

Spatiotemporal patterns of urbanization during the last four decades in Switzerland and their impacts on urban heat islands

Présentée le 20 mai 2021

Faculté de l'environnement naturel, architectural et construit
Communauté d'études pour l'aménagement du territoire
Programme doctoral en génie civil et environnement

pour l'obtention du grade de Docteur ès Sciences

par

Martí BOSCH PADROS

Acceptée sur proposition du jury

Prof. D. Licina, président du jury
Dr J. Chenal, Dr S. Joost, directeurs de thèse
Dr S.-E. Rabe, rapporteur
Dr M. Schlaepfer, rapporteur
Dr K. Javanroodi, rapporteur

The playground, asphalted and fenced in, is nothing but a pictorial acknowledgment of the
fact that 'play' exists as an isolated concept in our minds
In a natural city [. . .] play takes place in a thousand places [. . .] How can children become
filled with their surroundings in a fenced enclosure! They cannot.
— Christopher Alexander, "A city is not a tree" (1965)

To Ximena.

Acknowledgements

Following the timeline of events, I would like to start by thanking Lluís Solano and Dani Tost for introducing me to Linux, Python and Emacs during my undergraduate informatics courses at ETSEIB, which certainly contributed to the decision to address my career path towards computer science and scientific computing. Today, more than ten years after, these tools continue to be the central pillars of my development environment.

I express my most sincere gratitude to Pierre Genevès, Nabil Layaïda and all the members of the Tyrex team at INRIA Grenoble-Rhône-Alpes for giving me the opportunity to work in a great research environment where I had the joy of publishing my first academic paper. Such an internship made clear to me that my next steps should be directed towards pursuing a career in academia. I would like to continue by thanking Xavier Espinal, who supervised me as summer student at CERN, where I got to know first-hand the computing infrastructure beyond one of the most advanced research facilities in the world. It was then a pleasure to come back to INRIA Grenoble-Rhône-Alpes and join the STEEP team to work on my master thesis. I would thus like to thank all the team members, especially Luciano Gervasoni, Serge Fenet and Peter Sturm, who supported me greatly throughout such an endeavor.

This thesis would have not been possible without my friends at CEAT and EPFL, with whom I have had the privilege of working closely and sharing a fantastic atmosphere inside and outside working hours. I particularly thank Jérôme Chenal for giving me the opportunity to undertake this PhD thesis, granting me with trust and freedom to define and explore the research questions autonomously and with continuous support, and Stéphane Joost for his valuable guidance throughout my thesis. I am also very grateful to Perrine Hamel and Roy Remme for contributing to my thesis with their help and expertise. Finally, I would like to thank Nahid Mohajeri for her feedback and helpful comments as external expert of my candidacy exam, as well as the members of the thesis jury, Dusan Licina, Kavan Javanroodi, Sven-Erik Rabe and Martin Schlaepfer, for taking the time to review this manuscript and for providing constructive comments.

Als meus amics i a la meva família, especialment als meus pares i als meus germans pel seu suport incondicional, i al meu tiet Andreu, per donar-me la meva primera feina i compartir amb mi la seva manera particular de veure el món abans de marxar, malauradament massa aviat. A Eugenio y Rosy, por su gentileza y apoyo. Per acabar, a la Ximena, per haver compartit aquest últims anys amb mi, i per tots els anys que queden per compartir.

Sant Feliu de Llobregat, May 3, 2021

Martí Bosch.

Abstract

Urbanization is nowadays a global phenomenon which is increasingly concentrating the world's population in cities. In Switzerland, recent decades have seen an unprecedented loss of arable land due to urbanization, which has triggered amendments in the spatial planning laws with the aim of promoting urban densification. Nevertheless, despite remarkable efforts, the environmental impacts of distinctive urban patterns such as compact cities and urban sprawl remain poorly understood. One of the most remarkable environmental impacts of urbanization is the urban heat island effect, a phenomenon by which urban temperatures are warmer than in its rural surroundings. Central Europe, and therefore Switzerland, is among the regions in the world where temperatures are rising faster and the urban heat island effect is most prominent, which represents a central challenge for spatial planning. Most studies suggest that the urban heat island effect can be aggravated in compact cities, especially when considering the larger share of urban dwellers that are exposed to the highest temperatures. At the same time, the literature on the subject has seen a growing development of mitigation strategies, which suggest that the urban heat island effect can be significantly alleviated by an adequate planning of the building materials and urban green spaces.

This doctoral dissertation intends to address the issues expressed above by performing a quantitative evaluation of the spatiotemporal patterns of urbanization in Switzerland and their impact on the urban heat island effect. To that end, the thesis adopts a landscape ecology perspective to quantify urban patterns and to spatially simulate the biophysical processes that underpin the urban heat island effect. The first article presents PyLandStats, an open-source library to compute landscape metrics in a repeatable and reproducible manner. In the second article, such a library is used to evaluate the spatiotemporal patterns of urbanization observed in the urban agglomerations of Bern, Lausanne and Zurich from 1980 to 2016. The results reveal that the outer zones of Bern and Lausanne are still undergoing diffusive urban expansion, whereas infill development is the dominant growth mode in both the inner and outer zones of Zurich. The thesis follows with the development of a spatially-explicit method to simulate urban heat mitigation using a recent model of urban cooling based on three biophysical mechanisms, namely tree shade, evapotranspiration and albedo. The study introduces an automated procedure to calibrate the parameters of the model, and shows that the proposed approach can outperform regression models based on remote sensing features. Then, in the fourth article, such an approach is applied to Lausanne in order to evaluate heat mitigation in a variety of urban greening scenarios which modify both the abundance and spatial configuration of the tree canopy cover. The simulations suggest a potential alleviation

Acknowledgements

of the maximum nighttime temperatures of 2°C, which represents a major reduction of the human exposure to the urban heat island effect.

Finally, a concluding chapter summarizes the main contributions of the dissertation and reviews key implications for urban planning in Switzerland. Overall, rather than prescribing urban densification as the customary strategy for spatial development, land use regulations and local plans should incorporate spatially-explicit evaluations of the ecosystem services provided by urban green spaces. Future research should extend the proposed approach to include further ecosystem services and explore trade-offs and spatially design solutions.

Contents

Acknowledgements	v
Abstract	vii
Table of contents	ix
List of figures	xi
List of tables	xiv
1 Introduction	1
1.1 Context and motivation: urban sprawl, spatial planning and urban heat islands in Switzerland	2
1.2 Thesis goal and research objectives	3
1.3 State of the art and research gaps	4
1.3.1 Characteristics and impacts of urban sprawl	4
1.3.2 The effects of urban patterns and environmental performance	6
1.3.3 Urban green infrastructure and heat mitigation	9
1.4 Conceptual framework and theoretical background	12
1.5 Outline	13
2 Quantifying spatial patterns of landscapes	15
2.1 Introduction	15
2.2 Analysis of a single landscape	16
2.2.1 Computing data frames of landscape metrics	16
2.2.2 Customizing the landscape analysis	18
2.3 Spatiotemporal analysis	20
2.3.1 Computing spatiotemporal data frames	20
2.3.2 Customizing the spatiotemporal analysis	21
2.3.3 Plotting the evolution of metrics	22
2.4 Zonal analysis	23
2.4.1 Buffer analysis around a feature of interest	23
2.4.2 Generic zonal analysis	26
2.5 Spatiotemporal buffer analysis	28
2.6 Improvements of PyLandStats over existing software packages	30

3	Spatiotemporal patterns of urbanization in three Swiss urban agglomerations	33
3.1	Introduction	33
3.2	Materials and Methods	35
3.2.1	Study area	35
3.2.2	Data sources	36
3.2.3	Area-radius scaling in urban agglomerations	37
3.2.4	Quantifying spatiotemporal patterns of urbanization	39
3.3	Results	40
3.3.1	Area-radius relationship	40
3.3.2	Time series of landscape metrics	41
3.3.3	Growth modes	43
3.4	Discussion	44
3.4.1	Testing hypothesis of urbanization patterns	44
3.4.2	Identifying characteristic extents in urban agglomerations	46
3.5	Conclusion	46
4	Spatially-explicit simulation of urban heat islands	49
4.1	Introduction	49
4.2	Materials and methods	51
4.2.1	Study area	51
4.2.2	Data	51
4.2.3	Simulation with the InVEST urban cooling model	53
4.2.4	Spatial regression of air temperature based on satellite data	57
4.3	Results	58
4.3.1	Spatial regression of air temperature based on satellite data	58
4.3.2	Simulation with the InVEST urban cooling model	60
4.3.3	Model comparison	61
4.4	Discussion	62
4.5	Conclusion	64
5	Urban greening scenarios for urban heat mitigation	67
5.1	Introduction	67
5.2	Materials and Methods	68
5.2.1	Study area	68
5.2.2	Simulation with the InVEST urban cooling model	69
5.2.3	Refining LULC classes based on tree cover and building density	69
5.2.4	Generation of urban greening scenarios	70
5.3	Results	72
5.3.1	Proportion of transformed pixels by their original LULC class	72
5.3.2	Simulated LULC, temperature and heat mitigation maps	73
5.3.3	Spatial patterns of tree canopy cover	74
5.3.4	Effects on human exposure	76
5.4	Discussion	77

5.4.1	Validity and applicability of the proposed approach	77
5.4.2	Implications for urban planning in Lausanne	78
5.5	Conclusion	79
6	Synthesis and outlook	81
6.1	Summary of main contributions	81
6.2	Implications of the key findings	83
6.3	Methodological aspects and outlook for future research	84
	Bibliography	114
A	Appendix	115
A.1	Quantifying spatial patterns of landscapes	115
A.1.1	The PyLandStats library	115
A.1.2	S1 Text	117
A.1.3	S1 Code	117
A.1.4	S2 Code	117
A.1.5	S3 Code	117
A.1.6	S4 Code	118
A.1.7	S5 Code	118
A.1.8	S6 Code	118
A.2	Spatiotemporal patterns of urbanization in three Swiss urban agglomerations .	118
A.2.1	Code S1	118
A.2.2	Code S2	118
A.2.3	Code S3	118
A.3	Spatially-explicit simulation of urban heat islands	119
A.3.1	Data	119
A.3.2	Results	120
A.4	Urban greening scenarios for urban heat mitigation	122
A.4.1	Data	122
A.4.2	Results	124
	Curriculum Vitae	127

List of Figures

1.1	Conceptual framework	13
2.1	Example spatiotemporal plot for a class-level metric	22
2.2	Example spatiotemporal plot for a class and landscape-level metric	23
2.3	Example landscapes of a buffer analysis	24
2.4	Example buffer analysis plot for a class level metric	25
2.5	Example landscapes of a buffer ring analysis	26
2.6	Example buffer ring analysis plot for a class level metric	26
2.7	Example masks for a landscape transect analysis	27
2.8	Example landscapes of a transect analysis	28
2.9	Example zonal analysis plot for a class level metric	29
2.10	Example spatiotemporal buffer analysis plot for a landscape-level metric	30
3.1	Population change	36
3.2	Evolution of urban patches	38
3.3	Area-radius scaling	40
3.4	Time series of landscape metrics	42
3.5	Three growth modes	43
4.1	Study area — Lausanne urban agglomeration	52
4.2	Spatial regression errors	59
4.3	Air temperature maps predicted by the spatial regression	60
4.4	InVEST urban cooling model errors	61
4.5	Air temperature maps predicted by the InVEST urban cooling model	62
4.6	Spatial regression vs. InVEST urban cooling model comparison maps	63
5.1	Transformed pixels by original LULC class	73
5.2	Comparison of transformed pixels by selection approach	73
5.3	Simulated LULC, air temperature and heat mitigation maps	74
5.4	Scenario landscape metrics and temperature	74
5.5	Human exposure to urban heat	76
5.6	Comparison of human exposure by selection approach	77
A.1	Reference temperatures and magnitude of the urban heat island	120

List of Figures

A.2 Predicted vs. observed temperatures (linear regression model) 121

A.3 Predicted vs. observed temperatures (InVEST urban cooling model) 121

A.4 Location of the monitoring stations 123

A.5 Transformed pixels vs. average temperature regression plot 124

A.6 Simulated temperature histograms 124

List of Tables

2.1	Example data frame of patch-level metrics	17
2.2	Example data frame of class-level metrics	17
2.3	Example data frame of landscape-level metrics	18
2.4	Example customized data frame of class-level metrics	19
2.5	Example data frame of class-level metrics for a spatiotemporal analysis	20
2.6	Example data frame of landscape-level metrics for a spatiotemporal analysis	21
2.7	Example customized data frame of landscape-level metrics for a spatiotemporal analysis	21
2.8	Example data frame of class-level metrics for a buffer analysis	24
2.9	Example data frame of class-level metrics for a buffer ring analysis	26
2.10	Example data frame of class-level metrics in a zonal transect analysis	28
2.11	Example data frame of class-level metrics in a spatiotemporal buffer analysis	30
2.12	Comparison of FRAGSTATS, landscapemetrics, LecoS and PyLandStats	31
3.1	Selected landscape metrics	39
5.1	Selected landscape metrics	72
A.1	F-test of variable significance of the linear regression.	120
A.2	Biophysical table	123

1 Introduction

The world's population is undergoing an unprecedented trend of migration to urban areas. While, in 1800 roughly 5% of the world population lived in cities (United Nations, 1980, Table 3, page 7), recent estimates (United Nations, 2015) state that currently one out of two people lives in cities, and this proportion is expected to reach 60% by 2030. Although such trend seems to indicate that at a global scale human activity is becoming increasingly concentrated, the local densities of most urban agglomerations have been decreasing (Angel et al., 2005; Seto et al., 2011, 2012; Fragkias et al., 2013). At the same time, the degree and timing of such urban density downturn varies considerably among different regions of the world. By the end of the twentieth century, densities in cities of developing countries were found to be around three times lower than their counterparts in industrialized countries, with significant differences in the rate of density decline. However, many of such countries have recently experienced abrupt economic development accompanied by urbanization at declining densities, which suggests a global connection between these phenomena (Seto et al., 2014).

The first large-scale manifestations of urban migrations can be attributed to the industrial revolutions in Great Britain, where the poorest segment of the rural population migrated to the emerging industrial settlements (Hall and Tewdwr-Jones, 2010, pages 12-18). The rapid densification and posterior suburban expansion were actually closely linked, since “the same factories that helped create wealth for a rapidly expanding middle class also created pollution and overcrowding” (Bruegmann, 2006, pages 25-27). Consequently, the concurrent development of cheaper modes of transportation allowed such middle class to migrate towards the outskirts. Such pattern is commonly referred to as urban sprawl, and was first observed in London around 1870, and replicated then in Paris, and shortly after in North-American cities, in an even more abrupt way. Despite the fact that it lacks an accepted definition (Burchell et al., 1998; Galster et al., 2001), urban sprawl has been a persistent feature of post-industrial urbanization. As noted by Bruegmann (2006) “as cities have become economically mature and prosperous, they have tended to spread outward at a decreasing densities” (page 18).

Between 1940 and 1969, urban sprawl transformed in the United States three times the amount of converted land during the previous 30 years. Throughout the following decade, the suburbs

became undoubtedly the main population hosts of the U.S. as 95% of its demographic growth took place in suburban areas (Gillham, 2002). This situation, is nevertheless not exclusive to North America but rather a global challenge. In the beginning of the 21st century the amount of land occupied by cities roughly accounted for a 3% of the world's arable land, but with current demographic prospects at decreasing urban densities it might rise to as much as 5-7% by 2030 (Angel et al., 2005, 2011; Seto et al., 2011, 2012; Fragkias et al., 2013). Although the numbers might still appear relatively small, the environmental footprint of cities has significant implications at the global scale, for their functioning produces 78% of the earth's greenhousegases (Grimm et al., 2008).

One of the major impacts of urbanization is the urban heat island effect, a phenomenon by which urban temperatures are warmer than in its non-urbanized surroundings (Oke, 1973, 1982; Arnfield, 2003; Voogt and Oke, 2003; Grimmond, 2007; Phelan et al., 2015). Although the term urban heat island (UHI) first appeared in the 1940s (e.g., Balchin and Pye, 1947), evidence of higher air temperatures in the city than in the surrounding countryside was first introduced by Luke Howard in the first half of the nineteenth century (Howard, 1818). The main physical explanations for the UHI effect are a combination of the increased absorption of solar radiation of artificial surfaces, reduced evapotranspiration, anthropogenic heat releases and low ventilation (Oke, 1982; Taha et al., 1988; Taha, 1997; Phelan et al., 2015).

Recent estimates show that annual mean air temperatures in urban areas are up to 4 °C warmer than in its rural surroundings (Oleson et al., 2011). In European cities, the maximum UHI intensity ranges from 1 to 10 °C, with an average maximum value of 6 °C (Santamouris, 2016). With the ongoing global rise of temperatures and expansion of urban areas, the magnitude of the UHI effect is expected to intensify, which will increase extreme heat risks for a large share of the future urban population (Meehl and Tebaldi, 2004; Huang et al., 2019). Therefore, the mitigation of urban heat has become a key research and planning priority (Arnfield, 2003; Gago et al., 2013; Akbari and Kolokotsa, 2016; Kabisch et al., 2016; Deilami et al., 2018; Grădinaru and Hersperger, 2019; Geneletti et al., 2020).

1.1 Context and motivation: urban sprawl, spatial planning and urban heat islands in Switzerland

Likewise many developed countries, urbanization has been a major force of landscape change in Switzerland, especially in the Central Plateau region. Between 1985 and 2009, the extent of urban areas expanded by 23.4%, which represents an increase from 6.0% to 7.5% of the proportion of total surface area in Switzerland (SFSO, 2013). During the same period, the average surface of built-up area per inhabitant has increased to 407 m², exceeding the target of 400 m² per inhabitant set by the Swiss Federal Council to ensure an efficient use of land resources (Swiss Federal Council, 2012). Overall, the urban growth observed since the second half of the twentieth century in Switzerland has been characterized by a dispersed and low-density expansion of urban areas, matching most of the connotations of urban sprawl (Jaeger

and Schwick, 2014).

In line with the federalist government structure, the Swiss spatial planning system is distributed between the federal state, the 26 cantons and 2495 municipalities. The federal state specifies the framework legislation and coordinates the spatial planning activities of the cantons, while cantons check the compliance of municipal development plans with cantonal and federal laws. With some exceptions, municipal administrations are in charge of their local development plans, namely the land use plan and building ordinance, and might therefore be viewed as the most important spatial planning entities. In order to prevent urban sprawl and ensure that land is used economically, the Swiss Federal Act on Spatial Planning of 1979, municipalities were required to provide land use plans, which specify the boundaries between building and non-building zones. While the designation of building zones have generally been able to effectively manage the spatial development of the largest Swiss urban agglomerations (Gennaio et al., 2009), the Federal Act has not prevented the extension of built-up areas in Switzerland, mainly because small and mid-sized municipalities with enough available farmland can designate new building zones almost entirely autonomously (Mann, 2009; Jaeger and Schwick, 2014; Rudolf et al., 2018). Forecasts based on the current urbanization trends predict significant increases of urban land use demands over the next decades, mostly at the expense of agricultural land located at the fringe of existing urban agglomerations (Price et al., 2015), which might result in a reduction of recreation opportunities, crop production, biodiversity and increased flooding risk and heat island effects (Gerecke et al., 2019). Nonetheless, the foregoing predictions might be challenged by a major revision of the Federal Act in 2013, which limits the amount of building zones that municipalities can designate and encourages infill development and densification by means of tax incentives (ARE, 2013).

Central Europe, and therefore Switzerland, is among the regions where extreme heat events have become more frequent in recent decades (Swiss Academy of Sciences, 2018; National Center for Climate Services, 2018). Future climate scenarios for Swiss urban areas forecast a notable increase in the number of tropical nights, i.e, where the temperature does not sink below 20 °C (Burgstall, 2019). In view of such a situation, many Swiss municipalities and cantons have started incorporating adaptation strategies in their planning framework (FOEN, 2018). However, most of the hitherto measures correspond to generic recommendations to raise awareness among the population, urban planners and decision makers. Therefore, little is known about how the urban densification promoted by the new Swiss regulations might impact the UHI effect or urban ecosystem services in general.

1.2 Thesis goal and research objectives

The main goal of this thesis is to spatially evaluate the impacts of urban form on the UHI effect. Such an endeavor is divided into three key objectives:

1. Quantify the landscape changes associated to urbanization that have taken place in

Switzerland, and most importantly, in the main Swiss urban agglomerations. This is a required preliminary step to have a quantifiable basis against which variations in the observed UHI effect can be assessed.

2. Develop reusable methods to spatially model the UHI effect and map the potential urban heat mitigation that can be attained in a given urban agglomeration.
3. Based on the outputs of the first two, is to formulate distinct future urbanization scenarios and spatially evaluate how each might affect the UHI effect as well as the urban heat mitigation potential.

These inquiries are of major relevance to the urbanization context of Switzerland reviewed above. More precisely, the results are expected to map the heat mitigation provided by the existing urban green infrastructure, and therefore estimate the potential effects of replacing urban green patches by artificial surfaces. Additionally, the methods and tools developed to attain the results are intended to support urban planning, by allowing planners and decision makers to spatially quantify the impacts of potential interventions, explore alternatives and select the most desirable configurations. Altogether, in line with the foregoing endeavors, this thesis intends to test the central hypothesis that the urban patterns that have the greatest heat mitigation potential are incompatible with severe densification and infill development of the existing Swiss urban agglomerations.

1.3 State of the art and research gaps

1.3.1 Characteristics and impacts of urban sprawl

The first reference to the term urban sprawl was made by Earle Draper, as part of a conference of urban planners of the southeastern United States in 1937. The topic acquired striking relevance during the second half of the twentieth century, and ever since then, it has been continuously spreading to a wide range of domains. In one of the early efforts to characterize urban sprawl, Harvey and Clark (1965) criticized the lack of accepted definitions of the term and delineated three physical patterns of sprawl, namely continuous low density, ribbon development and leapfrog development. However, besides a set of archetypes, “sprawl is a matter of degree” (Ewing, 1995, page 520). For instance, to what extent polycentric urban forms might be considered sprawl is not clear (Gordon and Wong, 1985). On the other hand, sprawl has also been associated to a dysfunctional spatial segregation of land uses (Burchell et al., 1998). Despite remarkable efforts to assemble different acceptations of sprawl (Galster et al., 2001), the research community still fails to agree on a common definition of urban sprawl, especially since the term can be heard from very diverse practitioners and its interpretation is likely to depend on the discipline and the context of application. Be that as it may, some prominent characteristics of sprawl reappear often in the literature, such as scattered development, low density, decentralization to the urban periphery, segregation of land uses and low accessibility.

From the semantic ambiguity of urban sprawl follows a lack of consensual methods to measure it. In consonance with the preceding traits, the prevalent approach is to treat sprawl as a multidimensional phenomena, and several dimensional decompositions have been proposed throughout the literature. Some of them are rather simple, such as the four dimensions proposed by Ewing et al. (2002), i.e., density, land use mix, centering and accessibility, whereas Galster et al. (2001) unravel sprawl further and identify eight dimensions, i.e., density, continuity, concentration, clustering, centrality, nuclearity, land use mix and proximity. Nevertheless, such decompositions seem fuzzy, even for the simplest cases, e.g., the accessibility to a given facility is related to the density, the number of activity centers and the land use mix. In point of fact, when computing the dimensions of sprawl for the largest metropolitan areas of the United States, concentration, proximity clustering and centrality are significantly correlated in Galster et al. (2001), and the same holds for density and connectivity in Ewing et al. (2002). When calculating aggregate indices, such intricateness might result in overemphasizing certain features of sprawl. In the discussion between different views towards urban sprawl of Ewing et al. (2014), some authors argue that many of the research results rely heavily on how the sprawl indices are constructed, which is “highly subjective and depend upon very specific and not necessarily generally accepted definitions of sprawl” (page 15).

While the multiplicity of perspectives adopted to investigate urban sprawl highlights the relevance of the topic, the involved ambiguity paves the way for incomplete assessments, endogenous biases and premature claims, which are often accused to be politically motivated. The vast report of the Real Estate Research Corporation (RERC, 1974) has been a noteworthy source of controversy. For instance, Altshuler et al. (1979) accounted that it includes few rigorous calculations on the car use decrease, while Windsor (1979) concluded that the claimed energy savings in their alternative scenarios are more a result of their assumptions rather than of the density. Also as response to the report, Gordon and Wong (1985) pointed to the evidence of reduced trip lengths of the suburban residents of large polycentric cities to suggest that as cities grow, travel demands are accommodated through decentralization of the employment centers. More broadly, Haines (1986) determined that studies that consider only centralization and sprawl resolve that centralization is the most energy-efficient option, whereas studies that additionally consider polycentric urban forms favor the latter. Similar controversies arose from the global strong correlations between density and gasoline consumption established empirically by Newman and Kenworthy (1989), mainly because density alone neglected the complexity and diversity of the analyzed urban patterns. Overall, in a thorough review of empirical studies, Hall (2001) discerned that literature findings relating transportation and urban form when compared with each other are equivocal, and resolved that travel is globally more linked to income than density.

Although the sprawl debate has focused more on transportation issues, additional environmental implications of urban form require careful consideration. Urban areas exert significant influence on its surrounding ecosystems and the services that they provide to humans and other living beings (Bolund and Hunhammar, 1999). While many studies have reported empirical correlations between environmental indicators and aggregate measures of urban-

ization such as density or the extent of the built-up area, such an approach presents two key methodological shortcomings (Alberti, 1999). On the one hand, disagreement in the planning literature on the environmental impacts of alternative urban development patterns can be attributed to how environmental performance is defined and measured. The environmental performance of cities concerns the effects of their functioning on the surrounding environment, which includes direct transformations of the physical landscape patterns, the use of natural resources, the release of emissions and wastes as well as impacts on human health and well being (Alberti, 1996). On the other hand, aggregate measures do not reflect the complexity and diversity of existing urban forms, and are strongly affected by the different definitions of city boundaries. For instance, the comparative study of five UK cities of Tratalos et al. (2007) associated higher density to poorer urban biodiversity and environmental services such as carbon sequestration, storm water interception or alleviation of maximum temperatures, yet sites with similar densities show substantial variability on the environmental performance, even within the comparable conditions among the UK. Overall, the effects of urban density and form are hard to isolate since their impact on environmental performance is mediated by the local environmental characteristics of the site.

1.3.2 The effects of urban patterns and environmental performance

The approach to quantifying urban sprawl and its costs reviewed above, which is characteristic of the viewpoints of urban economics and the regional sciences, has been prevalent among the early studies of urban sprawl (Bosch et al., 2019). In order to assess the impacts of urban sprawl, such studies often explore the empirical correlations between the alleged sprawl indices and a variety of indicators of travel behavior, environmental performance and public health. Nevertheless, such an approach presents two main drawbacks when it comes to evaluating the environmental impacts of urban sprawl. On the one hand, as discussed above, many of the aggregate measures of urban form used in the literature of urban economics and sprawl do not reflect the spatial complexity of contemporary cities. On the other hand, the way in which environmental systems respond to the disturbances of urbanization shows complex nonlinear dynamics, such as thresholds, reciprocal feedback loops, time lags, resilience, heterogeneity, surprises and legacy effects (Alberti, 1999; Collins et al., 2000; Liu et al., 2007). Therefore complexity of such interactions can hardly be apprehended by means of statistical methods.

Quantifying urbanization with spatial metrics from landscape ecology

Landscape ecology is the study of how the spatial pattern of landscapes influences the ecological processes that occur upon them (Forman and Godron, 1981; Forman et al., 1986; Turner, 1989). Urban landscapes can be characterized as a mosaic of land use patches. From this perspective, measuring urban sprawl can benefit from a set of spatial metrics from landscape ecology (Torrens and Alberti, 2000), which serve to quantify two main characteristics of the urban landscape, namely the geometric configuration of patches and their functional composition. From the reviewed definitions, an urban landscape might be considered sprawling

when its configuration is irregular and fragmented and its land use composition is segregated (Frenkel and Ashkenazi, 2008).

Urbanization throughout the world has happened under very different geographical constraints, historical periods and available technologies, resulting in distinctive spatial signatures. However, despite the apparent complexity and diversity of cities and regions, spatial metrics from landscape ecology suggest that remarkable regularities exist among the spatio-temporal evolution of their land use patterns. In a comparative study of four Chinese cities, Seto and Fragkias (2005) determined that in spite of significant differences on the initial urban structures, economic context and local policies, synergies exist in terms of shape, size and growth rates of land use patches. Similarly, Jenerette and Potere (2010) explored a global set of 120 cities and resolved that while individual cities show continued increases in complexity and fragmentation of land use patches, the inter-city diversity of patterns diminishes, suggesting a tendency towards global urban homogenization. After a thorough comparison of hypotheses regarding the spatio-temporal patterns of urban land use change, Liu et al. (2016) determined that under the contemporary Western socioeconomic context, urbanization globally leads to increasing dispersion of land use, structural fragmentation and shape complexity. Notably, such urban landscape significantly matches many of the connotations of sprawl.

Unlike many of aggregate indices of urban sprawl reviewed above, landscape metrics are inherently conceived to represent complex and fractal spatial patterns, such as those observed in contemporary cities (Frankhauser, 1990; Batty and Longley, 1994; Frankhauser, 1994). Furthermore, while multidimensional indices of sprawl are often hard to interpret and relate to environmental performance, a key advantage of spatial metrics is that they are also good predictors of the ecosystem's ability to support important ecosystem functions (Turner and Gardner, 2015).

Characteristics of the spatial and temporal scales in urban ecosystems

Urban ecosystems are governed by the same ecological laws as rural and natural environments, with the main difference being the relative importance of anthropogenic processes (Niemelä, 1999). Nevertheless, the study of urban landscapes has received little attention among ecologists throughout most of the 20th century. In the context of rapid rates of land use change due to urbanization, the urge to understand such interactions has recently fostered the emergence of the field of urban ecology, which integrates the theory and methods of both natural and social sciences to study urban ecosystems (Collins et al., 2000; Grimm et al., 2008; Wu, 2014; McPhearson et al., 2016). Like other ecosystems, urban ecosystems constantly exposed to changes. Urbanization results in major disturbance of the resource flows by altering the land use and cover, biogeochemical cycles, local climatic conditions, hydrological processes and biodiversity. Therefore, anthropogenic changes in urban areas are likely to occur in much shorter time scales (Collins et al., 2000).

When modeling cities as ecosystems, two central issues arise regarding the spatial scale. On

the one hand, as urban areas expand, the demarcation between urban and rural spaces is better characterized by a continuum than by a dichotomy, which can result in equivocal comparison of environmental impacts of cities (Stewart and Oke, 2006). The reliance upon the definitions of metropolitan areas and administrative boundaries is also problematic, since they are constructed manually based on subjective criteria that does not necessarily match the actual spatial extent of cities, and can thus lead to misleading outcomes (Rozenfeld et al., 2008; Tannier and Thomas, 2013; Oliveira et al., 2014; Liu et al., 2014). In order to address the issue of the spatial extent, the environmental gradient paradigm can be applied to study the urban-rural continuum by evaluating the spatial variation of the environmental characteristics as one moves progressively from the highly-developed urban cores to the less intense suburbs until the rural and natural hinterlands (McDonnell and Pickett, 1990). On the other hand, when compared to natural landscapes, urban areas tend to show greater patchiness and spatial heterogeneity. Land cover maps often rely on coarse-scale classifications aimed at separating the human and natural components of systems, yet such a scheme fails to characterize how human and natural components are strongly interspersed in urban areas. For instance, some classifications distinguish residential land uses according to the density of buildings but ignore the associated abundance and variety of vegetation types and building materials, which can have a strong influence on the flux of water, carbon, nutrients, and energy (Band et al., 2005). With the aim of better understanding how urban landscapes interact with ecological processes, urban ecologists have devised frameworks to quantify the fine-scale heterogeneity of the built and natural components of cities. The work of Ridd (1995) suggests representing the biophysical composition of urban cover in terms of its proportion of vegetation, impervious and soil components, and shows how these can be mapped using remote sensing. Similarly, Cadenasso et al. (2007) propose a reconceptualization of urban land use which consists of six main features, namely coarse-textured vegetation (trees and shrubs), fine-textured vegetation (herbs and grasses), bare soil, pavement, buildings, and the building typology. Finally, Zhang et al. (2013) highlight the importance of a multiscale perspective and present hierarchical model of the structure of urban landscape pattern. By considering six nested hierarchical levels (i.e., individual plant, plant population, land-cover (or local ecosystem), land-use, landscape and region), multiple natural and anthropogenic processes can be modeled at their appropriate level, which allows assessing how multiple anthropogenic controls from different scales modify the environmental factors that constrain ecosystem functions, and thus facilitate linking ecosystem processes and socioeconomic drivers.

Spatial modeling of urban ecosystem services

As reviewed above, ecological research in cities is concerned with how anthropogenic changes affect the ecological processes that take place in urban environments. Understanding the links between spatial landscape patterns and ecosystem processes is crucial in order to develop planning strategies that maximize the provision of beneficial ecosystem services at the urban scale, which include (among others) reduction of air pollution, alleviation of maximum temperatures, absorption of storm water, noise reduction, carbon sequestration, improvement of

aesthetic and cultural values as well as the preservation of ecological habitats and biodiversity (Bolund and Hunhammar, 1999; Gómez-Baggethun and Barton, 2013).

Given the drawbacks of using aggregate measures to evaluate complex phenomena such as urban ecosystems, using integrated and spatially-explicit models becomes crucial in order to understand the links between landscape patterns, biophysical and socioeconomic processes (Bagstad et al., 2013; Haase et al., 2014; Turner et al., 2016; Costanza et al., 2017). While there exists a wide range of models to evaluate ecosystem services, very few have been implemented in a spatially-explicit manner. Available open source platforms of spatially-explicit models of ecosystem services include the ARIES (Villa et al., 2014), MIMES (Boumans et al., 2015) and InVEST (Sharp et al., 2020) platforms. The latter is being adapted into the Urban InVEST platform, which focuses on modelling the ecosystem services that are most relevant at the scale of urban agglomerations. In the beginning 2020, NatCap released the first two urban models, which focus on urban flood risk mitigation and urban cooling respectively. The study of Kadaverugu et al. (2020) applied the flood risk mitigation model to spatially quantify the flood risk mitigation provided by the urban green spaces of Hyderabad, India, and found that they retain 44-50% of the precipitation. Nonetheless, slight additional increases of rainfall intensity can result in major water run-off generation with potential major economic damages, which highlights the importance of mitigation measures such as the promotion of urban green infrastructure, open space as well as the preservation of urban water bodies and their connectivity. In the study of the impacts of urban form on heat mitigation in Milan, Italy, Ronchi et al. (2020) use the urban cooling model to 13 urban districts characteristic of four different historical planning periods, with distinct characteristics in terms of green areas, permeability, built-up footprint, and tree density and cover. Their results suggest that the proportion of permeable surfaces, size of green areas and the proportion of tree cover have the most significant positive effects in the cooling capacity of the district, whereas the footprint and volume of buildings have the most notable negative influence. Finally, Kadaverugu et al. (2021) apply the urban cooling model to evaluate the heat mitigation in the present and future plausible scenarios for Nagpur City, India. Their simulations suggest that promoting urban green spaces results in a 0.5 °C decrease of the average temperature of the study area, with important impacts on the energy demand for cooling indoor environments.

1.3.3 Urban green infrastructure and heat mitigation

Urban green infrastructure has been identified as a flexible, cost effective and broadly applicable approach to provide urban cooling as well as other beneficial ecosystem services to urban dwellers (Gill et al., 2007; Bowler et al., 2010; Young, 2010; Block et al., 2012; Gago et al., 2013; Zardo et al., 2017; Koc et al., 2018; Santamouris et al., 2018). However, the contribution of urban green spaces to urban heat mitigation is complex and is affected by both its abundance and spatial configuration (Kong et al., 2014; Li et al., 2017; Zhou et al., 2017; Jiao et al., 2017; Yan et al., 2019; Yu et al., 2020). While increasing the abundance of urban green spaces shows a very consistent relationship with reduced temperatures, contradicting results have been

reported regarding the cooling effects of spatial configuration. In fact, several studies have found that patterns with patches with complex shapes and further edge density between natural and artificial patches lead to greater heat mitigation (Zhou et al., 2011; Rhee et al., 2014; Maimaitiyiming et al., 2014; Estoque et al., 2017), whereas other studies resolve the opposite (Li et al., 2012; Connors et al., 2013; Fan et al., 2015; Myint et al., 2015). Similarly, larger patches of urban green spaces are usually associated with increasing heat mitigation, yet such a relationship is poorly understood as it displays scale dependencies and nonlinear thresholds (Chang et al., 2007; Bowler et al., 2010; Kong et al., 2014; Jaganmohan et al., 2016; Ziter et al., 2019; Yu et al., 2020; Jung et al., 2021). Additionally, some results suggest that the cooling effect of the patch shapes depends on their size, as smaller patches with increased edge provide a longer interface through which the cool air can be transported, yet larger green spaces can form stable microclimates that also have a positive cooling effect (Chang et al., 2007; Jaganmohan et al., 2016; Yu et al., 2020). Overall, as suggested by Zhou et al. (2017), the foregoing contradicting results are related to how the cooling mechanisms of trees, namely shading and evapotranspiration, operate in urban areas, which strongly depends on the existing urban fabric and canopy cover as well as the local climatic context (Li et al., 2017; Yu et al., 2018; Sun et al., 2019; Yu et al., 2020; Wang et al., 2020a,b).

The effects of the intensity and configuration of urban patches on the UHI effect and human exposure to such additional heat also present complex trade-offs that require considering the specific circumstances of each region of study. In the case study for the Strasbourg-Kehl urban region (France-Germany), Kohler et al. (2017) determine that realistic planning scenarios of urban sprawl and compact cities show no significant differences in the predicted UHI intensity. Nonetheless, as noted by Lemonsu et al. (2015), this might be largely due to the fact that such scenarios do not change the morphology of the historic city center, where maximum temperatures are usually observed. In the study of distinct urban sprawl and compact city scenarios in Paris, Lemonsu et al. (2015) resolve that urban sprawl results in lower nighttime UHI because of the abundance of low-density vegetated outskirts, while the daytime UHI is lower in the compact city scenario because of the limited penetration of solar radiation. In a similar case study for Beijing, Yang et al. (2016) determine that the compact city scenario can enhance the UHI magnitude while sprawl scenario can reduce it. While both studies conclude that human exposure to the UHI effect is aggravated in the compact city scenarios because of the large share of urban dwellers residing at the city center, Yang et al. (2016) further find that urban sprawl produces a larger regional warming effect with greater thermal perturbation in the vertical extent, which results in higher potential for increased instability at the planetary boundary layer height. Overall, the design of urban heat mitigation solutions requires place-based awareness that takes into account the existing urban fabric as well as the larger synoptic climate context (Georgescu et al., 2015).

Planning the urban green infrastructure for ecosystem services and heat mitigation

The effects of the spatial pattern of urban green infrastructure on heat mitigation highlight the importance of spatial planning for urban resilience and climate adaptation. As reviewed above, the complexity of such a relationship is evidence that such a planning endeavor cannot be addressed with aggregate measures and thus requires an explicit consideration of space.

The work of Locke et al. (2010) presents a spatially-explicit model to prioritize tree planting sites based on multiple criteria, which includes the alleviation of air pollution, flood risks, maximum temperatures as well as the improvement of the biodiversity, public health and neighborhood beautification. Similarly, Bodnaruk et al. (2017) use the i-Tree suite of tools Hirabayashi et al. (2011) to explore the tradeoffs between ecosystem services and benefits between different tree planting schemes in Baltimore, which comprise the reduction of air pollution and air temperature as well as metrics of heat risk based on the exposure to maximum temperatures of the urban dwellers, weighted by age groups to account for their different vulnerabilities to extreme heat. In another application of the i-Tree suite, Lin (2020) propose a composite index to prioritize tree planting and protection locations based on environmental and human indicators and design three distinct scenarios that target at optimizing a weighted combination of such indicators. Their results show that small differences in the weightings can lead to substantial changes in the spatial distribution of the priority areas, stressing the need for transparency, as well as engagement and communication among stakeholders, the public and policy makers (Müller and Burkhard, 2012; Kabisch et al., 2016). Finally, Werbin et al. (2020) present heat vulnerability index specific to the city of Boston to support and inform decision-making for planting new trees. Such an index is based on sociodemographic and land cover data, and is implemented as part of an interactive web application that includes additional information of potential tree pests and diseases, suitability of species, land ownership, maintenance tips, and alternatives to tree planting.

Nevertheless, the foregoing studies overlook the effects of spatial configuration reviewed above, and thus might prevent the achievement of more efficient greening strategies. For instance, Jaganmohan et al. (2016) find that increasing the complexity of smaller green spaces has a negative effect on their cooling efficiency but a positive effect in larger green spaces. Such a threshold effect is in consonance with the detailed study of the UHI in Madison, Wisconsin, by Ziter et al. (2019), which reveals that canopy cover in excess of 40% has larger cooling effects of the daytime urban heat. Accordingly, neighborhoods with intermediate amounts of impervious surfaces and 40% canopy cover could offer the greatest marginal increase in climate mitigation for urban residents. Moreover, the results of Ziter et al. (2019) reveal that the cooling effect of the tree canopy is lower at fine scales, likely because very small canopy areas cannot be isolated from the surrounding meteorological conditions. Finally, the study of the UHI of Seattle and Baltimore by Jung et al. (2021) also confirm the existence of such a threshold but further reveal that the relationship between patch size and its cooling effect might be hump-shaped, which suggests that an increase of canopy cover of the same area in moderate canopy cover areas might be less effective at mitigating heat than the same increase

of canopy cover area in either a low or a high canopy cover area.

1.4 Conceptual framework and theoretical background

The conceptual framework adopted in this thesis is concerned with how a set of features X influences a set of targets Y . Following the scientific method, the aim of the framework is the search for empirical regularities between X and Y . From this perspective, the central question of this thesis can be expressed as how urban form, represented by a set of the features X , influences the UHI effect, measured by a set of targets Y .

Such an inquiry belongs to the more general quest of evaluating the environmental performance of distinct urban forms. Based on the literature reviewed above, three key methodological considerations arise, which are addressed as follows:

- Contemporary cities are complex spatial entities. In order to be able to assess their spatial complexity, and to avoid the semantic ambiguity regarding the definitions and indices of urban sprawl, spatial metrics from landscape ecology are adopted in this thesis as the main tool to quantify the spatial patterns of urban areas.
- The choice of an appropriate spatial scale is central to the study of cities. The ecological concept of spatial scale encompasses both extent and grain (Forman et al., 1986; O'Neill et al., 1986; Wiens, 1989; Turner, 1989). To select the appropriate spatial extent to evaluate the environmental performance of urban areas, the approach in this thesis is inspired by the environmental gradient paradigm, evaluating the spatial variation of the environmental characteristics along the urban-rural continuum without assuming any predefined administrative boundary. Regarding the issue of spatial grain, most of the available land use and land cover classifications fail to represent the fine-scale heterogeneity of the built and natural components of cities. To overcome such a shortcoming, this thesis builds upon several schemes to classify urban structures have been developed with the specific purpose of studying the UHI effect (Stewart and Oke, 2012; Larondelle et al., 2014; Hamstead et al., 2016), which define composite classes that represent combinations of built and natural features such as the building volume, abundance of trees or fraction of pervious/impervious surfaces. Finally, cities influence and are influenced by environmental processes operating at multiple scales. Therefore, understanding such interactions requires crossing spatial and hierarchical scales (Wu and Loucks, 1995; Alberti, 1999; Zhang et al., 2013)
- Models are the central tools to scientific inquiry used in this thesis. The phenomena that they intend to represent, namely how biophysical and socioeconomic processes operate in urban areas, show complex behaviors in space and time. Therefore, the employed models must fulfill two major requisites. First, in view of the spatial complexity of urban landscapes, aggregate models and results cannot properly address the relationship between the spatial patterns and its environmental performance, which highlights the

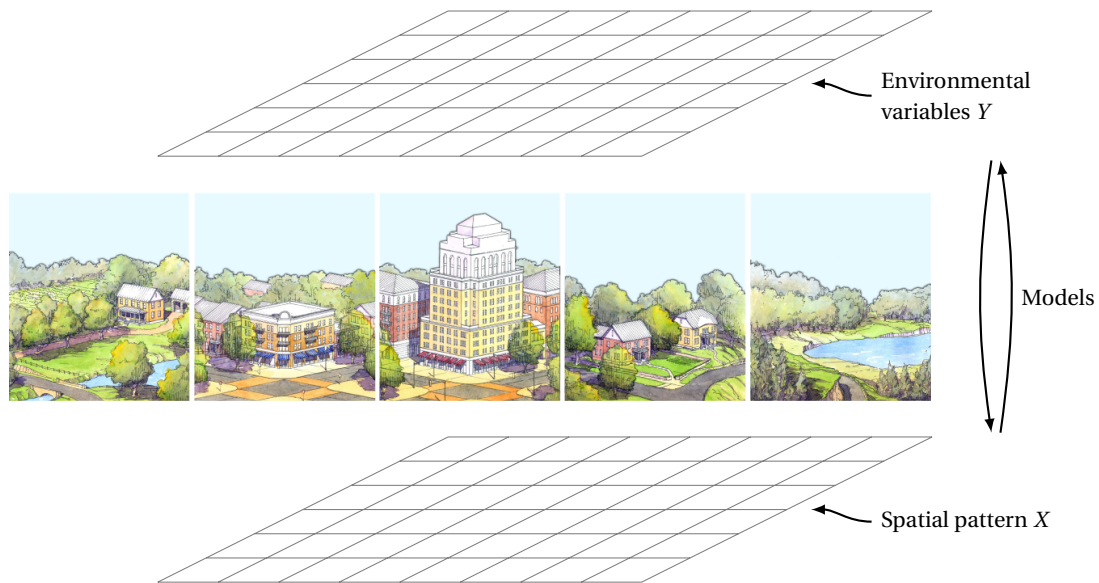


Figure 1.1 – Conceptual framework to scientific inquiry used in this thesis. Illustration of the urban transect by Dover, Kohl & partners, downloaded from the Center for Applied Transect Studies (transect.org).

need for an explicit representation of space in the inputs, functioning and outputs of the models. Secondly, the models need to be able to advance the domain knowledge and ultimately inform urban planning and decision making. From this perspective, models that incorporate an explicit representation of the underlying biophysical and socioeconomic processes present a major advantage with respect to statistical and black-box approaches such as artificial neural networks or similar machine learning models, which is that the parameters of the models can be straightforwardly interpreted in terms of their biophysical and socioeconomic meaning. Such an aspect of the models is crucial to improve the understanding of the complex couplings between the human and natural components of urban systems.

A schematic illustration of the conceptual framework to scientific inquiry of this thesis is shown in Figure 1.1.

1.5 Outline

The remainder thesis is organized in five main chapters, which are outlined below:

- **Chapter 2** presents PyLandStats, an open-source library developed with the aim of computing landscape metrics in a reusable and reproducible manner, which can be straightforwardly included as part of complex and automated computational workflows.
- In **Chapter 3**, the PyLandStats library is used to evaluate the spatiotemporal patterns of

urbanization in the Swiss urban agglomerations of Bern, Lausanne and Zurich over the period from 1980 to 2016. Fractal analysis of the area-radius relationship of the urban agglomeration is employed to separate it into two characteristic extents, namely the inner and outer zone. The computed landscape metrics and growth modes suggest that the two extents show very distinct urbanization patterns. More precisely, the inner zone of all agglomerations is dominated by infilling, whereas the outer zones of Bern and Lausanne are undergoing a diffusive urban expansion.

- **Chapter 4** develops a reusable spatially-explicit approach to simulate urban heat mitigation with the InVEST urban cooling model, which is based on three biophysical mechanisms, namely tree shade, evapotranspiration and albedo. An automated procedure is proposed to calibrate the parameters of the model to best fit temperature measurements from monitoring stations. The simulations performed in the urban agglomeration of Lausanne show that the calibrated model can outperform regression approaches based on remote sensing features. Additionally, a key advantage of the proposed approach is that the calibrated model can be used to evaluate synthetic scenarios such as master land use plans, urbanization prospects and the like.
- In **Chapter 5**, the foregoing workflow to simulate urban cooling is exploited to evaluate the potential heat mitigation that can be achieved by increasing the tree canopy cover in the urban agglomeration of Lausanne. The approach couples the cadastral land use/land cover map with a high-resolution tree canopy map to discern locations of the current urban fabric where the tree canopy can be increased, and then makes use of the calibrated InVEST urban cooling model to assess the potential heat mitigation. The results suggest a potential alleviation of the maximum nighttime temperatures at the city center of 2 °C, with substantial impact on the human exposure to extreme heat.
- **Chapter 6** summarizes the research contributions and concludes by reviewing implications for urban planning as well as perspectives for future research.

2 Quantifying spatial patterns of landscapes

As reviewed in the introductory chapter, landscape metrics have been widely applied to quantify the spatial patterns of urban areas and evaluate the landscape transformations associated to urbanization. Nevertheless, at the time when the study of the urbanization patterns of this thesis was conceived, none of the available tools to compute landscape metrics fulfilled key operational requirements in terms of their use in interactive computational environments and their inclusion as part of automated computational workflows. In order to address such a shortcoming, this chapter presents PyLandStats, an open-source library to compute landscape metrics using the Python programming language, which has been published in the following article:

Bosch, M. (2019a). PyLandStats: An open-source Pythonic library to compute landscape metrics. *PLoS One*, 14(12)

The candidate designed and developed the library and wrote the manuscript.

2.1 Introduction

Landscape ecology is based on the notion that the spatial pattern of landscapes strongly influences the ecological processes that occur upon them (Turner, 1989). From this perspective, quantifying the spatial patterns of landscapes becomes a central prerequisite to the study of the pattern-process relationships. Landscape ecologists often view landscapes as an heterogeneous spatial mosaic of discrete patches, each representing a zone of relatively homogeneous conditions, where the size, shape and configuration of patches significantly affects key ecosystem functions such as biodiversity and fluxes of organisms and materials (Pickett and Cadenasso, 1995).

Recent decades have seen the development of a series of landscape metrics that quantify several aspects of the spatial pattern of landscapes (O'Neill et al., 1988; Turner, 1990; McGarigal et al., 2012). In a context of significant advances in geographical information systems (GIS) and increasing availability of land use/land cover (LULC) datasets, landscape metrics have been

implemented within a variety of software packages (Steiniger and Hay, 2009). The present article introduces PyLandStats, an open-source library to compute landscape metrics, which represents an advance over previously available software because of its implementation within the most popular libraries of the scientific and data-centric Python stack. Additionally, its modular and object-oriented design allows it to be efficiently used in interactive environments such as Jupyter notebooks as well as in automated computational workflows, and eases the maintainability and extensibility of the code.

The remainder of the article describes the structure and use of PyLandStats by presenting a thorough example analysis case for a sequence of three raster landscape snapshots of the Canton of Vaud (Switzerland) for the years 2000, 2006 and 2012, which have been extracted from the Corine Land Cover (Heymann et al., 1994) inventory. The code snippets and materials to reproduce the figures of the following four sections can be found in the appendices A.1.3, A.1.4, A.1.5 and A.1.6 respectively.

2.2 Analysis of a single landscape

The basic unit of the PyLandStats library is the `Landscape` class, which represents the LULC mosaic of a particular region *at a given point in time*. A `Landscape` instance mainly consists of an array where each position represents the LULC class at the corresponding pixel of the landscape.

Since LULC data is most often stored in raster files (e.g., GeoTiff), the easiest way to instantiate a `Landscape` object is by passing a path to a raster file as first argument, as in:

```
> ls = Landscape('path/to/raster.tif')
```

The above call will use the `rasterio` Python library in order to read the raster files, and will extract the pixel resolution and no-data value from the file metadata. Alternatively, `Landscape` instances might also be initialized by passing a NumPy array (Van Der Walt et al., 2011) as first argument, which also requires specifying the x and y coordinates of pixel resolution as a tuple in the `res` keyword argument. By default, PyLandStats assumes that zero values in the array represent pixels with no data. Otherwise, the no-data value can be specified by means of the `nodata` keyword argument. A `Landscape` instance can be plotted at any moment by using its `plot_landscape` method. Note that all the plotting methods of PyLandStats make use of the `matplotlib` library (Hunter, 2007).

2.2.1 Computing data frames of landscape metrics

Landscape metrics might be classified into two main groups (see the section “List of implemented metrics” of appendix A.1.2 for the list of metrics implemented in PyLandStats, their classification and their description). The first concerns metrics that provide a scalar value for

2.2. Analysis of a single landscape

each patch of the landscape, which are often referred to as patch-level metrics. The second consists of metrics that provide a scalar value that aggregates a characteristic of interest over a set of the patches. This second group allows for an additional distinction between class-level metrics, which are computed over all patches of a given LULC class, and landscape-level metrics, which are those computed over all the patches of a landscape.

For a given Landscape instance, the patch-level metrics can be computed by means of the `compute_patch_metrics_df` method as in:

```
# `ls` is a given `Landscape` instance
> ls.compute_patch_metrics_df()
```

which will return a pandas data frame (McKinney, 2010) as depicted in Table 2.1, where each row corresponds to a patch of the landscape with its associated LULC class value and the computed metrics.

Table 2.1 – Example data frame of patch-level metrics.

patch_id	class_val	area	perimeter	perimeter_area_ratio	shape_index	fractal_dimension	euclidean_nearest_neighbor
0	1	115.0	10600.0	92.173913	2.409091	1.129654	1431.782106
1	1	13.0	2600.0	200.000000	1.625000	1.100096	223.606798
2	1	2.0	600.0	300.000000	1.000000	1.011893	223.606798
⋮	⋮	⋮	⋮	⋮	⋮	⋮	⋮
203	2	11.0	1800.0	163.636364	1.285714	1.052571	223.606798
204	2	2.0	800.0	400.000000	1.333333	1.069990	223.606798
205	2	14.0	2400.0	171.428571	1.500000	1.079705	282.842712

Similarly, metrics can be computed at the class level by using the `compute_class_metrics_df` method as in:

```
> ls.compute_class_metrics_df()
```

which will return a pandas data frame as depicted in Table 2.2, where each row corresponds to a LULC class and each column represents a metric computed at the row's class level.

Table 2.2 – Example data frame of class-level metrics.

class_val	total_area	proportion_of_landscape	number_of_patches	patch_density	largest_patch_index	total_edge	...
1	24729	7.701939	193	0.060111	2.069921	1431600	...
2	296346	92.298061	13	0.004049	89.451374	1431600	...

Lastly, the landscape-level metrics can be computed by using the `compute_landscape_metrics_df` method as in:

```
> ls.compute_landscape_metrics_df()
```

which will return a pandas data frame as depicted in Table 2.3, where the only row features the values of the metrics computed at the landscape level.

Table 2.3 – Example data frame of landscape-level metrics.

	total_area	number_of_patches	patch_density	largest_patch_index	total_edge	edge_density	landscape_shape_index	...
0	321075	206	0.064159	89.451374	1431600	4.458771	9.716931	...

2.2.2 Customizing the landscape analysis

While a vast collection of metrics have been proposed over the literature of the last decades, many of them are highly correlated with one another. As a matter of fact, Riitters et al. (1995) found that the characteristics represented by 55 prevalent landscape metrics could be reduced to only 6 independent factors. Therefore, analysis cases tend to consider a limited subset of metrics. To that end, the three methods that compute data frames of metrics showcased above can be customized by means of the `metrics` keyword argument as in:

```
> ls.compute_class_metrics_df(  
    metrics=['proportion_of_landscape', 'edge_density'])
```

which will return a pandas data frame where only the specified metrics will appear as columns.

On the other hand, certain metrics allow for some customization concerning the way in which they are computed. In PyLandStats, each metric is defined in its dedicated method in the `Landscape` class, which includes metric-specific keyword arguments that allow controlling how the metric is computed. For instance, when computing the edge density (ED), the user might decide whether edges between LULC pixels and no-data pixels (e.g., landscape boundaries) are considered, or whether the area should be converted to hectares. By default, PyLandStats computes the metrics according to the definitions specified in FRAGSTATS v4 (McGarigal et al., 2012) (see also the appendix A.1.7), and therefore does not consider edges between LULC pixels and no-data pixels, and converts areas to hectares. Nevertheless, the user might decide to change that by providing the `count_boundary` and `hectares` keyword arguments to the `edge_density` method as in:

```
> ls.edge_density()  
4.4587713151132915  
> ls.edge_density(count_boundary=True)  
6.863816865218407  
> ls.edge_density(count_boundary=True, hectares=False)  
0.0006863816865218407
```

Similarly, the `compute_patch_metrics_df`, `compute_class_metrics_df`, and `compute_landscape_metrics_df` accept the `metrics_kws` keyword argument in the form of a dictionary, which allows set-

ting the keyword arguments that must be passed to each metrics' method when computing the data frames. For instance, in order to compute a class-level data frame with the `proportion_of_landscape` as a fraction instead of a percentage, and include the landscape boundaries in `edge_density`, the `metrics_kws` keyword argument must be provided as in:

```
> ls.compute_class_metrics_df(
    metrics_kws={
        'proportion_of_landscape': {'percent': False},
        'edge_density': {'count_boundary': True}
    })
```

In the above example, the columns of the returned data frame will feature not only the proportion of landscape and edge density, but all the available metrics instead. In order to compute a reduced set of metrics, some of which with non-default arguments, both `metrics` and `metric_kws` keyword arguments must be defined. For instance, in the code snippet below:

```
> ls.compute_class_metrics_df(
    metrics=[
        'proportion_of_landscape', 'edge_density', 'fractal_dimension_am'
    ],
    metrics_kws={
        'proportion_of_landscape': {'percent': False},
        'edge_density': {'count_boundary': True}
    })
```

the returned data frame will be of the form depicted in Table 2.4.

Table 2.4 – Example of a data frame of class-level metrics computed with custom `metrics` and `metrics_kws` keyword arguments.

class_val	proportion_of_landscape	edge_density	fractal_dimension_am
1	0.077019	4.502998	1.129561
2	0.922981	6.819590	1.204003

Note that the `metrics` and `metric_kws` keyword arguments work in the same way for the `compute_patch_metrics_df` and `compute_landscape_metrics_df` methods. Additionally, a list of LULC class values might be provided to the `classes` keyword argument of `compute_class_metrics_df` in order to compute the metrics for the specified subset of classes only. The three keyword arguments are complimentary and might therefore be used in conjunction. For instance, adding a `classes=[1]` to the foregoing code snippet would return a data frame of the form depicted in Table 2.4 but featuring only the first row.

2.3 Spatiotemporal analysis

Landscape metrics are often applied to assess the spatiotemporal patterns of LULC change for a given region by computing landscape metrics over a temporally-ordered sequence of landscape snapshots. To this end, PyLandStats features the `SpatioTemporalAnalysis` class, which is instantiated with a temporally-ordered sequence of landscape snapshots.

```
> input_filepaths = [
    'snapshot00.tif', 'snapshot06.tif', 'snapshot12.tif'
]
> dates = [2000, 2006, 2012] # the dates of each snapshot
> sta = pls.SpatioTemporalAnalysis(input_filepaths, dates=dates)
```

When initializing a `SpatioTemporalAnalysis` instance, a `Landscape` instance will be created for each of the landscape snapshots provided as first argument. The `dates` argument might also be provided as string or `datetime` objects (see appendix A.1.4).

2.3.1 Computing spatiotemporal data frames

Similarly to `Landscape` instances, the data frames of class and landscape-level metrics of a `SpatioTemporalAnalysis` instance can be computed by means of the `compute_class_metrics_df` and `compute_landscape_metrics_df` methods respectively. For instance, following the snippet above, the data frame of class-level metrics can be obtained as in:

```
> sta.compute_class_metrics_df()
```

which will return a data frame indexed by both the class value and date, as depicted in Table 2.5.

Table 2.5 – Example data frame of class-level metrics for a spatiotemporal analysis.

class_val	dates	total_area	proportion_of_landscape	number_of_patches	patch_density	largest_patch_index	total_edge	...
1	2000	24729	7.70194	193	0.0601106	2.06992	1.4316e+06	...
	2006	24599	7.66145	200	0.0622907	2.02227	1.436e+06	...
	2012	24766	7.71346	201	0.0626022	2.02227	1.4459e+06	...
2	2000	296346	92.2981	13	0.0040489	89.4514	1.4316e+06	...
	2006	296476	92.3386	8	0.00249163	89.1318	1.436e+06	...
	2012	296309	92.2865	8	0.00249163	89.0916	1.4459e+06	...

Similarly, the data frame of landscape metrics can be obtained as follows:

```
> sta.compute_landscape_metrics_df()
```

where the resulting data frame will be indexed by the dates as depicted in Table 2.6.

Table 2.6 – Example data frame of landscape-level metrics for a spatiotemporal analysis.

dates	total_area	number_of_patches	patch_density	largest_patch_index	total_edge	edge_density	landscape_shape_index	...
2000	321075	206	0.0641595	89.4514	1.4316e+06	4.45877	9.71693	...
2006	321075	208	0.0647824	89.1318	1.436e+06	4.47248	9.73633	...
2012	321075	209	0.0650938	89.0916	1.4459e+06	4.50331	9.77998	...

Note that PyLandStats does not compute data frames for spatiotemporal analyses at the patch level, given that new patches emerge and others disappear over the years and therefore there is no common index upon which the data frames of patch-level metrics for different snapshots could be assembled.

2.3.2 Customizing the spatiotemporal analysis

As with the Landscape class, the `compute_class_metrics_df` and `compute_landscape_metrics_df` methods of the `SpatioTemporalAnalysis` class also allow customizing how each metric is computed by means of the `metrics` and `metric_kws` arguments. Additionally, the `classes` keyword argument might be provided to `compute_class_metrics_df` in order to compute the metrics for the specified subset of classes only. For instance, the code snippet below:

```
> sta.compute_class_metrics_df(
    metrics=['proportion_of_landscape', 'edge_density',
            'fractal_dimension_am', 'landscape_shape_index',
            'shannon_diversity_index'],
    classes=[1],
    metrics_kws = {
        'proportion_of_landscape': {'percent': False},
        'edge_density': {'count_boundary': True}})
```

will return a data frame of the form depicted in Table 2.7.

Table 2.7 – Example of a data frame of class-level metrics for a spatiotemporal analysis computed with custom `classes`, `metrics` and `metrics_kws` keyword arguments.

class_val	dates	edge_density	fractal_dimension_am	landscape_shape_index	proportion_of_landscape
1	2000	4.503	1.12956	22.9492	0.0770194
	2006	4.51608	1.12336	23.0892	0.0766145
	2012	4.54847	1.12347	23.181	0.0771346

Note that although provided within the `metrics` keyword argument, the Shannon's diversity index does not appear in the data frame of Table 2.7 since it can only be computed at the landscape level. Analogously, the proportion of landscape would not appear in the data frame of landscape-level metrics.

2.3.3 Plotting the evolution of metrics

One of the most important features of the `SpatioTemporalAnalysis` class is plotting the evolution of the metrics. To that end, the class features the `plot_metric` method, which takes the snake case label of the respective metric name as first argument, e.g., for proportion of landscape, the argument becomes `'proportion_of_landscape'` (see the section “List of implemented metrics” of appendix A.1.2 for the list of metrics implemented in `PyLandStats` and their respective snake case labels). In order to plot the evolution of a metric at the class level, the value of the LULC class must be passed to the `class_val` keyword argument as in:

```
# a class value of 1 represents "urban" LULC in this example
> sta.plot_metric('proportion_of_landscape', class_val=1)
```

which will produce a plot for the metric at the class level as depicted in Figure 2.1.

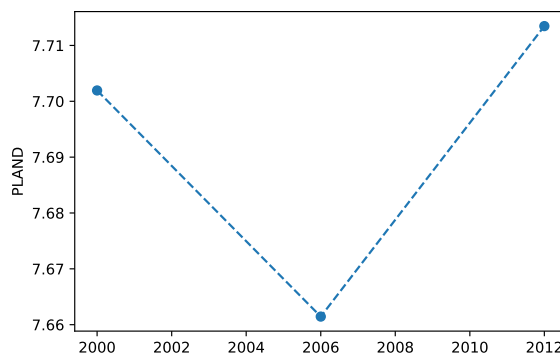


Figure 2.1 – Example of a plot for a class-level metric in a spatiotemporal analysis.

If the `class_val` keyword argument is omitted, the metric will instead be plotted at the landscape level. For instance, the following snippet will plot both the class and landscape-level area-weighted fractal dimension in the same matplotlib axis:

```
> ax = sta.plot_metric('fractal_dimension_am', class_val=1,
                      plot_kws={'label': 'class level (urban)'})
> sta.plot_metric(
    'fractal_dimension_am', ax=ax, plot_kws={'label': 'landscape level'})
> ax.legend()
```

producing a plot as depicted in Figure 2.2.

In order to customize the resulting plot, the `plot_metric` method accepts, among other keyword arguments, a `plt_kws` keyword argument that will be forwarded to the matplotlib's plot method (see the section “Spatiotemporal analysis” of appendix A.1.2).

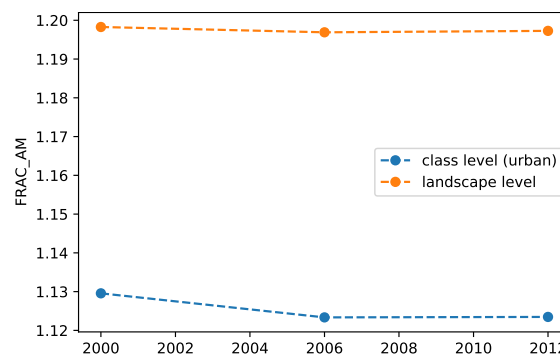


Figure 2.2 – Example with a metric plotted at both the class and landscape level in a spatiotemporal analysis.

2.4 Zonal analysis

Landscape metrics are very sensitive to scale, that is, to the pixel resolution and especially to the spatial extent of the considered map (Meentemeyer and Box, 1987; Turner, 1989; Saura and Martinez-Millan, 2001). To overcome such shortcoming, landscape ecologists often turn to methods of multiscale analysis which explicitly consider multiple scales, both in terms of resolution and map extents (Wu et al., 2000).

The PyLandStats library features two classes that might be used for such purpose. The first is `BufferAnalysis`, which segments a given landscape based on a series of buffers of increasing distances around a feature of interest, whereas the more generic `ZonalAnalysis` allows the user to freely choose how the landscape is segmented by providing a list of NumPy masks.

2.4.1 Buffer analysis around a feature of interest

In line with the classic concentric models of location and land use, evaluating the spatial variation of the environmental characteristics across the urban-rural gradient has become one of the central topics of landscape ecology (McDonnell and Pickett, 1990).

Consider a LULC raster file featuring a city and its rural hinterlands. Then, given a coordinate that represents the center of the feature of interest (e.g., a Shapely point with its coordinate reference system) and a list of buffer distances (in meters), a `BufferAnalysis` can be instantiated as follows:

```
> from shapely.geometry import Point
# latitude and longitude of the center of Lausanne in the OpenStreetMap
> base_mask = Point(6.6327025, 46.5218269)
> base_mask_crs = '+proj=longlat +ellps=WGS84 +datum=WGS84 +no_defs'
# buffer distances (in meters)
> buffer_dists = [10000, 15000, 20000]
```

Chapter 2. Quantifying spatial patterns of landscapes

```
# instantiation of `BufferAnalysis`  
> ba = pls.BufferAnalysis(  
    path_to_raster, base_mask, buffer_dists, base_mask_crs=base_mask_crs)
```

where the `BufferAnalysis` instance will generate the landscape of interest for each buffer distance by masking the pixels of the input raster, as illustrated in Figure 2.3.

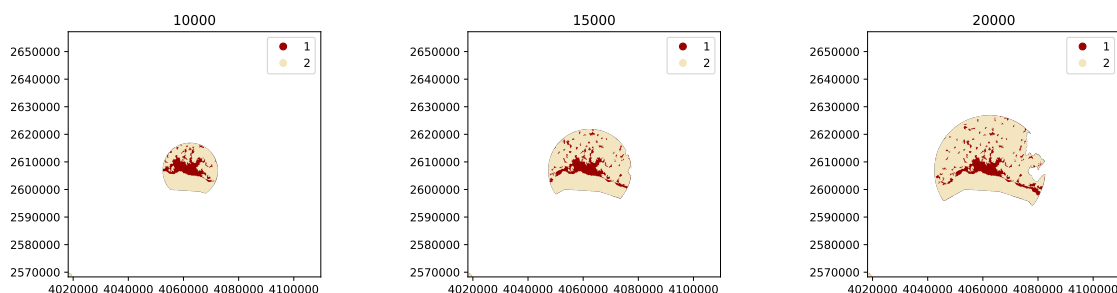


Figure 2.3 – Landscapes generated by instantiating a `BufferAnalysis` with a raster of urban and non-urban LULC classes (values of 1 and 2 respectively), the coordinates of the city center as base mask, and buffer distances of 10000, 15000 and 20000m (corresponding to the three subplots from left to right).

On the other hand, the `base_mask` argument might also be a polygon geometry (e.g., administrative boundaries) instead of a point. In such case, note that the list of buffer distances might start from zero in order to start computing the metrics for the region defined by the polygon geometry itself.

Like in the other classes, the data frames of class and landscape-level metrics can be obtained through the `compute_class_metrics_df` and `compute_landscape_metrics_df` methods respectively. For instance, the following snippet:

```
> ba.compute_class_metrics_df()
```

will return a data frame indexed by both the class value and buffer distance, as depicted in Table 2.8.

Table 2.8 – Example data frame of class-level metrics for a buffer analysis.

class_val	buffer_dist	total_area	proportion_of_landscape	number_of_patches	patch_density	largest_patch_index	total_edge	...
1	10000	7261	24.9648	20	0.068764	21.5472	223900	...
	15000	9630	16.7106	46	0.0798223	11.5326	395200	...
	20000	12149	13.3476	76	0.0834981	7.30169	565200	...
2	10000	21824	75.0352	4	0.0137528	74.3614	223900	...
	15000	47998	83.2894	4	0.00694107	82.9493	395200	...
	20000	78871	86.6524	5	0.0054933	86.3151	565200	...

Again, the metrics that are considered in the analysis and how they metrics are computed can be customized by providing the `metrics` and `metrics_kws` keyword arguments respectively to

the `compute_class_metrics_df` and `compute_landscape_metrics_df` methods, while the considered classes can be set as the `classes` keyword argument of `compute_class_metrics_df`.

On the other hand, and analogously to the `SpatioTemporalAnalysis` class, the metrics computed for each buffer distance in a `BufferAnalysis` instance can be plotted by means of the `plot_metric` method. Again, `plot_metric` takes an optional `class_val` keyword argument that if provided, plots the metric at the class level, and otherwise, plots the metric at the landscape level. For instance, the following snippet:

```
> ba.plot_metric('proportion_of_landscape', class_val=1)
```

will produce a plot for the metric at the class level as depicted in Figure 2.4.

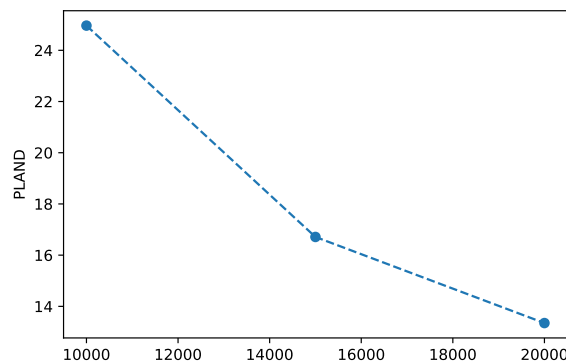


Figure 2.4 – Example of a plot for a class-level metric in a buffer analysis. The x axis corresponds to the buffer distances.

Another approach to examine how landscape patterns change across the urban-rural gradient is to compute the metrics for each buffer ring that defined between each pair of distances. For instance, for the buffer distances considered in latter example, i.e., 10000, 15000 and 20000, the metrics would be computed for the buffer rings that go from 0 to 10000 m, 10000-15000 m and 15000-20000 m. Such analysis can be performed in `PyLandStats` by setting the keyword argument `buffer_rings` to `True`, as in the snippet below:

```
> ba = pls.BufferAnalysis(
    input_filepath, base_mask, buffer_dists, base_mask_crs=base_mask_crs,
    buffer_rings=True)
```

where `BufferAnalysis` will generate the landscapes as depicted in Figure 2.5.

Under such circumstances, the buffer distance of each in the data frame of class and landscape-level metrics will be strings that represent the buffer distances that correspond to the start and end of each ring, as depicted in Table 2.9.

Chapter 2. Quantifying spatial patterns of landscapes

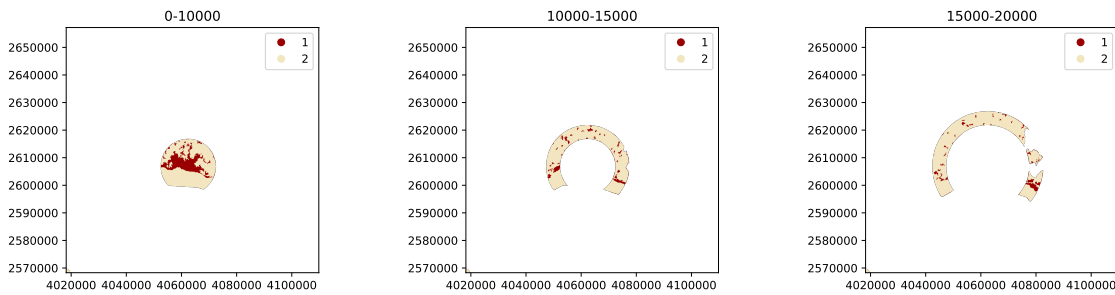


Figure 2.5 – Landscapes generated by instantiating a `BufferAnalysis` with a raster of urban and non-urban LULC classes (values of 1 and 2 respectively), the coordinates of the city center as base mask, and buffer distances of 10000, 15000 and 20000m (corresponding to the three subplots from left to right) and `buffer_rings` set to `True`.

Table 2.9 – Example data frame of class-level metrics for a buffer analysis computing the metrics for the buffer rings.

class_val	buffer_dist	total_area	proportion_of_landscape	number_of_patches	patch_density	largest_patch_index	total_edge	...
1	0-10000	7261	24.9648	20	0.068764	21.5472	223900	...
	10000-15000	2369	8.29976	37	0.129629	1.68518	168600	...
	15000-20000	2519	7.54372	37	0.110805	3.11152	169100	...
2	0-10000	21824	75.0352	4	0.0137528	74.3614	223900	...
	10000-15000	26174	91.7002	3	0.0105105	83.6282	168600	...
	15000-20000	30873	92.4563	8	0.0239578	76.117	169100	...

Accordingly, the `plot_metric` method of a `BufferAnalysis` will produce a figure as depicted in Figure 2.6, where the x axis represents the buffer distances of the rings.

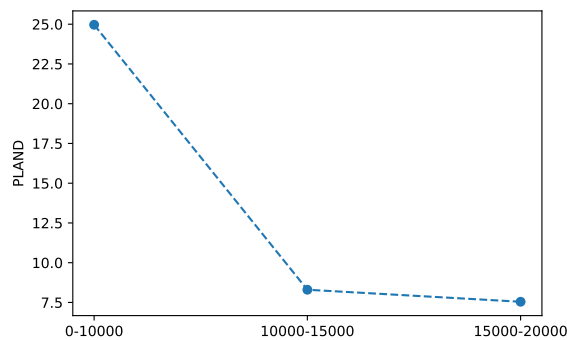


Figure 2.6 – Example of a plot for a class-level metric in a buffer analysis that computes the metrics for the buffer rings. The x axis delineates three discrete points, each corresponding to a buffer ring, and whose label represents the ring's start and end buffer distance.

2.4.2 Generic zonal analysis

In certain analysis cases, the user might consider more appropriate to compute the metrics along a decomposition of the landscape different than concentric buffers, for example, rectangular transects. To that end, `PyLandStats` features the `ZonalAnalysis` class, which instead of a base mask, accepts a list of boolean arrays of the same shape of our landscape

as masks to define our transects (or any other type of subregion). Consider the code snippet below:

```
# this reads the input raster landscape and creates a boolean base mask
# of the same shape of the landscape and filled with `False` values
with rasterio.open(input_filepath) as src:
    base_mask_arr = np.full(src.shape, False)

masks_arr = []
# for a pixel resolution of 100m, this corresponds to transects of 30km
transect_len = 300
# this will iterate over three transects (0-30km, 30-60km, 60-90km)
for transect_start in range(0, 900, transect_len):
    mask_arr = np.copy(base_mask_arr)
    # the 400 and 600 serve to slice the landscape vertically along the
    # 20km where the feature of interest is located
    mask_arr[400:600, transect_start:transect_start+transect_len] = True
    masks_arr.append(mask_arr)
```

where the variable `masks_arr` will be a list of three NumPy boolean arrays, each corresponding to a distinct rectangular transect, as plotted in Figure 2.7.

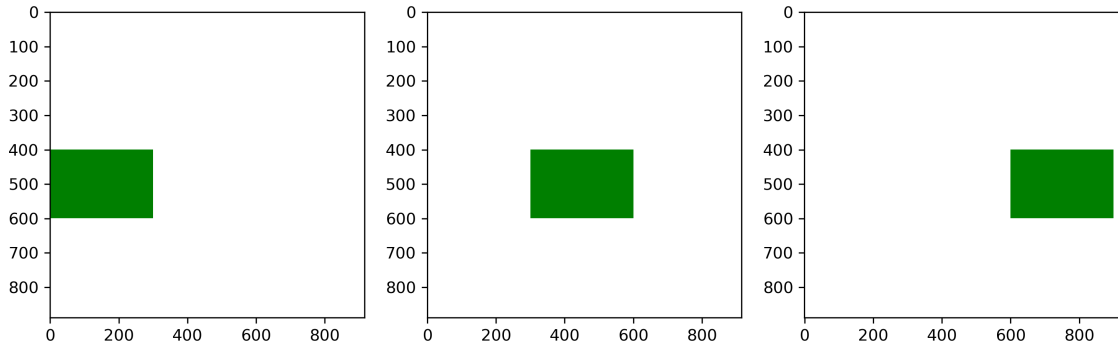


Figure 2.7 – Example of a list of three boolean mask arrays that delineate three rectangular transects of a landscape

The instantiation of `ZonalAnalysis` requires the list of mask arrays (e.g., the `masks_arr` variable created above) as second argument. Additionally, the keyword argument `attribute_values` might be used to map an identifying value or label to each of our landscapes. In this example, a list of strings will be provided in a form which denotes that each landscape corresponds to the transect from kilometers 0 to 30, 30 to 60 and 60 to 90 respectively:

```
> attribute_values = ['0-30', '30-60', '60-90']
> za = pls.ZonalAnalysis(
    input_filepath, masks_arr, attribute_values=attribute_values)
```

Chapter 2. Quantifying spatial patterns of landscapes

where `ZonalAnalysis` will generate the landscapes as depicted in Figure 2.8.

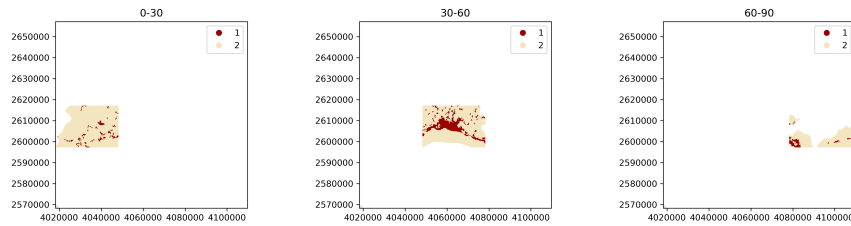


Figure 2.8 – Landscapes generated by instantiating a `ZonalAnalysis` for three rectangular transects.

In `ZonalAnalysis` instances, the data frames of metrics are indexed by the values provided to the keyword argument `attribute_values` as depicted in Table 2.10.

Table 2.10 – Example data frame of class-level metrics in a zonal analysis of three transects.

class_val	attribute_values	total_area	proportion_of_landscape	number_of_patches	patch_density	largest_patch_index	total_edge	...
1	0-30	2641	5.0768	37	0.0711251	0.707407	216700	...
	30-60	9577	17.6965	40	0.0739126	12.2806	370500	...
	60-90	1761	9.27281	9	0.0473909	6.90854	71900	...
2	0-30	49380	94.9232	2	0.0038446	94.9194	216700	...
	30-60	44541	82.3035	6	0.0110869	81.8859	370500	...
	60-90	17230	90.7272	6	0.0315939	53.2199	71900	...

Again, the data frames of metrics `ZonalAnalysis` can also be customized by providing the `metrics` and `metrics_kws` keyword arguments to the `compute_class_metrics_df` and `compute_landscape_metrics_df` methods, and additionally by the `classes` keyword argument in `compute_class_metrics_df`.

In order to plot a metric's computed value for each subregion, the class `ZonalAnalysis` features a `plot_metric` method which works in the same way as its counterpart in `SpatioTemporalAnalysis` and `BufferAnalysis`. For instance, the following snippet:

```
> za.plot_metric('proportion_of_landscape', class_val=1)
```

will produce a plot for the metric at the class level as depicted in Figure 2.9.

2.5 Spatiotemporal buffer analysis

The zonal analysis methods presented above are themselves multiscale analysis approaches since they explicitly consider multiple map extents. Accordingly, the `BufferAnalysis` and `ZonalAnalysis` classes might be employed to obtain scalograms, namely, response curves of the metrics to changing the map extent (Wu et al., 2002).

Nevertheless, when performing spatiotemporal analyses, it might also be useful to evaluate how the computed time series of metrics responds to changes in the map extent. To that

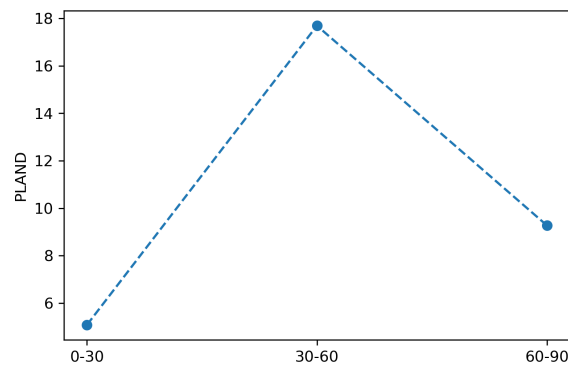


Figure 2.9 – Example of a plot for a class-level metric in a zonal analysis of three transects. The x axis corresponds to the values provided to the keyword argument `attribute_values` provided to the initialization of `ZonalAnalysis`

end, `PyLandStats` features an additional `SpatioTemporalBufferAnalysis` class, which is instantiated like a `BufferAnalysis` except that the first argument is a temporally-ordered list of landscape raster snapshots — like in the `SpatioTemporalAnalysis` class — instead of a single raster landscape. In addition, like the `SpatioTemporalAnalysis` class, a list with the dates that correspond to each of the landscape snapshots can be passed to the keyword argument `dates`. Putting it all together, `SpatioTemporalBufferAnalysis` can be instantiated as in:

```
# Note: `input_filepaths` is a list (like in `SpatioTemporalAnalysis`)
> stba = pls.SpatioTemporalBufferAnalysis(
    input_filepaths, base_mask, buffer_dists,
    base_mask_crs=base_mask_crs, dates=[2000, 2006, 2012])
```

Like `BufferAnalysis`, a `SpatioTemporalBufferAnalysis` can also be instantiated from a polygon geometry. The data frame of class and landscape-level metrics can be computed by means of the `compute_class_metrics_df` and `compute_landscape_metrics_df` methods respectively, which again, might also be customized by providing the `metrics` and `metrics_kws` keyword arguments, and additionally by the `classes` keyword argument in `compute_class_metrics_df`. In `SpatioTemporalBufferAnalysis` instances, the data frames are indexed by the buffer distances and the snapshot dates (and also by the LULC class values in the class-level data frame, as depicted in Table 2.11).

The `SpatioTemporalBufferAnalysis` class features a `plot_metric` method with the same signature of its counterparts in `SpatioTemporalAnalysis`, `BufferAnalysis` and `ZonalAnalysis`. For example, the snippet below:

```
> stba.plot_metric('fractal_dimension_am')
```

Chapter 2. Quantifying spatial patterns of landscapes

Table 2.11 – Example data frame of class-level metrics in a spatiotemporal buffer analysis.

buffer_dist	class_val	dates	total_area	proportion_of_landscape	number_of_patches	patch_density	largest_patch_index	total_edge	...
10000	1	2000	7261	24.9648	20	0.068764	21.5472	223900	...
		2006	7205	24.7722	20	0.068764	21.0211	226600	...
		2012	7205	24.7722	20	0.068764	21.0211	227000	...
	2	2000	21824	75.0352	4	0.0137528	74.3614	223900	...
		2006	21880	75.2278	4	0.0137528	74.5539	226600	...
		2012	21880	75.2278	4	0.0137528	74.5539	227000	...
15000	1	2000	9630	16.7106	46	0.0798223	11.5326	395200	...
		2006	9278	16.0998	49	0.0850281	11.2671	391300	...
		2012	9320	16.1727	50	0.0867634	11.2671	395500	...
	2	2000	47998	83.2894	4	0.00694107	82.9493	395200	...
		2006	48350	83.9002	4	0.00694107	83.5601	391300	...
		2012	48308	83.8273	4	0.00694107	83.4872	395500	...
20000	1	2000	12149	13.3476	76	0.0834981	7.30169	565200	...
		2006	11827	12.9938	78	0.0856955	7.1336	566200	...
		2012	11882	13.0543	79	0.0867941	7.1336	571400	...
	2	2000	78871	86.6524	5	0.0054933	86.3151	565200	...
		2006	79193	87.0062	6	0.00659196	86.6678	566200	...
		2012	79138	86.9457	7	0.00769062	86.604	571400	...

will plot the temporal evolution of the area-weighted fractal dimension at the landscape level for the three buffer distances in the same axis, producing an output as depicted in Figure 2.10.

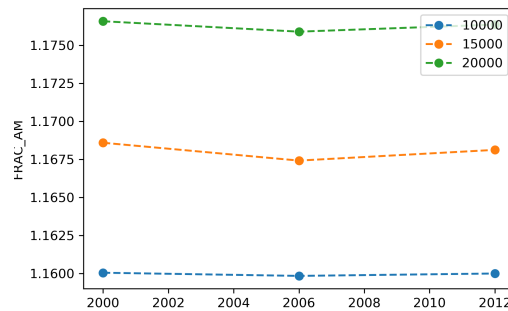


Figure 2.10 – Example of a plot for a landscape-level metric in a spatiotemporal buffer analysis.

Although this is beyond the scope of this article, the above plot suggests that the area-weighted fractal dimension shows a predictable response to changing the spatial extent of the considered landscape (Wu et al., 2002; Wu, 2004).

2.6 Improvements of PyLandStats over existing software packages

There have been many other freely-available software packages to compute landscape metrics (Steiniger and Hay, 2009) (see Table 2.12). By far, the most popular one has been FRAGSTATS (McGarigal and Marks, 1995), yet as a stand-alone software, its functions cannot be directly integrated into advanced computational workflows. Furthermore, FRAGSTATS is not open-source software. Recently, the open-source R package landscapemetrics (Hesselbarth et al., 2019) has been developed to overcome such shortcomings by relying on a well-established spatial framework in R. On the other hand, the only available tool to compute landscape metrics in Python is the LecoS package (Jung, 2016), which is designed as a QGIS plugin.

2.6. Improvements of PyLandStats over existing software packages

Table 2.12 – Comparison of FRAGSTATS, landscapemetrics, LecoS and PyLandStats.

Characteristic	FRAGSTATS	landscapemetrics	LecoS	PyLandStats
open source	no	yes	yes	yes
programming language	?	R	Python	Python
cross-platform compatibility	no	yes	yes	yes
integration into advanced workflows	no	yes	QGIS only	yes
Benchmark Vaud [s]	0.61	14.27	-	0.91
Benchmark Bern and Valais [s]	33.31	553.45	-	32.2

The two benchmarks consist in the computation of the 95 metrics implemented in PyLandStats for the landscape snapshots of the canton of Vaud (889x916 pixels of 2 LULC classes) and the cantons of Bern and Valais (1640x1319 pixels of 28 LULC classes) respectively (see appendix A.1.8 for more details). Both landscapes have been derived from the Corine Land Cover (Heymann et al., 1994) dataset for the year 2000. Note that LecoS has been excluded from the benchmarks since only features 20 landscape metrics.

The computed values for the landscape metrics in PyLandStats are the same as in FRAGSTATS, with a maximum relative difference of 0.1% (see appendix A.1.7). Furthermore, the performance of both packages is very similar. Nevertheless, unlike FRAGSTATS, PyLandStats is open source and it is therefore straightforward for users to contribute to its development on its GitHub repository. On the other hand, PyLandStats is an alternative to landscapemetrics for those users that prefer to write their computational workflows in Python rather than R. Additionally, the cache mechanisms included within PyLandStats lead to significantly better performance and make it more suitable for experimentation in interactive environments such as Jupyter notebooks (Kluyver et al., 2016), since it ensures that the marginal cost of subsequent calls to compute a metric are minimal (see appendix A.1.8).

Finally, although LecoS is based on the NumPy and SciPy stack (like PyLandStats), only 20 metrics have been implemented, and its design as a QGIS plugin forces the users to adapt the computational workflows to QGIS. In sharp contrast, PyLandStats is designed as a Python package which can be directly used in Python scripts, Jupyter notebooks and in other Python packages including QGIS plugins.

In view of the growing popularity of Jupyter notebooks and continuous releases of new Python packages to visualize geospatial data interactively, it is reasonable to expect that geospatial scientists, including landscape ecologists, will increasingly turn to the Jupyter environments for their analyses. From this perspective, PyLandStats intends to offer a Python package that geospatial scientists can use in order to compute landscape metrics, and whose modularity and object-oriented design allows it to evolve and adapt to new developments in the Python and Jupyter ecosystem.

3 Spatiotemporal patterns of urbanization in three Swiss urban agglomerations

Switzerland has undergone important landscape changes during the last decades, especially in the form of urbanization in the Central Plateau region. In the scope of this thesis, quantifying the characteristics of such physical transformations is crucial in order to evaluate its impacts on the UHI effect and identify which urbanization patterns can exacerbate its magnitude. To that end, this chapter presents a study of the spatiotemporal patterns of urbanization that have occurred during the last four decades in the Swiss urban agglomerations of Bern, Lausanne and Zurich, which has been published as a scientific article in:

Bosch, M., Jaligot, R., and Chenal, J. (2020a). Spatiotemporal patterns of urbanization in three swiss urban agglomerations: insights from landscape metrics, growth modes and fractal analysis. *Landscape Ecology*, pages 1–13

The candidate contributed by designing the study, performing the processing and analysis of the data and writing the manuscript.

3.1 Introduction

The last centuries have seen an unprecedented growth of urban areas, which has resulted in dramatic conversion of natural land and profound changes in landscape patterns and the ecosystem functions that they support (Alberti, 2005). The combination of current demographic prospects and the observed trends of decreasing urban densities suggest that the global amount of land occupied by cities might increase threefold by 2030 (Angel et al., 2005). Although the land use and land cover changes associated to urbanization have occurred on less than a 3% of the earth's terrestrial surface, the environmental footprint of cities has significant implications at the global scale, for their functioning produces 78% of the earth's greenhouse gases (Grimm et al., 2008). Given that urbanization will continue to be a major form of landscape change in the next decades, quantifying urban landscape patterns in space and time is crucial to understand the driving forces and ecological impacts of urbanization (Wu, 2014).

Chapter 3. Spatiotemporal patterns of urbanization in three Swiss urban agglomerations

Recent decades have witnessed an increasing number of studies of the spatiotemporal patterns of land use change associated to urbanization (Dietzel et al., 2005; Seto and Fragkias, 2005; Schneider and Woodcock, 2008; Jenerette and Potere, 2010; Wu et al., 2011; Li et al., 2013a; Liu et al., 2016; Nong et al., 2018). Building upon previous ideas of urban growth phases and wave-like urban development, initial attempts to synthesis suggested that urbanization can be characterized as a two-step alternating process of diffusion and coalescence (Dietzel et al., 2005; Schneider and Woodcock, 2008). Nonetheless, subsequent studies challenged the empirical validity of such hypothesis. The thorough study of Jenerette and Potere (2010) examined the spatiotemporal patterns of land use change of a sample of 120 cities distributed throughout the world from 1990 to 2000, and determined that overall, urbanization leads to fragmented landscapes with more complex and heterogeneous structures. Similarly, in a comparative analysis of the metropolitan regions of Phoenix and Las Vegas, Wu et al. (2011) revealed that throughout the 20th century, the two agglomerations did not display signs of distinct urban growth phases, but instead showed a strikingly similar trend towards a landscape that is more diverse in land use, fragmented in structure and complex in shape. Subsequently, Li et al. (2013a) determined that the two-phase diffusion and coalescence model can be over-simplistic and that urbanization might be better characterized by means of three growth modes, namely infilling, edge expansion and leapfrogging, which operate simultaneously while alternating their relative dominance. Such results were confirmed by the thorough study of 16 world cities over the 1800-2000 period by Liu et al. (2016), who further resolved that urbanization generally leads to an increasingly diverse and complex landscape.

Nevertheless, such models of urbanization missappreciate the way in which contemporary cities are multi-scaled systems, organized in different levels that show its own characteristic spatiotemporal patterns (Batty, 2005, 2008; White et al., 2015). While both the diffusion and coalescence model of Dietzel et al. (2005) and the three growth modes model of Li et al. (2013a) make use of a hierarchical framework and evaluate the spatial patterns at different extents, the choice of such extents is not based on quantitative criteria and neglects the characteristic scales of complex systems such as urban patterns. Despite the apparent complexity and diversity of urban forms, cities comply with well-defined principles of spatial organization, which can be characterized quantitatively by means of fractal geometry. A remarkable regularity is found in the relationship between the total built-up area and the distance from the city center, which has been shown to empirically follow a scaling law with very stable exponents for a wide variety of cities (Frankhauser, 1994; Batty and Longley, 1994). In a thorough examination of a global sample of cities, Frankhauser (1994) noted the existence of a kink in the area-radius relationship, which reveals a change on the spatial structure of cities at a certain distance from their center. The same pattern was found in the urban cellular automata simulations of White and Engelen (1993), suggesting that the area-radius scaling could be better approximated through two scaling exponents, a first steeper one for small distances to the city center, reflecting an inner zone where urbanization was essentially complete, and a second lower slope for the outer zone that is still undergoing urbanization.

The objective of this study is therefore to build upon fractal analysis in order to enlighten

the current hypotheses of the spatiotemporal patterns of urbanization. More precisely, the area-radius relationship will be used to detect characteristic extents in urban agglomerations, such as the inner and outer zones reviewed above. Thereupon, the time series of landscape metrics and growth modes will be computed at such extents in order to evaluate the degree to which the spatiotemporal patterns of urbanization operate differently at each scale. The results will serve to assess the validity of the diffusion and coalescence and three growth modes hypothesis and provide critical insights into how they could be revised from a multi-scale perspective.

3.2 Materials and Methods

3.2.1 Study area

Switzerland is a highly developed country in central Europe, with a population distributed into several interconnected mid-sized cities and a large number of small municipalities. Mainly because of the country's topography, most urban settlements are located in its Central Plateau region, which accounts for about one third of the total Swiss territory, (42,000 km²) and is highly urbanized (450 inhabitants per km²). The Central Plateau is characterized by elevations that range from 400 to 700m, a continental temperate climate with mean annual temperatures of 9-10 °C and mean annual precipitation of 800-1400 mm, and a dominating vegetation of mixed broadleaf forest.

In line with the country's federalist government structure, the Swiss spatial planning system is distributed between the federal state, the 26 cantons and 2495 municipalities. The federal state specifies the framework legislation and coordinates the spatial planning activities of the cantons, while cantons check the compliance of municipal development plans with cantonal and federal laws. With some exceptions, municipal administrations are in charge of their local development plans, namely the land use plan and building ordinance, and might therefore be viewed as the most important spatial planning entities. While the Federal Statute on regional planning of 1979 limited the number of new buildings constructed outside the building zones, built-up areas have since increased continuously, mainly because the municipalities can designate new building zones almost entirely autonomously (Jaeger and Schwick, 2014). A major revision of the Federal Statute was accepted in 2013, which limits the amount of building zones that municipalities can designate and encourages infill development and densification by means of tax incentives. Forecasts based on the current urbanization trends predict significant increases of urban land use demands over the next decades, mostly at the expense of agricultural land located at the fringe of existing urban agglomerations (Price et al., 2015).

Given that a significant part of the cross-border urban agglomerations of Geneva and Basel (the second and third largest in Switzerland) lie beyond the Swiss boundaries (SFSO, 2014), in order to ensure coherence of the land use/land cover data, this study comprises only three

Chapter 3. Spatiotemporal patterns of urbanization in three Swiss urban agglomerations

of the five largest Swiss urban agglomerations, namely Bern, Lausanne and Zurich (SFSO, 2018). As shown in Figure 3.1, the three agglomerations have undergone important population growth over the last 30 years, especially during the most recent years and at the agglomeration extent. With a total population over 1.3 million and land area of 1305 km² (1038 hab/km²), Zurich is the largest Swiss urban agglomeration. As a leading global city and one of the world's largest financial centers, Zurich has the country's largest airport and railway station, and also hosts the largest Swiss universities and higher education institutions. Bern is the capital of Switzerland and fourth most populous urban agglomeration in Switzerland, with a total population of 410000 inhabitants and occupying a land area of 783 km² (531 hab/km²). As the fifth largest Swiss urban agglomeration and the second most important student and research center after Zurich, the Lausanne agglomeration has a total population of 409000 inhabitants over a land area of 773 km² (537 hab/km²). Given its larger population growth rate, Lausanne is likely to soon surpass Bern and become the fourth largest urban agglomeration in Switzerland. Overall, the three urban agglomerations are characterized by a pervasive public transportation system and a highly developed economy, with a 85% of the employment devoted to the tertiary sector.

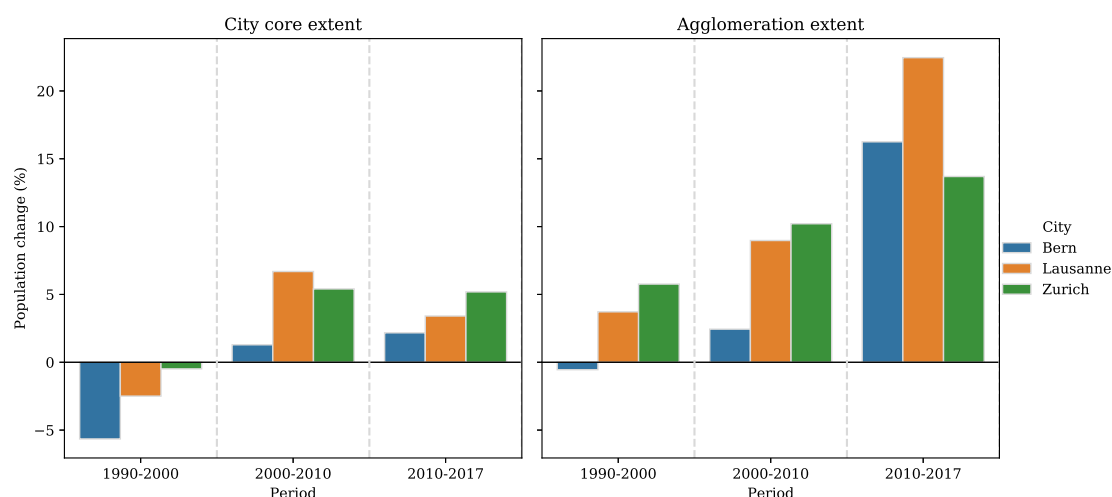


Figure 3.1 – Population change of the three regions of study at the city core (left) and agglomeration extent (right) over the periods of 1990-2000, 2000-2010 and 2010-2017. Data from the Urban Audit collection (SFSO, 2018).

3.2.2 Data sources

The Swiss Federal Statistical Office (SFSO) provides an inventory of land statistics datasets (SFSO, 2017), namely a set of land use/land cover maps for the national extent of Switzerland, which comprise 72 base categories. Four datasets have been released for 1979/85, 1992/97,

2004/09 and 2013/18¹, at a spatial resolution of one hectare per pixel. The pixel classification is based on computer-aided interpretation of satellite imagery, which includes special treatment and field verification of pixels where the category attribution is not clear.

The SFSO land statistics datasets have been used to produce a series of categorical maps for each urban agglomeration and time period. In order to process the SFSO datasets in an automated and reproducible manner, an open source reusable toolbox to manage, transform and export categorical raster maps has been developed in Python (Bosch, 2019b). The boundaries of each urban agglomeration have been adopted from the definitions provided also by the SFSO (2014), which comprise multiple municipalities and have been established in consideration of population density, proximity between centers, economic activities and commuting behavior. As stated above, Geneva and Basel are excluded from this study because a significant portion of their urban agglomeration lies beyond the extent covered by the SFSO land statistics inventory, namely the administrative boundaries of Switzerland. The spatiotemporal evolution of the urban footprint for the three selected urban agglomerations (i.e., Bern, Lausanne and Zurich) over the study period (i.e., 1980-2016¹) is displayed in Figure 3.2.

3.2.3 Area-radius scaling in urban agglomerations

In order to quantitatively detect characteristic spatial extents of urban agglomerations, the relationship between the built-up area and the distance from the main city center will be evaluated from the perspective of fractal geometry. If cities are to be considered fractal objects, such relationship should follow a scaling rule of the form (Mandelbrot, 1983):

$$A(r) \sim r^D \quad (3.1)$$

where A denotes the total area of the urban built-up extent that lays within a distance r from the city center, and D corresponds to the radial dimension, analogous to the fractal dimension of two-dimensional complex objects such as Sierpinski carpets.

With the aim of assessing whether the urban agglomerations follow the bi-fractal city model suggested by White and Engelen (1993), a piecewise linear regression with two segments will be compared to that of a simple linear regression. The optimal breakpoint of the two-segment regression, namely, the breakpoint location that minimizes the sum of squared residual will be computed with the `pwlf` Python library², which is based on the differential evolution optimization algorithm (Storn and Price, 1997). In this context, such breakpoint corresponds to the kink in the area-radius scaling noted by Frankhauser (1994), namely the radial distance to the city center at which cities show a distinct spatial structure that is less space-filling.

¹The exact dates of each surveying period 1979/85, 1992/97, 2004/09 and 2013/18 are determined according to the production process of the national maps and vary across the Swiss territory (SFSO, 2017)

²See https://github.com/cjekel/piecewise_linear_fit_py

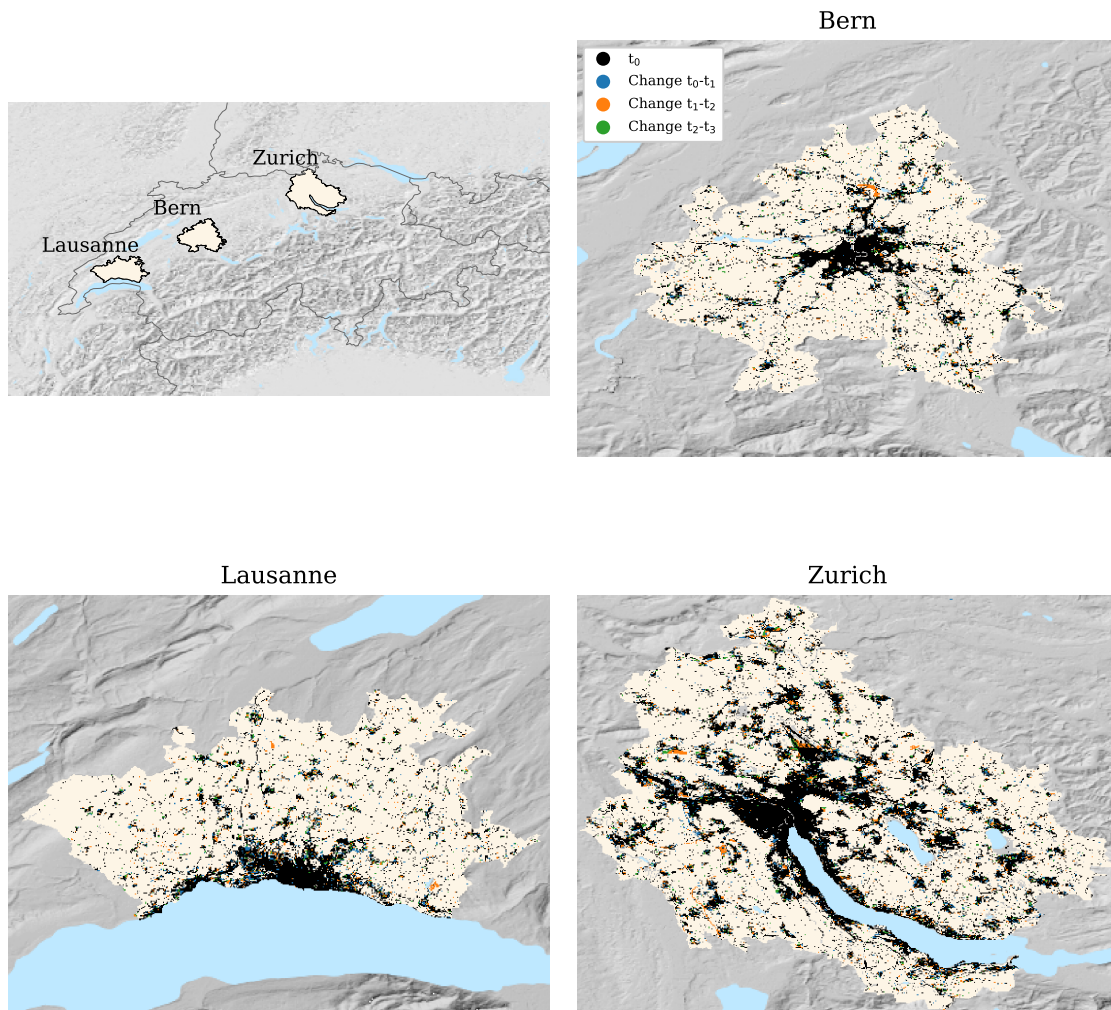


Figure 3.2 – Evolution of urban patches of the three urban agglomerations throughout their respective periods of study. The times t_0 , t_1 , t_2 and t_3 correspond to 1981, 1993, 2004 and 2013 for Bern; 1980, 1990, 2005 and 2014 for Lausanne and 1982, 1994, 2007 and 2016 for Zurich.

Thereupon, three spatial extents will be considered in the analysis of the spatiotemporal patterns of urbanization. The first extent corresponds to the whole urban agglomeration defined by the SFSO (SFSO, 2014), which is described in the foregoing section. The second and third extents will be derived from the location of the kink, i.e., the breakpoint of the two-segment regression of the area-radius relationship. More precisely, in line with White and Engelen (1993), the second extent will be defined as the inner zone, i.e., a circle with the city core as center and the breakpoint distance as radius, while the third extent will be defined as the outer zone, i.e., the area that lies outside the inner zone circle and the agglomeration boundaries.

3.2.4 Quantifying spatiotemporal patterns of urbanization

Time series of landscape metrics

While a plentiful collection of landscape metrics can be found in the literature, many of them are highly correlated with one another. As a matter of fact, Riitters et al. (1995) found that the characteristics discerned by 55 prevalent landscape metrics could be reduced to only 6 independent factors. On the other hand, landscape metrics can be very sensitive to the resolution and the extent of the maps. However, several metrics empirically exhibit consistent responses to changing scales that conform to predictable scaling relations (Wu et al., 2002; Wu, 2004). Based on such remarks, and in order to enhance comparability with other studies, ten landscape metrics have been selected for the present study, whose details are listed in Table 3.1.

Table 3.1 – Selected landscape metrics to quantify the spatiotemporal patterns of urbanization. A more thorough description can be found in the documentation of the software FRAGSTATS v4 (McGarigal et al., 2012)

Metric name	Category	Description
Percentage of landscape (PLAND)	Area and edge	Percentage of landscape, in terms of area, occupied by patches of a given class
Patch density (PD)	Aggregation	The number of patches per area unit
Edge density (ED)	Area and edge	Sum of the lengths of all edge segments per area unit
Area-weighted mean fractal dimension (AWMFD)	Shape	Mean patch fractal dimension weighted by relative patch area
Mean euclidean nearest neighbor distance (ENN)	Aggregation	Mean patch shortest edge-to-edge distance to the nearest neighboring patch of the same or different class

While complying with the FRAGSTATS v4 definitions (McGarigal et al., 2012), the landscape metrics have been computed with the open source library PyLandStats (Bosch, 2019a). Like in most of the related studies, the categorical maps have been reclassified into urban and natural classes, and the metrics have computed at the urban class level, namely aggregating their values across all the urban patches of the landscape. Pixels that correspond to land unavailable for development, such as water bodies, have been excluded from the computation of the metrics.

Modes of urban growth

In addition to the conventional landscape metrics, which are computed over a single snapshot of a landscape, Liu et al. (2010) proposed a quantitative method to classify the types of urban growth occurring between two time points. To that end, for each new urban patch, the

Landscape Expansion Index (LEI) is computed as³:

$$LEI = \frac{L_c}{P} \quad (3.2)$$

where L_c denotes the length of the interface between the new urban patch and pre-existing urban patches, and P is the perimeter of the new urban patch. Then, the type urban growth attributed to a new urban patch will be identified as infilling when $LEI > 0.5$, edge-expansion when $0 < LEI \leq 0.5$ and leapfrog when $LEI = 0$.

3.3 Results

3.3.1 Area-radius relationship

The area-radius relationship of the three urban agglomerations at each temporal snapshot is plotted in Figure 3.3.

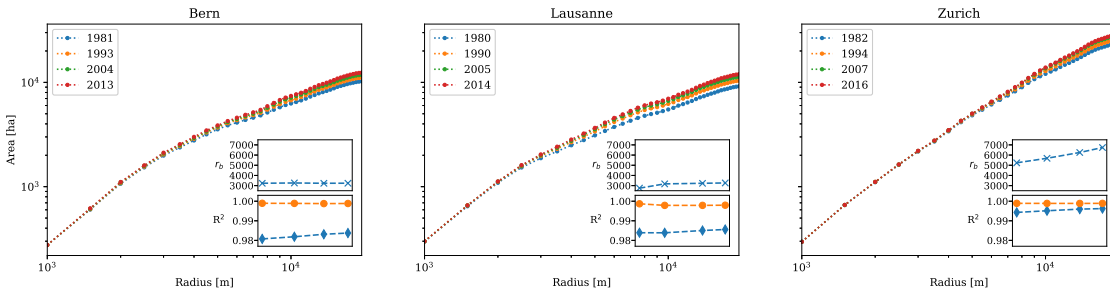


Figure 3.3 – Area-radius relationship of the three urban agglomerations at each temporal snapshot. The plot is produced by computing the total area occupied by urban land uses laying within a series of radius values (noted by the dot-shaped markers) from 1000 to 20000m, successively increasing by a step of 500m. The reference center points correspond to the town hall location of each urban agglomeration, and have been manually retrieved from the OpenStreetMap⁴. The upper inset shows the evolution along the temporal snapshots of the breakpoint r_b (in meters) for the two-segment regression that minimizes the sum of squared residuals, while the lower inset shows the evolution along the temporal snapshots of the coefficient of determination R^2 of the single-segment fit (blue) and of the two-segment piecewise fit (orange). See appendix A.2.1.

On the one hand, the urban agglomerations of Bern and Lausanne show an area-radius relationship that is significantly better approximated by two line segments in a log-log scale (as suggested by the R^2 values of the ordinary linear regression and the piecewise regression

³The LEI definition of (3.2) is taken from Nong et al. (2018) and is equivalent to the initial formula proposed by Liu et al. (2010)

⁴<https://www.openstreetmap.org/>

with two line segments respectively, see appendix A.2.1), hence consistent with the bifractal city model suggested by White and Engelen (1993). In the two urban agglomerations, the breakpoints that separate the inner and outer zones are located around a 3 km distance of the city center and remain very stable through time in the case of Bern, while a slight tendency to increase might be noted in Lausanne, from 2.7 km in 1980 to 3.3 km in 2014. On the other hand, area-radius relationship of Zurich is significantly steeper than its counterparts. Considering the R^2 of the simple and the piecewise regressions, such relationship might also be approximated by a single straight line in the log-log scale (see appendix A.2.1). Nonetheless, the two-segment fit for Zurich yields a breakpoint that is initially located at 5.2 km from the city center in 1982 and increases to 6.7 km in 2016.

Overall, the results suggest that Zurich fills a higher proportion of the available space, especially at large radial distances from the agglomeration center. At the same time, the area-radius relationship becomes steeper through time in the three urban agglomeration — a trend that is more notable in the outer zones. This suggests that as the two agglomerations become more urbanized, their area-radius relationship could tend towards the almost straight line in the log-log scale observed in Zurich (see appendix A.2.1).

3.3.2 Time series of landscape metrics

The computed time series of landscape metrics for Bern, Lausanne and Zurich at the extents of the whole agglomeration, the inner zone and outer zone are displayed in Figure 3.4 (see appendix A.2.2).

The proportion of landscape occupied by urban patches has increased monotonically for the three agglomerations and at the three extents. At the agglomeration extent, Bern and Lausanne show almost indistinguishable trends, starting from a 13% in the early 1980s and surpass the 16% in the last snapshot of 2013 and 2014 respectively, while Zurich shows a parallel tendency with the percentage of urbanized land increasing from 22% in 1982 to a 27% in 2016. The inner zones of Bern and Lausanne are strongly urbanized, with the proportion of urbanized landscape showing a steady increase and surpassing the 70% and 80% respectively, whereas the inner zone of Zurich shows a smaller proportion of urbanized land, gradually increasing from a 54% in 1982 to a 58% in 2016. In the outer zone, Bern and Lausanne show a limited degree of urbanization, increasing from an initial 11% to 14% and 16% respectively, while in the outer zone of Zurich, the proportion of urbanized landscape is initially at almost 20% and surpasses the 25% in the last survey period.

The number of urban patches per area unit, namely the patch density, shows the most irregular pattern. At the agglomeration extent and in the outer zone, none of the urban areas exhibit a discernable trend. In the inner zone, an overall decrease is observed in the three urban areas, nonetheless, such a trend is only monotonic in Zurich. On the other hand, the density of edges between urban and natural patches displays at the three extents similar trends for Bern and Lausanne, which differ significantly from those observed in Zurich. Bern and Lausanne show

Chapter 3. Spatiotemporal patterns of urbanization in three Swiss urban agglomerations

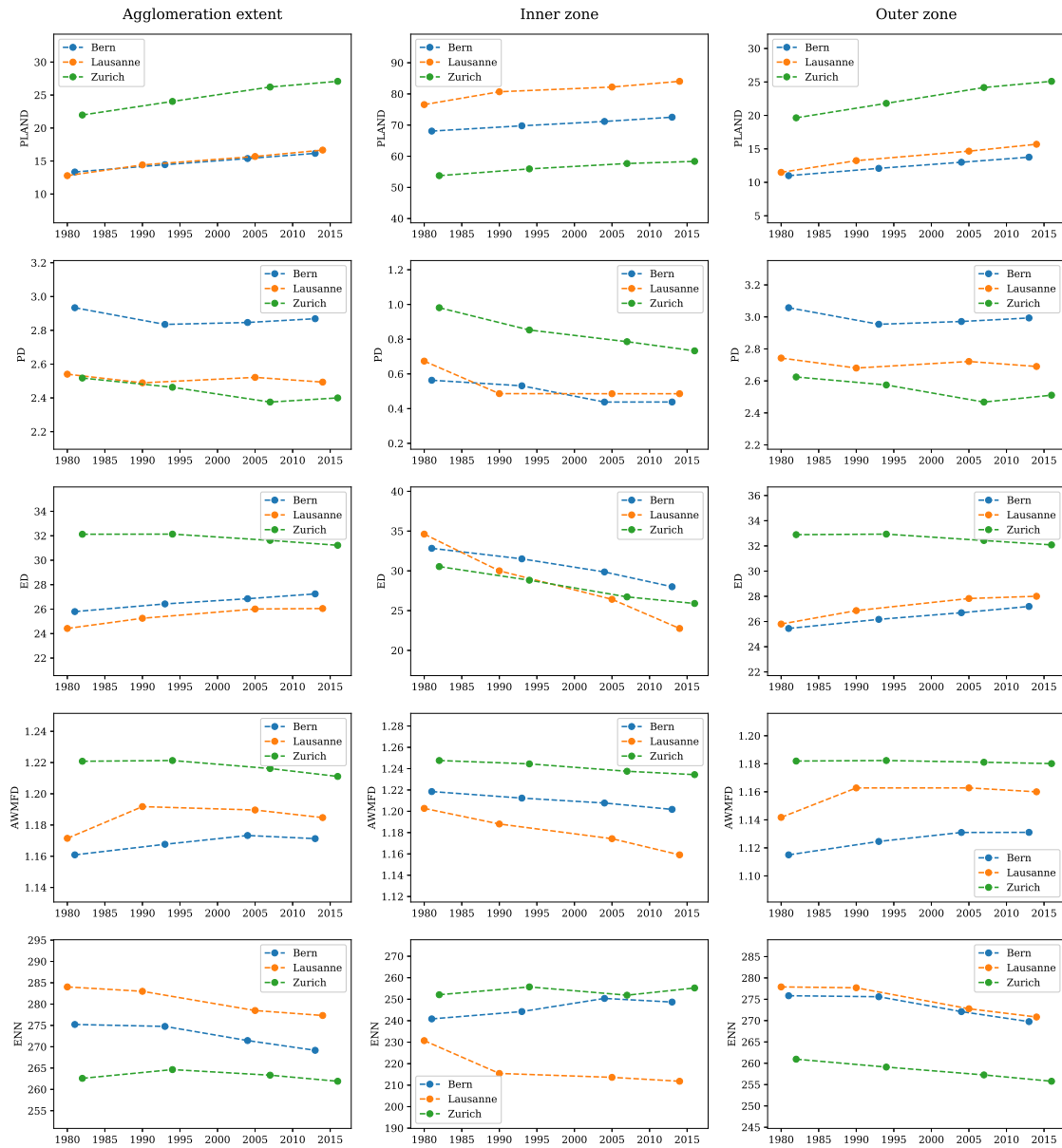


Figure 3.4 – Time series of landscape metrics, computed at the urban class level.

a monotonic increase at the agglomeration extent as well as in the outer zone, which contrasts with the monotonic decrease exhibited by Zurich. In contrast, the three urban agglomerations show a clear decrease in the inner zone, which is more notable in Lausanne.

Regarding the shape complexity of urban patches, represented by the area-weighted mean fractal dimension, the three urban agglomerations show distinctive patterns. In Bern, an overall increase might be noted at the agglomeration extent and in the outer zone, in both cases with a slight decline in the latter period which is reminiscent of an unimodal pattern. In Lausanne, a clearer unimodal pattern is observed also at the agglomeration and outer zone

extents. At the inner zone, the three urban agglomerations display a monotonic decrease, which likewise for the edge density, is most pronounced in Lausanne.

Finally, the distance between urban patches, reflected by the mean euclidean-nearest neighbor metric, shows an overall decrease at the agglomeration extent for Bern and Lausanne, while an unimodal pattern is observed in Zurich. The latter suggests that urban patches in the Zurich agglomeration became more distant between the first and second temporal snapshots and became more connected throughout the third and fourth temporal snapshots. In the inner zone, a monotonic decrease is observed in Lausanne whereas Bern and Zurich do not exhibit any discernable trend. In the outer zone, the three urban agglomerations show a monotonic decrease, suggesting that at that extent, urban patches are becoming more connected on average.

3.3.3 Growth modes

The changes in the relative dominance of the three growth modes, namely infilling, edge expansion and leapfrog, are displayed in Figure 3.5 (see appendix A.2.3).

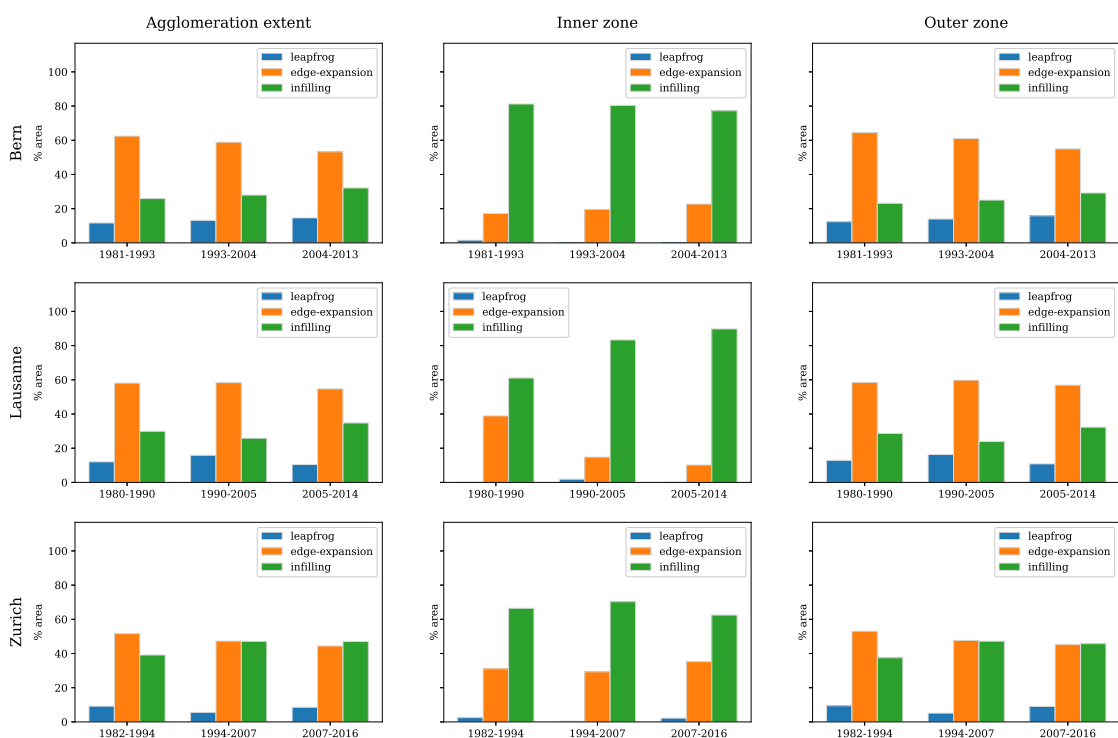


Figure 3.5 – Changes in the relative dominance of infilling, edge expansion and leapfrog over the three time periods in terms of the area of the new urban patches, for the urban agglomerations of Bern (upper row), Lausanne (middle row) and Zurich (bottom row) and at the extents of the whole agglomeration (left), inner zone (center) and outer zone (right). See appendix A.2.3.

Chapter 3. Spatiotemporal patterns of urbanization in three Swiss urban agglomerations

The relative dominance of the three growth modes shows almost indistinguishable trends at the agglomeration extent and in the outer zone, while a completely different pattern is observed in the inner zone. As with the time series of several landscape metrics, similar patterns might be noted in Bern and Lausanne. At the agglomeration extent and in the outer zone, edge-expansion is the most dominant mode of growth in the two urban areas, although its influence decreases throughout the period of study from a 62% to a 53% in Bern and from a 58% to a 55% in Lausanne (at the agglomeration extent). Such decrease is mostly at the expense of an increase on the relative dominance of infilling, which grows from 26% to 32% in Bern and from 30% to 35% (at the agglomeration extent). A similar trend is observed at the agglomeration extent and outer zone of Zurich, yet in this case the dominance of infilling surpasses that of edge expansion in the last period (47% of infilling versus a 44% of edge expansion at the agglomeration extent). Lastly, at the agglomeration extent and in the outer zone, leapfrog is by far the least dominant growth mode albeit there is no observable diminishment of its influence.

The inner zones of Bern and Lausanne are clearly dominated by infilling, with the evolution of its influence exhibiting a slight decline in Bern from 81% to 77% that contrasts with the noticeable increment from 61% to 90% observed in Lausanne. In the inner zone of Zurich, infilling is also the most dominant growth mode with a dominance that remains between 60% and 70% without a discernable trend. Additionally, the influence of edge expansion in the inner zone of Zurich, i.e., 35% in the last period, is significantly above its counterparts in Bern and Lausanne, i.e., 23% and 10% respectively in the last period. Lastly, in the three urban agglomerations, the influence leapfrog is practically irrelevant in the inner zone.

3.4 Discussion

3.4.1 Testing hypothesis of urbanization patterns

The results of this study can be used to explore whether there exist generalities and regularities in the spatiotemporal patterns of urbanization. In this respect, a central question is to what extent the observed transformation of the landscapes conform to the prominent models of urbanization defined by the diffusion and coalescence hypothesis and the three growth mode hypothesis.

The idea of urban growth as a two-phase alternating process of diffusion and coalescence was formulated by Dietzel et al. (2005) as a testable temporal pattern of landscape metrics: during the diffusion stage, the patch density, edge density, area-weighted mean fractal dimension and mean euclidean nearest-neighbor distance of urban patches should increase at first, reach an apex at different times and then decrease as patches start to coalesce, showing an overall unimodal pattern. The time series of landscape metrics of this study show mixed support for the diffusion and coalescence hypothesis. At the agglomeration extent, the trends of the edge density and the area-weighted mean fractal dimension, which reflect the structural complexity

of the landscape, suggest that Zurich is already at the coalescence stage, whereas Bern and Lausanne are seemingly undergoing a transition between diffusion and coalescence. Nevertheless, the irregular pattern exhibited by the density of urban patches is in strong dissonance with the unimodal pattern supposed by the diffusion and coalescence model. Examining the time series of landscape metrics in the inner and outer zones provides additional insights that enlighten the peculiarities of the undergoing urbanization patterns. In Bern, the decreases of the patch density, edge density and area-weighted mean fractal dimension in the inner zone suggest that such extent is undergoing a coalescence process which contrasts with the pattern observed in the outer zone, where the increases of the edge density and area-weighted mean fractal dimension are characteristic of the diffusion stage. A similar pattern might be noted in Lausanne, however, the area-weighted mean fractal dimension at the outer extent does not show an increase but rather an unimodal pattern, which reflects that the shape complexity of urban patches in the outer zone has reached an apex after the first period and then progressively started to decline. This suggests that the inner zone of Lausanne is undergoing a coalescence process while the outer zone is seemingly at the transition between diffusion and coalescence. Finally, with the modest exception of the increase in the last period of the patch density in the agglomeration and outer extents of Zurich, the three metrics show monotonic decreases at the three considered extents, which indicates that both the inner and outer zone of Zurich show the characteristics of the coalescence stages.

The irregular trend of the patch density observed in the three urban agglomerations is evidence that new urban patches might emerge at any period. Such a remark is reminiscent of the critique to the diffusion and coalescence model by Li et al. (2013a), who suggested that such dichotomy can be misleadingly over-simplistic because, in reality, the three growth modes of infilling, edge-expansion and leapfrog operate simultaneously, and thus “it is more plausible to view urbanization as a spiraling process that involves three growth modes of leapfrogging, edge-expanding and infilling [where] leapfrog and infilling tend to alternate in their relative dominance while edge-expansion is likely to remain its importance throughout much of the urbanization process” (pages 1885-1886). The results of this study are primarily consistent with such model, nevertheless, a thorough examination allows for further clarifications. On the one hand, at the agglomeration extent, the importance of leapfrog growth does not necessarily decrease over time, instead it seems that infilling is becoming increasingly influent at the expense of edge-expansion. On the other hand, the influence of the three growth modes changes dramatically when inspecting the results in the inner zone, which is mostly dominated by infilling, and the presence of leapfrog growth is either completely inexistent or practically insignificant. This challenges the overall validity of the three growth modes hypothesis, especially since the alleged simultaneous action of the three growth modes does not hold for the inner zone extent. Overall, the results of this study suggest that both the diffusion and coalescence as well as the three growth modes models of urbanization should be extended by clarifying the patterns that are to be expected at each extent — and that such extent should be systematically defined according to quantitative criteria, as for example, the breakpoint location in the area-radius relationship.

3.4.2 Identifying characteristic extents in urban agglomerations

In the present study, a fractal analysis of the area-radius relationship has been exploited to define the extents at which the landscape metrics and growth modes have been computed. More precisely, the employed approach is based on the bifractal city model suggested by White and Engelen (1993), which is characterized by the existence of a kink in the area-radius relationship that separates an urban agglomeration into a inner zone where urbanization is essentially complete, and an outer zone that is still undergoing active development of natural land into urban uses. Although the existence of such a kink is also noted in the extensive fractal analysis of a number of cities around the world by Frankhauser (1994), the bifractal city model lacks an established method to validate it quantitatively. In consonance with the area-radius plots, comparing the coefficients of adjustments of the simple and piecewise regressions suggests that Bern and Lausanne can be significantly better approximated by two curves. However, it is trivial to show that increasing the number of segments in such a piecewise regression will always lead to a greater or equal coefficient of adjustment. In this study, the bifractal model has been assumed by exogenously fixing the number of segments to two before the piecewise regression, yet further deliberation is required in order to develop methods to properly identify distinct scaling regimes in urban area-radius curves.

Another issue of concern arises from the assumption of a monocentric organization that underlies the bifractal city model. While such assumption is statistically confirmed in the three urban agglomerations by the way in which the slope of the area-radius relationship decreases with increasing radius, this might be largely attributable to how the extents of the urban agglomerations adopted in this study have been constructed, i.e., based on functional criteria such as employment and commuting behavior (SFSO, 2014). Furthermore, the boundaries between neighboring urban agglomerations in the Swiss Plateau are starting to permeate — for instance, the urban agglomerations of Lausanne and its neighboring Vevey-Montreux practically configure an urban continuum, and the same might be noted for the urban agglomerations of Zurich and Baden-Brugg. Therefore, it might be appropriate to employ other quantitative approaches to detect urban agglomeration boundaries based on land use/land cover characteristics, such as those based on percolation theory (Rozenfeld et al., 2008) or fractal analysis (Tannier and Thomas, 2013), which would likely yield more polycentric patterns.

3.5 Conclusion

The present study combines three different approaches to study the spatiotemporal patterns of land use change associated to urbanization in three of the main Swiss urban agglomerations over four surveys in the period from 1980 to 2016. Fractal analysis of the area-radius relationship of urban land is employed to separate the urban agglomeration into two characteristic extents, the inner and outer zones, in which the landscape metrics and the growth modes are computed. The results show that the three urban agglomerations can show very distinct

spatiotemporal patterns in the inner and outer zones. On the one hand, Bern and Lausanne present most characteristics of the coalescence stage in the inner zone, whereas the outer zone displays many traits of the diffusion stage. On the other hand, leapfrog growth is practically nonexistent in the inner zone, which is mainly dominated by infilling. Therefore, spatiotemporal hypotheses of urban land use change should be revised to consider the way in which contemporary cities are configured by a different characteristic extents where urbanization exhibits distinct spatial signatures.

4 Spatially-explicit simulation of urban heat islands

At the scale of an urban area, the UHI effect is strongly related to the spatial composition and configuration of the urban landscape. In order to understand how the landscape transformations occurred in the Swiss urban agglomerations influence the UHI effect, this chapter presents a reusable and spatially-explicit approach to simulate the UHI effect from LULC features based on three key biophysical mechanisms, i.e., shade, evapotranspiration and albedo. The work of this chapter has been submitted for publication and has been accepted for publication to the *Geoscientific Model Development* journal and is currently in press:

Bosch, M., Locatelli, M., Hamel, P., Remme, R. P., Chenal, J., and Joost, S. (in press). A spatially-explicit approach to simulate urban heat mitigation with InVEST (v3.8.0). *Geoscientific Model Development*

Contributions of the candidate include the design of the study, the conduction of the analysis and wrote the manuscript.

4.1 Introduction

Since the industrial revolution, the earth has seen a global increase of temperature which has been especially prominent in urban areas (Oke, 1973; Arnfield, 2003; Clinton and Gong, 2013). Such a trend concurs with an unprecedented growth of urban areas, making contemporary cities a major source of landscape changes and greenhouse gas emissions (Angel et al., 2005; Grimm et al., 2008; United Nations, 2015). By modifying the energy and water balance processes and influencing the movement of air, urban surfaces alter local climatic characteristics, often resulting in warmer temperatures than its rural surroundings (Oke, 1982). This phenomenon is known as the urban heat island (UHI) effect.

The quantification of UHIs can be broadly divided into two main approaches (Schwarz et al., 2011), namely the canopy-layer UHI, measured by the air temperature, usually at 2 m height (Stewart, 2011), and the surface UHI, measured by land surface temperatures (LST) derived from remote sensing data (Voogt and Oke, 2003). The increasing availability of satellite

raster datasets has fostered a large body of research on the spatial distribution of LST and its relationship with the spatial composition and configuration of urban landscapes (Voogt and Oke, 2003; Zhou et al., 2019), which contrasts with the spatial sparsity of meteorological stations that measure air temperature. Despite exhibiting some correlations, air temperature and LST are essentially different physical quantities. Air temperature is closer to thermal comfort felt by humans, and can therefore be employed to evaluate the influence of UHIs on key matters such as energy demand for air conditioning or human health. Additionally, depending on the satellite overpass time, the differences between air temperature and LST can range from a few degrees (°C) up to tens of degrees (Jin and Dickinson, 2010; Sobrino et al., 2012), which calls for special caution when employing satellite-derived LST data for the study of UHIs.

Although notable studies have explored the relationship between satellite-derived LST raster data and air temperature measurements to provide high-resolution insights of the canopy-layer UHI (Fabrizi et al., 2010; Schwarz et al., 2012; Anniballe et al., 2014; Sheng et al., 2017; Shiflett et al., 2017), they have mostly focused on finding statistical relationships between UHIs and the spatial distribution of terrain features such as vegetation indices, without exploring how the observed patterns relate to the biophysical mechanisms that explain canopy-layer UHI. Such a limitation is important when models are used in simulations, for example to examine the effect of urban planning scenarios on air temperatures. As part of the Integrated Valuation of Ecosystem Services and Tradeoffs (InVEST) software, a suite of spatial models to quantify and value the goods and services from nature that sustain and fulfill human life (Sharp et al., 2020), an urban cooling model has been developed following recent research on the effects of surface materials and vegetation cover on UHI (Phelan et al., 2015; Zardo et al., 2017). The aim of the urban cooling model is to simulate the spatial distribution of UHIs based on three key mechanisms, namely the shade provided by trees, the evapotranspiration of urban vegetation and the albedo of the urban surface. In a preliminary application of the model, Hamel et al. (2020) showed its capability to represent the spatial pattern of nighttime air temperature of the 2003 heatwaves in the Île-de-France region.

The main objective of this study is to extend such preliminary experiments by proposing a reusable computational workflow to apply the InVEST urban cooling model to predict the spatial distribution of air temperature in a given study area. The validity of the simulated results is optimized by calibrating some key parameters to best fit a set of air temperature measurements from monitoring stations. Additionally, the simulated spatial pattern of air temperature is compared with the one obtained with an alternative approach, namely a spatial regression over features extracted from satellite data.

4.2 Materials and methods

4.2.1 Study area

Situated at the western end of the Swiss Plateau and on the shores of the Lake Léman, Lausanne is the fourth largest Swiss urban agglomeration with 420757 inhabitants as of January 2019 (Swiss Federal Statistical Office, 2018). As the second most important student and research center in Switzerland (after Zurich), the urban agglomeration of Lausanne has experienced substantial growth during recent decades, which has mostly occurred in the form of suburbanization (Bosch et al., 2020a).

A notable geographic feature of Lausanne is its elevation difference of about 500 m between the lake shore at 372 m.a.s.l. and the northeastern part of the agglomeration (see Figure 4.1 below). The area is characterized by a continental temperate climate with mean annual temperatures of 10.9 °C and mean annual precipitation of 1100 mm, and a dominating vegetation of mixed broadleaf forest.

Spatial extent of the study

In line with urban economics and regional sciences, many works rely on administrative boundaries to define the spatial extent of the study. However, the way in which boundaries are constructed overlooks the characteristic scales in which landscape changes and environmental processes unfold, and might thus lead to equivocal results (Liu et al., 2014; Oliveira et al., 2014). In consideration of such issues, the spatial extent for this study has been determined quantitatively by following the method employed in the Atlas of Urban Expansion (Angel et al., 2012). The core idea is that a pixel is considered part of the spatial extent depending on the proportion of built-up pixels that surround it. In this study, a pixel is considered part of the spatial extent when more than 15 % of the pixels that lay within a 500 m radius are built-up. Additionally, in order to evaluate how temperatures change across the urban-rural gradient, the spatial extent has been extended by a 1000 m buffer. The above procedure has been applied to the rasterized LULC map by means of the Python library Urban footprinter (Bosch, 2020c). The obtained spatial extent, displayed in Figure 4.1, has a surface of 112.46 km².

4.2.2 Data

Land use/land cover data

The land use/land cover (LULC) maps have been obtained by rasterizing the vector geometries of the official cadastral survey of August 2019 to the 10 m resolution. Such dataset is provided and maintained (i.e., weekly updated) by the cantonal administration of Vaud, and features the whole spatial extent of the canton of Vaud (Association pour le Système d'information du Territoire Vaudois, 2018). The classification distinguishes 25 LULC classes which are relevant

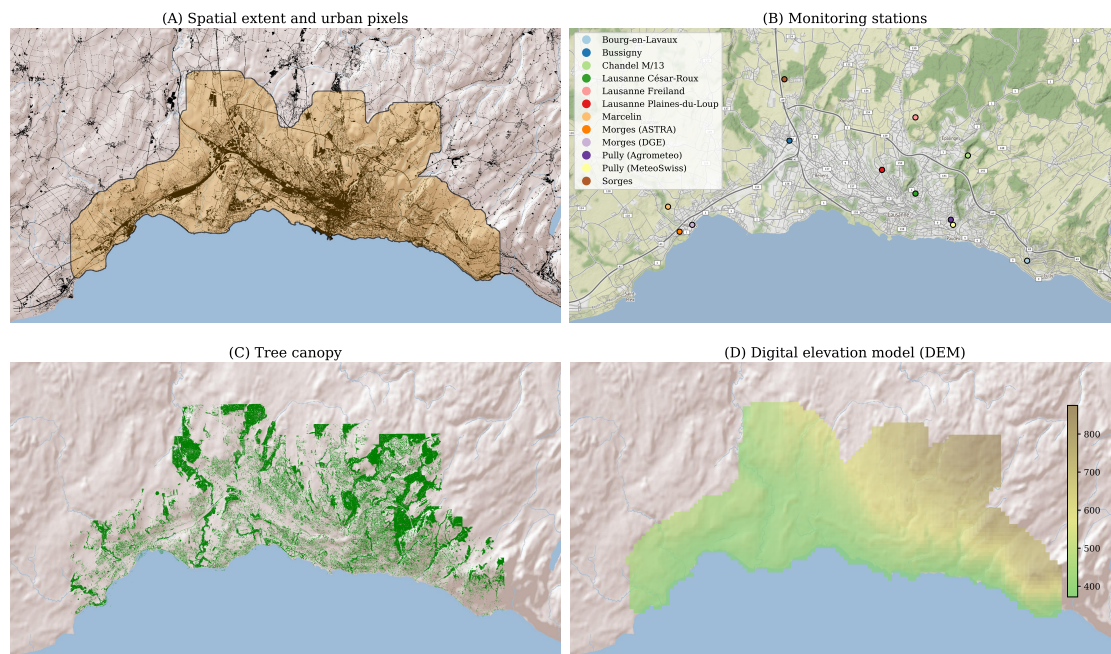


Figure 4.1 – Study area. The upper left plot (A) shows the computed spatial extent (in orange) over the repartition of urban pixels (in black) derived from the rasterized cadastral survey (Association pour le Système d’information du Territoire Vaudois, 2018). The upper right plot (B) shows the locations of the air temperature measurement stations (see Appendix A.3.1). The bottom row shows, for the computed spatial extent of the study, (C) the tree canopy map derived from the SWISSIMAGE orthomosaic (Federal Office of Topography, 2019) and (D) the altitude map derived from the free version of the digital height model of Switzerland (Federal Office of Topography, 2004). The basemap of plots A, C and D is based on the World Shaded Relief (Copyright: ©2009 Esri). The basemap tiles of plot B have been provided by Stamen Design, under CC BY 3.0, with data from OpenStreetMap, under ODbL.

to the urban, rural and wild landscapes encountered in Switzerland (Confédération suisse, 2011). On the other hand, a 1 m binary tree canopy mask has been derived from the SWISSIMAGE orthomosaic (Federal Office of Topography, 2019), by means of the Python library DetecTree (Bosch, 2020a), which implements the methods proposed by Yang et al. (2009). The tree canopy mask of the spatial extent of the study is shown in Figure 4.1.

Elevation data

The elevation map for the study area, which is displayed in Figure 4.1, is extracted from the free version of the digital height model of Switzerland (Federal Office of Topography, 2004), provided at the 200 m resolution by the Federal Office of Topography.

Satellite data

The satellite dataset consists of the 8 Landsat 8 images in 2018 and 2019 which do not feature clouds over the study area and for days in which the maximum observed air temperature is over 25 °C (see the list of selected image tiles in Appendix A.3.1). Data from Landsat 7 has been excluded because of the scan line corrector malfunction.

Air temperature data

A dataset of consistent air temperature measurements in the study area has been assembled by combining data from 11 stations operated by various governmental and research sources, which are shown in Figure 4.1. The temporal resolution of the stations ranges from 10 minutes to 30 minutes. Given that the UHI effect in Switzerland reaches its maximal intensity around 9 p.m. (Burgstall, 2019), the remainder of this study evaluates it based on the air temperature observations of that hour.

4.2.3 Simulation with the InVEST urban cooling model

The simulation of the spatial distribution of UHI employs the InVEST urban cooling model, version 3.8.0 (Sharp et al., 2020), which is based on the heat mitigation provided by shade, evapotranspiration and albedo. The main inputs are a LULC raster map, a reference evapotranspiration raster and a biophysical table containing model information of each LULC class of the map. Each row of the biophysical table represents a LULC class, and features the following columns:

- lcode the LULC class code as represented in the LULC raster map
- Shade a value between 0 and 1 representing the proportion of tree cover in such LULC class

- K_c the evapotranspiration coefficient
- Albedo a value between 0 and 1 representing the proportion of solar radiation directly reflected by the LULC class
- Green_area whether the LULC class should be considered a green area
- Building_intensity a value between 0 and 1 representing the ratio between floor area and land area (for nighttime simulations)

Model description

The data inputs described above are used to compute the cooling capacity index, which is based on the physical mechanisms that contribute to cooling urban temperatures. More precisely, the cooling capacity index used in InVEST urban cooling model builds upon the indices proposed by Zardo et al. (2017), which are based on shading and evapotranspiration, and extends them by adding a factor to account for the albedo. For each pixel i of the LULC raster map, the cooling capacity index is computed as in:

$$CC_i = w_S \cdot S_i + w_{AL} \cdot AL_i + w_{ET} \cdot ETI_i \quad (4.1)$$

where S_i , AL_i and ETI_i respectively represent the tree shading, albedo and evapotranspiration values of pixel i as defined in the biophysical table, and w_S , w_{AL} and w_{ET} represent the weights attributed to each component respectively. The values of S_i and AL_i are retrieved from the biophysical table according to the LULC class k of the pixel i (see Appendix A.3.1). The tree shading is computed by overlaying the binary tree canopy mask with the rasterized LULC map so that for each LULC class k , the shade coefficient S_k corresponds to the average proportion of tree cover over all the LULC pixels of class k , as in:

$$S_k = \frac{1}{|\Omega_k|} \sum_{j \in \Omega_k} x_j \quad (4.2)$$

where Ω_k is the set of pixels of the tree canopy mask whose location corresponds to class k in the LULC raster, and x_j is the value of pixel j of the tree canopy mask, i.e., 1 if j corresponds to a tree and 0 otherwise. The albedo coefficients are based on the local climate zone classification by Stewart and Oke (2012).

The evapotranspiration index ETI is computed as a normalized value of the potential evapotranspiration as in:

$$ETI = \frac{K_c \cdot ET_{ref}}{ET_{max}} \quad (4.3)$$

where K_c is the evapotranspiration coefficient, ET_{ref} is the reference evapotranspiration raster for the period and area of interest and ET_{max} is the maximum evapotranspiration value observed in the area of interest.

In line with the studies of Nistor et al. (Nistor and Porumb, 2015; Nistor et al., 2016; Nistor, 2016), the evapotranspiration coefficients are attributed to each LULC class by distinguishing four cases, namely the crop coefficient for single crops for vegetation LULC classes, the water evaporation coefficient for surface water, the rock and soil evaporation coefficient for bare soils and rocks, and evaporation coefficients for artificial LULC classes (e.g., urban areas). The evapotranspiration coefficients attributed to the LULC classes of the Swiss cadastral survey are listed in subsection A.3.1.

Following the recommendations of Allen et al. (1998), the daily evapotranspiration ET_{ref} (in mm/day) has been estimated for each pixel using the Hargreaves equation (Hargreaves and Samani, 1985) as in:

$$ET_{ref} = 0.0023 \cdot (T_{avg} + 17.8) \cdot (T_{max} - T_{min})^{0.5} \cdot R_a \quad (4.4)$$

where T_{avg} , T_{max} and T_{min} respectively correspond to the average, maximum and minimum T_{air} (in $^{\circ}C$) of each day and R_a is the extraterrestrial radiation (in mm/day), which is in turn estimated for the latitude of Lausanne (i.e., 46.519833°) for each date following the methods of (Allen et al., 1998, Equation 21). The temperature values of each day have been extracted from the inventory of gridded datasets provided by the Federal Office of Meteorology and Climatology (MeteoSwiss), which feature the minimum, average and maximum daily T_{air} for the extent of the whole country at a resolution of 1 km. Such a dataset is obtained by interpolating 100 T_{air} stations across Switzerland (including the MeteoSwiss Pully station of Figure 4.1) based on non-linear thermal profiles of major basins and non-Euclidean distance weighting that accounts for terrain effects (Frei, 2014).

In order to account for the cooling effect of large green spaces, the computed cooling capacity index of pixels that are part of large green areas (> 2 ha) is adjusted as in:

$$CC_i^{green} = \sum_{j \in \Omega_i} g_j \cdot CC_j \cdot e^{-\frac{d(i,j)}{d_{cool}}} \quad (4.5)$$

where g_i is 1 when the pixel i is a green area and 0 otherwise (as defined in the biophysical table), $d(i, j)$ is the distance between pixels i and j , d_{cool} is a parameter that defines the distance over which a green space has a cooling effect, and Ω_i is the set of pixels whose distance to i is lower than d_{cool} .

Then, a heat mitigation index is computed as:

$$HM_i = \begin{cases} CC_i & \text{if } i \text{ is part of a large green area or } CC_i > CC_i^{green} \\ CC_i^{green} & \text{otherwise} \end{cases} \quad (4.6)$$

In order to simulate the spatial distribution of T_{air} , the model requires two additional inputs. The first is the rural reference temperature T_{ref} , where the UHI effect is not observed, e.g., in the rural surroundings of the city. The second is the magnitude of the urban heat island effect

UHI_{max} , namely the difference between the rural reference temperature and the maximum T_{air} observed in the city center. The two parameters are combined with HM_i to compute the T_i for each pixel i of the study area as in:

$$T_i^{nomix} = T_{ref} + (1 - HM_i) \cdot UHI_{max} \quad (4.7)$$

Finally, the T_{air} values of each pixel T_i^{nomix} are spatially averaged using a Gaussian function with a kernel radius r defined by the user.

Calibration and evaluation of the model

To compare the InVEST urban cooling model with the spatial regression based on satellite features, the urban cooling model is used to simulate the spatial distribution of T_{air} for the same 8 dates used to train the spatial regression model, i.e., the dates of the selected Landsat images. It is implicitly assumed that no significative LULC changes have occurred throughout study period (i.e., from May 2018 to August 2019), and therefore all simulations depart from the same LULC raster, i.e., the rasterized cadastral survey of the canton of Vaud as described above. Given the rugged terrain of the study area, the T_{ref} has been set as the minimum average T_{air} observed among the monitoring stations, while UHI_{max} has been set as the difference between the maximum average T_{air} observed among the monitoring stations and T_{ref} . The values of T_{ref} and UHI_{max} for the 8 days considered in this study are displayed in Figure A.1.

Although the documentation of the InVEST urban cooling model (Sharp et al., 2020) provides some suggested values for several parameters of the model, their suitability depends strongly on the local geographic conditions of the study area. Therefore, calibration of the parameters is required in order to better understand how the physical mechanisms beyond the emergence of UHIs take place in the context of Lausanne. Following the manual calibration approach drafted by Hamel et al. (2020), the target parameters are the weights attributed to the tree shading w_S , albedo w_A and evapotranspiration w_{ET} , the distance over which green spaces have a cooling effect d_{cool} and the T_{air} mixing radius r . As an additional contribution, this article implements an automated calibrated procedure based on simulated annealing optimization (Kirkpatrick et al., 1983) that aims at the minimization of the R^2 between the T_{air} values observed in the monitoring stations and those predicted by the model¹. The parameter values suggested in the documentation of the model are set as the initial state of the simulation annealing procedure, which corresponds to a T_{air} mixing radius of $r = 500$ m, a green area cooling distance of $d_{cool} = 100$ m, and weights attributed to tree shading, albedo and evapotranspiration of $w_S = 0.6$, $w_A = 0.2$ and $w_{ET} = 0.2$ respectively. The number of calibration iterations is set to 100.

¹The calibration module has been designed as a reusable open-source Python package, see <https://github.com/martibosch/invest-ucm-calibration>

Given that the T_{ref} and UHI_{max} parameters were here obtained from observations from each simulated day, metrics such as the mean absolute error (MAE) and the root mean squared error (RMSE) are effectively constrained to the $[0, UHI_{max}]$ range, which affects the interpretation of these metrics. Therefore, in order to evaluate the ability of the InVEST urban cooling model to spatially simulate UHIs, the coefficient of adjustment R^2 , MAE and RMSE of the calibrated model are compared with those computed in two additional experiments. The first experiment consists in randomly sampling the T_{air} values from a uniform distribution over the $[T_{ref}, UHI_{max}]$ range of each date. In the second experiment, the T_{air} values of each date are randomly sampled from a normal distribution with the mean and standard deviation of the T_{air} measurements of the monitoring stations. For both experiments, the three evaluation metrics are reported as their average over 10 runs.

4.2.4 Spatial regression of air temperature based on satellite data

The spatial regression to predict T_{air} from features derived from satellite data is performed over a raster dataset on a per-pixel basis. A regression model is then trained to fit the observed T_{air} measurements by minimizing the error at the pixels that correspond to the locations of the monitoring stations.

The regression operates in each pixel with the T_{air} as the target variable, and the elevation, the LST and the normalized difference water index (NDWI) (Gao, 1996) as independent variables. Additionally, to account for the influence of temperature and moisture surface conditions of each pixel, the LST and NDWI are spatially averaged over a series of circular neighborhoods with radii 200, 400, 600 and 800 m, thus reckoning 8 supplementary features. Based on previous research on the sensitivity of the landscape patterns-UHI relationships to the spatial resolution (Weng et al., 2004; Song et al., 2014), the target resolution has been set to 200 m.

Computation of satellite-derived features

The estimation of LST from Landsat 8 images follows the methods of Avdan and Jovanovska (2016). On the one hand, the data from the near-infrared (NIR) and red bands of Landsat 8 (i.e., bands 4 and 5 respectively) to compute the normalized difference vegetation index (NDVI), which is then used to estimate the ground emissivity ϵ_λ . On the other hand, following the Landsat 8 data users handbook (Zanter, 2015), the data from the thermal band of Landsat 8 (i.e., band 10) is first converted to top of atmosphere spectral radiance L_λ , from which brightness temperature BT is estimated (in °C) as in:

$$BT = \frac{K_2}{\ln((K_1/L_\lambda) + 1)} - 273.15 \quad (4.8)$$

where the K_1 and K_2 are band-specific thermal conversion constants embedded in the Landsat

image metadata. Finally, the ground emissivity ϵ_λ and the brightness temperature BT are used to compute the LST by inversion of Planck's Law as in:

$$LST = \frac{BT}{1 + \lambda \cdot (BT/\rho) \cdot \ln(\epsilon_\lambda)} \quad (4.9)$$

where $\rho = 1.438 \cdot 10^{-2}$ m K is a constant computed as a product of Boltzmann constant and Planck's constants divided by the velocity of the light, and $\lambda = 10.895 \cdot 10^{-9}$ is the average of the limiting wavelengths of the thermal band.

The NDWI is computed from the green and near infrared (NIR) bands of Landsat 8 (i.e., bands 3 and 5 respectively) as in:

$$NDWI = \frac{X_{green} - X_{NIR}}{X_{green} + X_{NIR}} \quad (4.10)$$

Model selection and evaluation

Based on the work of Ho et al. (2014), three regression models have been considered, namely a multiple linear regression, support-vector machine (SVM) and random forest. The accuracy of each regression model is assessed by means of a k -fold cross-validation procedure, where the regression samples are first shuffled and partitioned into 3 folds. Then, for each fold k , a regression model is trained using the other 2 folds and validated using the samples of such k fold. Finally, the model that shows the best validation score (i.e., the R^2 averaged over 10 repetitions of the k -fold procedure) is selected. Additionally, the MAE and RMSE are computed in order to evaluate the deviations between the observed T_{air} and the predictions of each model.

On the other hand, the importance of each feature is evaluated by computing its permutation importance (Breiman, 2001), namely the average decrease of the regression accuracy when such feature is randomly shuffled. The training of the regression models, cross-validation and permutation feature importance described above have been implemented by means of the Scikit-learn library (Pedregosa et al., 2011).

4.3 Results

4.3.1 Spatial regression of air temperature based on satellite data

When including all the samples, the R^2 for the linear regression, SVM and random forest are respectively 0.832, 0.014 and 0.960, with MAE of 1.198, 2.671 and 0.580 °C, and RMSE of

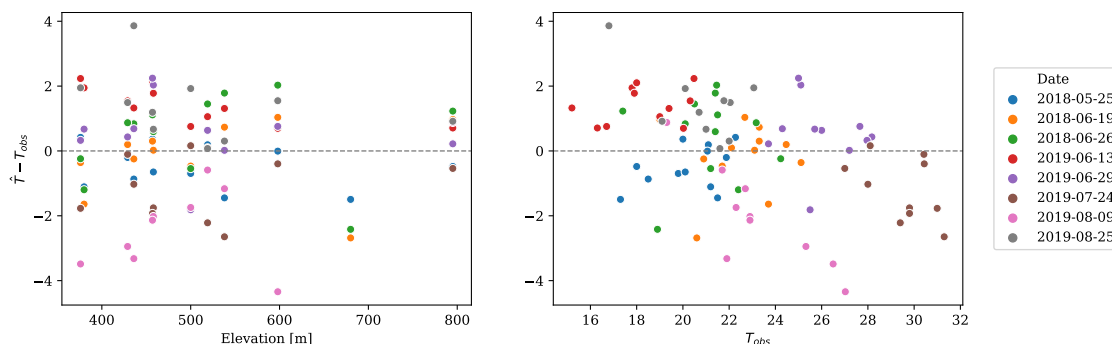


Figure 4.2 – Scatter plot of the spatial regression residuals (vertical axis) against the elevation of the monitoring station (horizontal axis of the left plot) and the observed T_{air} (horizontal axis of the right plot), colored by the sample date. See Appendix A.3.2.

1.508, 3.652 and 0.738 °C respectively. The coefficients suggest that SVM is not well suited for such a regression in this study area, whereas the linear regression and random forest models obtain a very strong fit — the latter achieving the best performance. Nevertheless, the average cross-validation scores suggest that the linear regression (average score $R^2 = 0.733$) is more robust to missing data and also less likely to over-fit the observations than the random forest regressor (average score $R^2 = 0.658$). The remainder of the article thus considers only the results obtained with a linear regression model trained with all the samples.

The feature importances of the chosen linear regression model can be evaluated by means of an F-test (as implemented in the Python library statsmodels (Seabold and Perktold, 2010), see A.1. With a significance level of $p = 0.05$, the results of the F-test suggest that the significant variables for the linear regression are the NDWI when spatially averaged over a 800m, 600m and 400m radius (in decreasing order of significance). The following most significant variable is the NDWI spatially averaged over a 200m radius ($p = 0.071$) and without spatial averaging ($p = 0.231$), and the LST spatially averaged over a 400m radius ($p = 0.277$). With a $p = 0.420$, the does not appear to be significant in this particular regression. The low significance obtained for the LST features in this study might be attributable to the large time lag between the acquisition time of the Landsat images (which ranges from 11:15 to 11:23 CET) and the time of the T_{air} measurements (i.e. 21:00 CET).

The relationship between the predicted and the observed values is displayed in Figure A.2. The MAE and RMSE of 1.198 and 1.508 °C respectively demonstrate a stronger fit than the 1.82 and 2.31 °C obtained in the study of Ho et al. (2014) in Vancouver. The two plots of Figure 4.2 show the relationship between the elevation and T_{obs} of each sample and the regression errors. While there is no discernable relationship regarding the elevation of the samples (i.e., the elevation of the monitoring stations), the regression errors seem to be negatively correlated with T_{obs} . This pattern, which was also noted by Ho et al. (2014), indicates that high temperature samples are systematically underestimated by the regression model whereas low temperature samples are consistently overestimated.

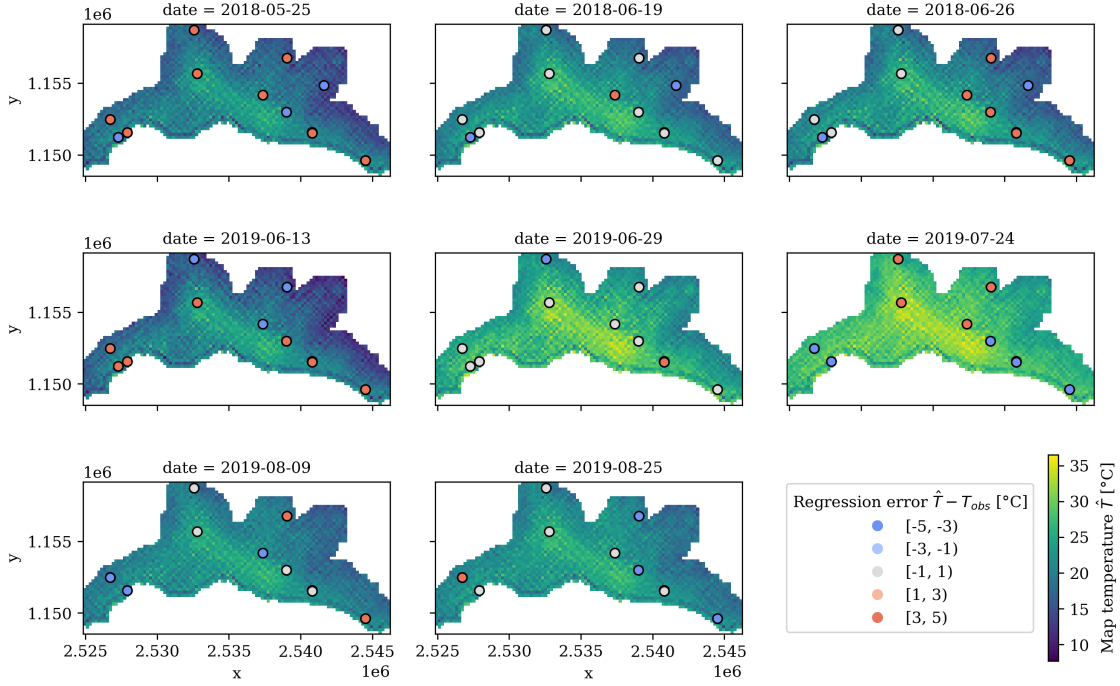


Figure 4.3 – Maps of the T_{air} predicted by the spatial regression for the 8 dates. The points in the map correspond to the location of the monitoring stations, and are colored according to the regression errors.

The series of predicted T_{air} maps for the 8 dates as well as the prediction errors at the locations of the monitoring stations are displayed in Figure 4.3. While the range of temperatures exhibits important differences throughout the dates, the spatial distribution of T_{air} is seemingly consistent. The highest temperatures persistently occur in the most urbanized areas, whereas the lowest temperatures are take place in the higher elevations located east and north-east of the map. Finally, there seems to be no discernable pattern in space nor time regarding the prediction errors at the monitoring stations.

4.3.2 Simulation with the InVEST urban cooling model

The parameters of the model that result in the best fit of the station measurements are a T_{air} mixing radius of $r = 236.02$ m, a green area cooling distance of $d_{cool} = 89.21$ m, and the weights attributed to tree shading, albedo and evapotranspiration of $w_S = 0.59$, $w_A = 0.24$ and $w_{ET} = 0.17$ respectively (see Appendix A.3.2). The R^2 , MAE and RMSE of the calibrated model are respectively 0.903, 0.955 °C and 1.144 °C, which suggest a better model performance than randomly sampling from the station measurements. The latter yields a R^2 , MAE and RMSE of 0.573, 1.947 °C and 2.405 °C when sampling from a uniform distribution and 0.550, 1.952 °C and 2.468 °C when sampling from a normal distribution. Furthermore, the values of R^2 , MAE and RMSE obtained with the calibrated parameters reveal a stronger fit than the spatial regression reported above.

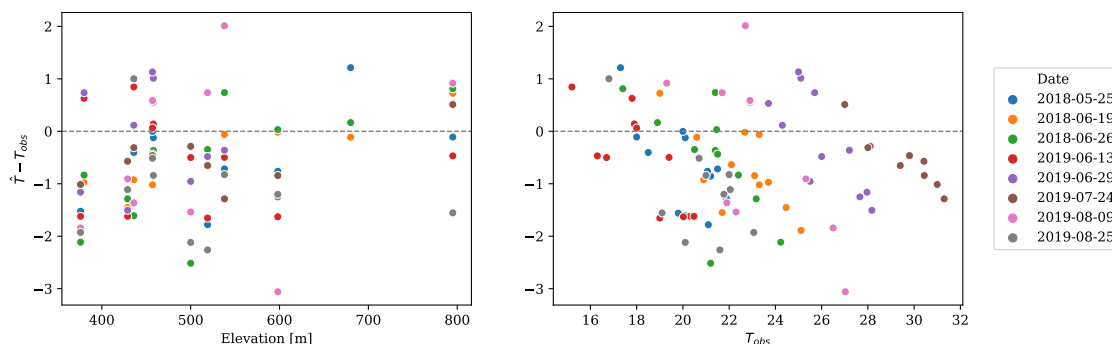


Figure 4.4 – Scatter plot of the differences between the T_{air} simulated by the InVEST urban cooling model and the ones observed in the monitoring stations (vertical axis) against the elevation of the monitoring station (horizontal axis of the left plot) and the observed T_{obs} (horizontal axis of the right plot), colored by the sample date.

The relationship between the T_{air} values at the monitoring stations simulated with the calibrated parameters and the actual observed measurements is shown in Figure A.3. The differences between T_{air} simulated at the monitoring stations and the observed values are plotted against the elevation and the observed temperatures T_{obs} in Figure 4.4. The pattern of such relationships is very similar to that observed in the spatial regression. On the one hand, there is no clear relationship between the prediction error of the urban cooling model and elevation. On the other hand, the prediction errors exhibit a negative correlation with the observed temperature, denoting a systematic tendency to both underestimate high temperatures and overestimate low temperatures — the former being more prominent in this case, as noticeable from the asymmetry of the vertical axis in Figure 4.4.

The simulated T_{air} maps for the 8 dates and the prediction errors at the monitoring stations are shown in Figure 4.5. As in the spatial regression, the temperature ranges show important differences across dates yet the same spatial pattern of T_{air} persists. The simulated distribution of T_{air} shows its highest values in the center of Lausanne and along the most urbanized (and hence less forested) zones along the main transportation axes, whereas the lowest temperatures are found in the forested areas located in the eastern and western extremes of the upper-half of the study area.

4.3.3 Model comparison

A comparison of the maps predicted by the spatial regression and the urban cooling model is displayed in Figure 4.6. In line with the temporal consistency of the spatial patterns predicted by the two approaches respectively, the comparison maps also show a spatial distribution of T_{air} that persists throughout the dates. Such spatial pattern is strongly reminiscent of the elevation maps (see Figure 4.1 above) and reflects the fact that the elevation is explicitly considered in the spatial regression but not in the urban cooling model. The overall distribution of the T_{air} pixel differences between the two approaches follows a normal distribution

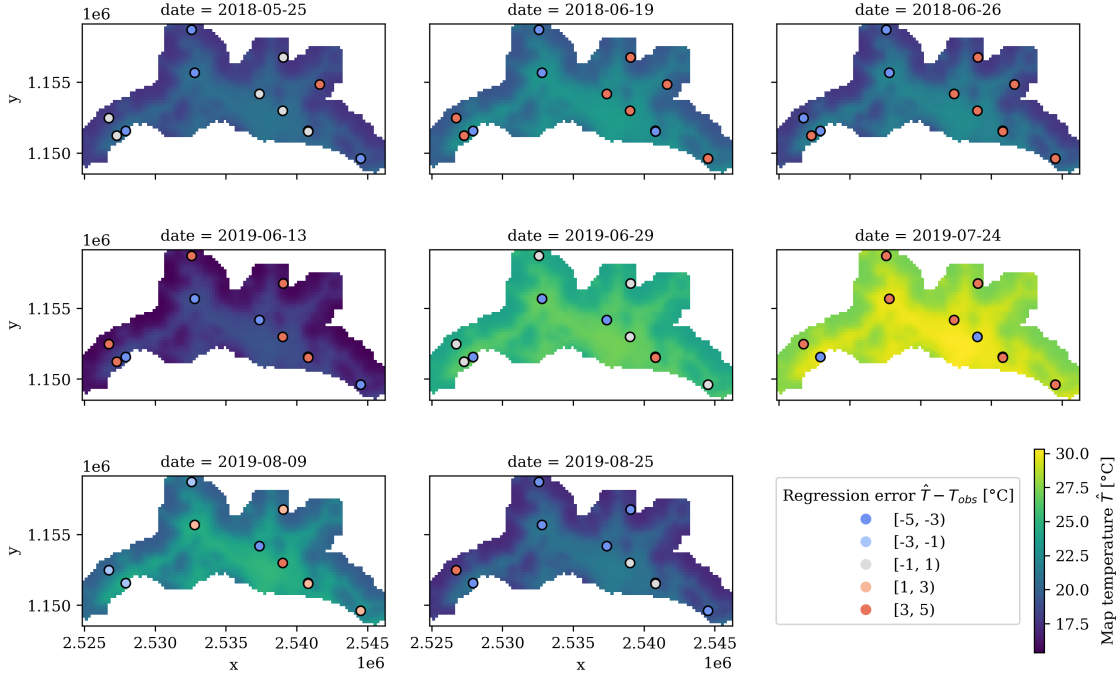


Figure 4.5 – Maps of the T_{air} simulated by the InVEST urban cooling model for the 8 dates. The points in the map correspond to the location of the monitoring stations, and are colored according to the simulation errors.

that ranges from $-9.620\text{ }^{\circ}\text{C}$ to $11.929\text{ }^{\circ}\text{C}$ (respectively reflecting lower and higher temperatures predicted in the spatial regression), which is considerably large range when compared to the small overall MAE and RMSE of both approaches. Nonetheless, the way in which the histogram is centered around $0\text{ }^{\circ}\text{C}$ suggests that the differences between the two approaches follow no particular correlation other than the spatial regression predicting more extreme T_{air} values, which is not surprising considering that the range of T_{air} is systematically bounded in the urban cooling model by the T_{ref} and UHI_{max} parameters.

4.4 Discussion

The results obtained of this study suggest that both the spatial regression based on satellite data and the InVEST urban cooling model are capable of predicting the spatial distribution of air temperature with a large degree of statistical determination. Furthermore, the fact that a similar spatial pattern is predicted by both models suggests that the biophysical mechanisms embedded in the urban cooling model are well represented. If that is the case, the urban cooling model presents two central advantages with respect to the spatial regression.

Firstly, unlike regressions and black-box approaches, the fact that the biophysical mechanisms that drive the emergence of UHIs are represented explicitly allows for a physical interpretation of the parameters of the model. For example, in a comparative study of the relationship between the LST and the spatial configuration of trees in Baltimore and Sacramento, Zhou

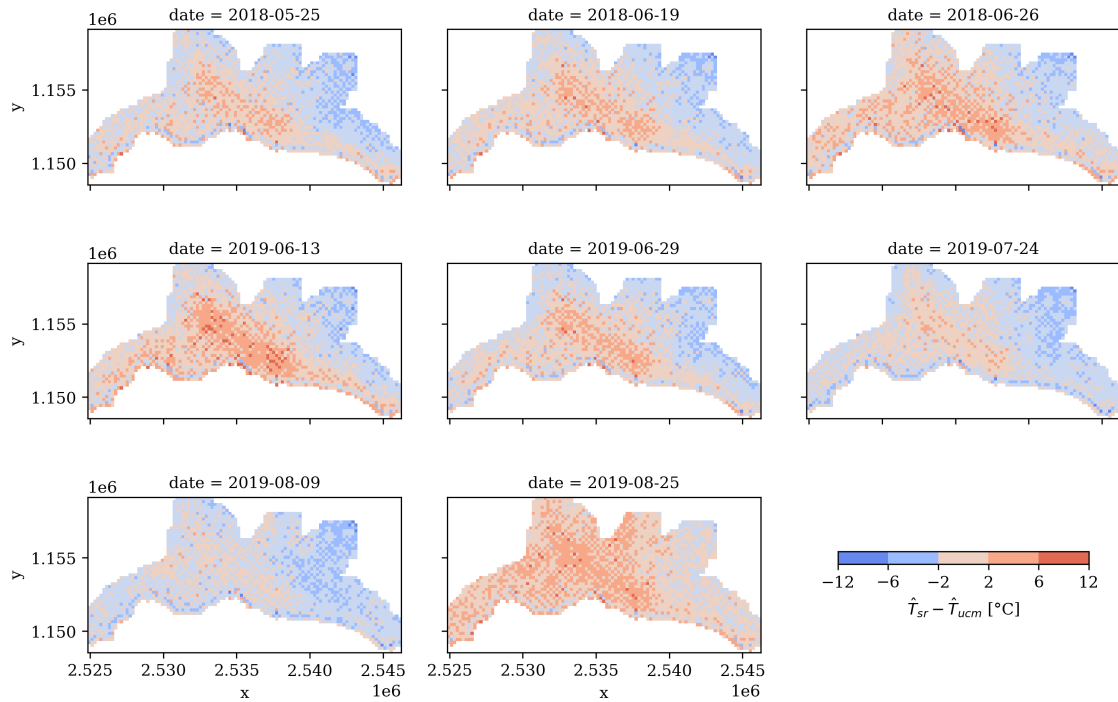


Figure 4.6 – Maps comparing the difference between the T_{air} predicted by the spatial regression \hat{T}_{sr} and the InVEST urban cooling model \hat{T}_{ucm} for the 8 dates. See Figure A.3.2.

et al. (2017) suggest that the distinctive results observed in each city might be related to how the shading of trees and evapotranspiration contribute differently to urban cooling in the climatic context of each city. More precisely, they suggest that in the dry climate of Sacramento, large patches of trees ameliorate the efficiency of the evapotranspiration, whereas with the humid climate of Baltimore, the gains from the tree shading are likely more important. The urban cooling model provides a suitable mean to quantitatively address such matters, i.e., by calibrating the model in the two cities, we can explore the weights obtained for each factor support such hypothesis. In the case study of Lausanne reported above, the weight attributed to the tree shading $w_S = 0.59$ is higher than the one attributed to the evapotranspiration $w_{ET} = 0.17$. This is consistent with the local climatic conditions being more similar in Lausanne and Baltimore than in Sacramento, yet the weights obtained in this study might be partly determined by the initial solution provided. Nonetheless, to further understand this issue, validation and calibration of the InVEST urban cooling model in a broader variety of cities is required. Overall, the way in which the calibrated parameters differ from the recommendations in the documentation of the model are in consonance with the particular characteristics of Lausanne. More precisely, the smaller mixing radius and cooling distances are consistent with the uneven relief of the study area.

The second major advantage of the urban cooling model is that once the model is calibrated for a given city, it can be used to evaluate synthetic scenarios such as those stemming from master plans, urbanization prospects or the like, and to spatially design solutions. This kind of

spatially-explicit evaluation of the impacts of alternative scenarios on ecosystem services is in fact one of the central purposes of the InVEST suite of models (Tallis and Polasky, 2009). Statistical models like the spatial regression are not well suited to such a purpose since they rely on features such as the LST that are hard to obtain other than empirically.

The approach proposed in this article is nevertheless subject to some limitations that merit thoughtful consideration. On the one hand, as acknowledged in its user guide (Sharp et al., 2020), the design of the InVEST urban cooling model presents a number of limitations, the most relevant to this study being the simplified and homogeneous way in which the air is mixed and the cooling effects of large green spaces. In complex terrains such as the Lausanne agglomeration, models with uniform weighting of space show considerable deviations from the observed distribution of air temperature (Frei, 2014). On the other hand, the relationship between the calibration parameters and the resulting R^2 is likely to define a complex optimization landscape with multiple local optima. As a metaheuristic that strongly depends on random decisions, the simulated annealing procedure is susceptible to convergence to local optima, arbitrarily leading to different solutions in each run. A sensitivity analysis of the parameters of the urban cooling model as undertaken preliminarily by Hamel et al. (2020) for the Île-de-France region could serve as a basis to improve the simulated annealing procedure by careful design of appropriate neighborhood search and annealing schedule. Finally, the approach of the present study based on observations at the moment of maximal UHI intensity (i.e., 9 p.m. in Switzerland), however the factors that influence UHIs are likely to operate differently across the diurnal UHI cycle. In fact, several studies point to distinct relationships between the spatial patterns of vegetation and daytime and nighttime UHIs (Anniballe et al., 2014; Sheng et al., 2017; Shiflett et al., 2017; Hamel et al., 2020). Considering the nature of the implications of UHI, e.g., energy consumption, work productivity or human health (Koppe et al., 2004; Santamouris et al., 2015; Zander et al., 2015), a sound understanding of the full diurnal UHI cycle becomes crucial towards the design of robust solutions.

Nevertheless, the limitations on how the urban cooling model represents the spatial air mixing and the cooling effects of green spaces seem hard to overcome with the current spatial sparsity of monitoring stations. Such major shortcoming, which contrasts with the growing availability of high-resolution LST datasets, is one of the main reasons why most of the UHI studies have focused on the latter (Jin and Dickinson, 2010; Zhou et al., 2019). As illustrated in this article, spatial regressions based on remote sensing features such as LST and NDWI do not necessarily replicate the air temperature measurements better than biophysical models such as the InVEST urban cooling model. Therefore, improving the spatial density of the monitoring network becomes an imperative for further enlightening of the UHIs phenomena.

4.5 Conclusion

The present article presents a spatially-explicit approach to simulate UHIs with the InVEST urban cooling model, which is based on three biophysical mechanisms, namely tree shade,

evapotranspiration and albedo. The proposed approach shows how LULC and air temperature data can be combined to calibrate the parameters of the model to best fit measurements from monitoring stations by means of an automated procedure. The simulations performed for the urban agglomeration of Lausanne show that the InVEST urban cooling model can outperform spatial regressions based on satellite-derived features such as LST, NDWI and elevation. The way in which both approaches consistently predict the highest temperatures in the most urbanized parts of the agglomeration suggests that the enhancement of green infrastructure can be an effective heat mitigation strategy, yet further exploration in other climatic contexts is required to fully understand this issue. To that end, the reusability of the computational workflow paves the way for further application of the urban cooling model to a broad variety of cities, which can serve to improve the understanding of the UHI phenomena and support the design of heat mitigation strategies.

5 Urban greening scenarios for urban heat mitigation

The model of the UHI effect presented in the foregoing chapter can be used to simulate the urban heat mitigation provided by altering the abundance and spatial configuration of urban elements such as buildings or green infrastructure. In this chapter, such an approach is applied to the urban agglomeration of Lausanne with the aim of mapping the heat mitigation potential that can be achieved within the current urban fabric. The study of this chapter has been submitted for publication to the Royal Society Open Science journal, where it is currently under review:

Bosch, M., Locatelli, M., Hamel, P., Jaligot, R., Chenal, J., and Joost, S. (2020b). Evaluating urban greening scenarios for urban heat mitigation: a spatially-explicit approach. *Preprint under review in Royal Society Open Science*

The candidate contributed by designing the study, developing of the code and executing the analysis workflow, and finally writing the manuscript.

5.1 Introduction

Urbanization is a global phenomenon that increasingly concentrates the world's population in urban areas, with the latter expected to grow in both the number of dwellers and spatial extent over the next decades (Seto et al., 2011; Angel et al., 2012; United Nations, 2018). As a major force of landscape change, urbanization is characterized by the conversion of natural to artificial surfaces, which alters the energy and water exchanges as well as the movement of air. Such changes often result in the urban heat island (UHI) effect, a phenomenon by which urban temperatures are warmer than its rural surroundings (Oke, 1973, 1982; Arnfield, 2003; Voogt and Oke, 2003; Grimmond, 2007; Phelan et al., 2015). The negative impacts of UHI have been widely documented and include increased energy and water consumption (Akbari et al., 2001; Golden et al., 2006; Santamouris et al., 2015), reduced workplace productivity (Kjellstrom et al., 2009; Zander et al., 2015) and aggravation of health risks (Chestnut et al., 1998; Kovats and Hajat, 2008; Laaidi et al., 2012). As urban areas grow and global temperatures rise, the

UHI effect is expected to become more intense (Meehl and Tebaldi, 2004; Huang et al., 2019), which makes urban heat mitigation a major priority for urban planning and policy-making (Geneletti et al., 2020).

Increasing urban green space, especially the urban tree canopy, has been one of the most widely advocated strategies of urban heat mitigation. Nevertheless, the impacts of the urban tree canopy on air temperature show a complex spatial behaviour that remains poorly understood (Bowler et al., 2010; Phelan et al., 2015; Koc et al., 2018). While many case studies have reported evidence of the cooling effects of urban green areas, the relationship between their size and their cooling capacity is non-linear (Zardo et al., 2017), and little is known about how the overall spatial configuration of urban green spaces affects the heat mitigation at the urban agglomeration scale (Lin and Fuller, 2013; Jim, 2013; Haaland and van Den Bosch, 2015; Artmann et al., 2019). Therefore, the extent to which cities can use green infrastructure to reduce heat stress remains uncertain, largely because of the lack of fine-grained approaches to evaluate the cooling effects of the spatial pattern of the tree canopy at the urban agglomeration scale.

With the aim of addressing the above shortcomings, the present work introduces a novel spatially-explicit method to evaluate the heat mitigation potential of altering the abundance and spatial configuration of the urban tree canopy cover in realistic settings. The proposed method consists of two major parts. First, synthetic scenarios are generated by increasing the tree canopy cover in candidate locations where the existing urban fabric permits it. Then, the spatial distribution of air temperature of each synthetic scenario is estimated with the InVEST urban cooling model, which simulates urban heat mitigation based on three biophysical processes, namely shade, evapotranspiration and albedo. Finally, the simulated temperature map is coupled with a gridded population census in order to evaluate the human exposure to urban heat in the scenario. By applying such a procedure in the urban agglomeration of Lausanne, Switzerland, this study aims to map the heat mitigation potential that can be achieved starting from the existing urban fabric. With the aim of quantifying the effects of the abundance and spatial configuration of the tree canopy cover on urban heat mitigation, a set of synthetic scenarios are generated by increasing different proportions of tree canopy cover in distinct spatial configurations.

5.2 Materials and Methods

5.2.1 Study area

Lausanne is the fourth largest Swiss urban agglomeration with 420757 inhabitants as of January 2019 (Swiss Federal Statistical Office, 2018). The agglomeration is located at the Swiss Plateau and on the shore of the Lake Léman, and is characterized by a continental temperate climate with mean annual temperatures of 10.9 °C and mean annual precipitation of 100 mm, with a dominating vegetation of mixed broadleaf forest. The spatial extent of the study has been

selected following the recent application of the InVEST urban cooling model to Lausanne by Bosch et al. (ress), and covers an area of 112.46 km^2 .

In order to evaluate the human exposure to UHI, the population data for the study area has been extracted from the population and households statistics (STATPOP) (Swiss Federal Statistical Office, 2020) provided at a 100 m resolution by the Swiss Federal Statistical Office (SFSO) with the Python library `swisslandstats-geopy` (Bosch, 2019b).

5.2.2 Simulation with the InVEST urban cooling model

The spatial distribution of air temperatures is simulated with the InVEST urban cooling model (version 3.8.0) (Sharp et al., 2020), which is based on the heat mitigation provided by shade, evapotranspiration and albedo. The main inputs are a land use/land cover (LULC) raster map, a reference evapotranspiration raster and a biophysical table containing model information of each LULC class of the map. The LULC maps have been obtained by rasterizing the vector geometries of the official cadastral survey of the Canton of Vaud (Association pour le Système d'information du Territoire Vaudois, 2018) as of August 2019 to a 10 m resolution. Such a dataset distinguishes 25 LULC classes which are relevant of the urban, rural and wild landscapes encountered in Switzerland. The reference evapotranspiration pixel values are estimated with the Hargreaves equation (Hargreaves and Samani, 1985) based on the daily minimum, average and maximum air temperature values of the 1 km gridded inventory of by the Federal Office of Meteorology and Climatology (MeteoSwiss) (Frei, 2014). The biophysical table used in this study is shown in Table A.2. A more thorough description of the model and the data inputs can be found in Bosch et al. (ress).

The parameters of the model are set based on its calibration to the same study area in previous work (Bosch et al., ress). Finally, the rural reference temperature (T_{ref}) and UHI magnitude (UHI_{max}) values are derived from the air temperature of 11 monitoring stations in the study area (see Figure A.4). More precisely, T_{ref} is set as the 9 p.m. air temperature measurement — the moment of maximal UHI intensity in Switzerland (Burgstall, 2019) — of the station showing the lowest temperature value, and UHI_{max} is set as the difference between the 9 p.m. temperature measurement of the station showing the highest temperature value and T_{ref} . With the above definitions, a reference day for the simulations has been selected from the 2018-2019 period as the day showing the maximum UHI_{max} with $T_{ref} > 20$. Such a date corresponds to July 27th 2018, with $T_{ref} = 20.60^\circ\text{C}$ and $UHI_{max} = 7.38^\circ\text{C}$.

5.2.3 Refining LULC classes based on tree cover and building density

A procedure to redefine the LULC classes from the cadastral survey has been designed to distinguish the LULC classes depending on their proportional cover of both trees and buildings. The reclassification is achieved by combining the 10 m raster LULC map with two 1 m binary raster masks, one for the tree canopy raster and another for the buildings. The 1 m binary

tree canopy mask has been derived from the SWISSIMAGE orthomosaic (Federal Office of Topography, 2019), by means of the Python library DetecTree (Bosch, 2020a), which implements the methods proposed by Yang et al. (2009). The estimated classification accuracy of the tree canopy classification is of 91.75%. On the other hand, the 1 m binary building mask has been obtained by rasterizing the buildings of the vector cadastral survey (Association pour le Système d'information du Territoire Vaudois, 2018).

The reclassification procedure consists of three steps. Firstly, each 10 m pixel is coupled with the tree canopy and building masks in order to respectively compute its proportion of tree and building cover. Secondly, the set of 10 m pixels of each LULC class are grouped into a user-defined set of bins to form two histograms, one based on their proportion of tree cover and the other analogously for the building cover. Lastly, the two histograms are joined so that each LULC class is further refined into a set of classes. For example, if two bins were used for both the tree and building cover, the “sidewalk” LULC code might be further refined into “sidewalk with low tree/low building cover”, “sidewalk with low tree/high building cover”, “sidewalk with high tree/low building cover” and “sidewalk with high tree/high building cover”.

In the present work, four equally spaced bins (i.e., distinguishing 0-25%, 25-50%, 50-75% and 75-100% intervals) have been used to reclassify each LULC class according to both the tree and building cover. Following the advice given by the directorate of resources and natural heritage in the Canton of Vaud (DGE-DIRNA), the threshold over which a pixel is considered to have a high tree canopy cover has been set to 75%, which corresponds to placing trees of a spheric crown with a 5 m radius spaced 10 m from one another so that they form a continuous canopy. Therefore, adjacent pixels with a tree canopy cover over 75% can Finally, in order to adapt the biophysical table of the InVEST urban cooling model to the reclassified LULC classes, the shade coefficients are computed as the midpoint of the bin interval of each level of tree cover (i.e., 0.125, 0.375, 0.625 and 0.875), whereas the albedo coefficients have been linearly interpolated based on the level of building cover (see Table A.2).

5.2.4 Generation of urban greening scenarios

Starting from the refined LULC map, a set of urban greening scenarios are generated by altering the LULC classes of certain candidate pixels in a way that corresponds to reasonable transformations that could occur in urban areas. More precisely, pixels whose base LULC class corresponds to “building”, “road, path”, “sidewalk”, “traffic island”, “other impervious” and “garden” are changed to the LULC code that has the same base class but with the highest tree cover, e.g., pixels of a post-refinement class “sidewalk with low tree/low building cover” are changed to “sidewalk with high tree/low building cover”. In order to ensure that such an increase of the tree canopy cover is performed only where the existing urban fabric permits it, pixels might only be transformed when two conditions are met. First, the proportion of building cover in the candidate pixels must be under 25%, i.e., there is a 75% of the pixel area which could be occupied by a tree crown. Secondly, pixels of the “road, path” class might only

be transformed when they are adjacent to a pixel of a different class, which prevents increasing the tree canopy cover in pixels that are in the middle of a road (e.g., a highway).

After mapping the candidate pixels where the tree canopy cover can be increased, scenarios are generated based on two key attributes: the extent of tree canopy conversion (expressed as a proportion of the total number of candidate pixels), and the selection of pixels to be converted. A set of scenarios is generated by transforming a 12.5, 25, 37.5, 50, 62.5, 75 and 87.5% of the candidate pixels respectively. For each of these canopy areas, three distinct selection approaches are used. The first consists in randomly sampling from the candidate pixels until the desired proportion of changed pixels is matched. In the second and third approaches, the candidate pixels are sampled according to the number of pixels with high tree canopy cover (i.e., greater than 75%) found in their Moore neighborhood (i.e., the 8 adjacent pixels). In the second approach, pixels with higher number of high tree canopy cover neighbors are transformed first, which intends to spatially cluster pixels of high tree canopy cover. The third approach intends to spatially scatter pixels of high tree canopy cover by prioritizing pixels with lower number of high tree canopy neighbors. Given that the three sampling approaches are stochastic, for each scenario configuration, i.e., each pair of proportion of transformed candidate pixels and sampling approach, the corresponding temperature maps will be computed by averaging a number of simulation runs. After observing little variability among the simulation results, the number of runs of a each configuration has been set to 10. Lastly, the set of scenarios is completed with a configuration where a 100% of the candidate pixels are transformed, which is independent of the sampling approach or scenario run since there exists a single deterministic way to transform all the candidate pixels. The final number of scenarios simulated scenarios is 211, i.e., 10 scenario runs for 3 different sampling approaches and 7 proportions of transformed candidate pixels, plus a last scenario where all the pixels are transformed.

For each scenario, the spatial pattern of the tree canopy is quantified by means of a set of spatial metrics from landscape ecology (O'Neill et al., 1988; McGarigal et al., 2012), which are computed for the pixels whose post-refinement LULC class has a tree canopy cover over 75%¹. Based on other studies that explore the relationship between the spatial of tree canopy and UHIs, four spatial metrics have been chosen to quantify both the composition and oconfiguration of the tree canopy, which are listed in Table 5.1. The proportion of landscape (PLAND) of pixels with high tree canopy cover serves to quantify the composition aspects, while the configuration is quantified by means of the mean patch size (MPS), edge density (ED) and the mean shape index (MSI) of patches of high tree canopy cover. The four metrics have been computed with the Python library PyLandStats (Bosch, 2019a).

¹Following the advice given by the directorate of resoures and natural heritage in the Canton of Vaud (DGE-DIRNA), the threshold over which a pixel is considered to have a high tree canopy cover has been set to 75%, which corresponds to placing trees of a spheric crown with a 5 m radius spaced 10 m from one another so that they form a continuous canopy.

Table 5.1 – Selected landscape metrics. A more thorough description can be found in the documentation of the software FRAGSTATS v4 (McGarigal et al., 2012)

Category	Metric name	Description
Composition	Percentage of landscape (PLAND)	Percentage of landscape, in terms of area, occupied by pixels with high tree canopy cover
Configuration	Mean patch area (AREA_MN)	Average size (in hectares) of the patches formed by pixels with high tree canopy cover
	Mean shape index (SHAPE_MN)	Average shape index of the patches formed by pixels with high tree canopy cover
	Edge density (ED)	Sum of the lengths of all edge segments between pixels with high tree canopy cover and other pixels, per area unit (in m/hectare)

5.3 Results

5.3.1 Proportion of transformed pixels by their original LULC class

The relationship between the number of transformed candidate pixels by their original LULC class and the overall proportion of transformed candidate pixels is shown in Figure 5.1. Changing a 25, 50, 75 and 100% of the candidate pixels corresponds to a total number of pixels changed of 118880, 237760, 356640 and 475520, which account for a total area of 1188.8, 2377.6, 3566.4 and 4755.2 hectares respectively. In the latter case, i.e., increasing the tree canopy in all the possible pixels, 61.50% of the pixels correspond to the “garden” LULC class, followed by “road, path”, “building”, “other impervious”, (18.01, 10.81 and 7.69%, respectively). Finally, the LULC classes of “sidewalk” and “traffic island” constitute only 1.67 and 0.3% of the pixels where the tree canopy can be increased. The differences when considering the sampling approaches separately are small relative to the total number of transformed candidate pixels. The largest differences between sampling approaches can be noted in the number of transformed pixels that originally belong to the “garden” class. When transforming 25, 50 and 75% of the candidate pixels, clustering respectively transforms (on average among the simulation runs) a 0.90, 0.38 and 0.12% more garden pixels than random sampling, and 1.28, 0.76 and 0.43% more garden pixels than the scattering approach (Figure 5.2).

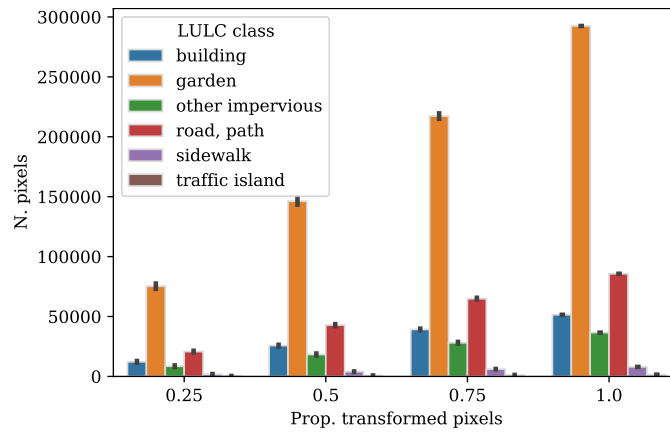


Figure 5.1 – Number of transformed pixels by its original LULC class for an overall proportion of transformed pixels of 25, 50, 75 and 100%. The lines at the top of the bars represent the 95% confidence intervals. The bar heights and the confidence intervals are computed out of all the simulation runs and sampling approaches. See the Jupyter Notebook at section S2.1 for the detailed numbers of the figure.

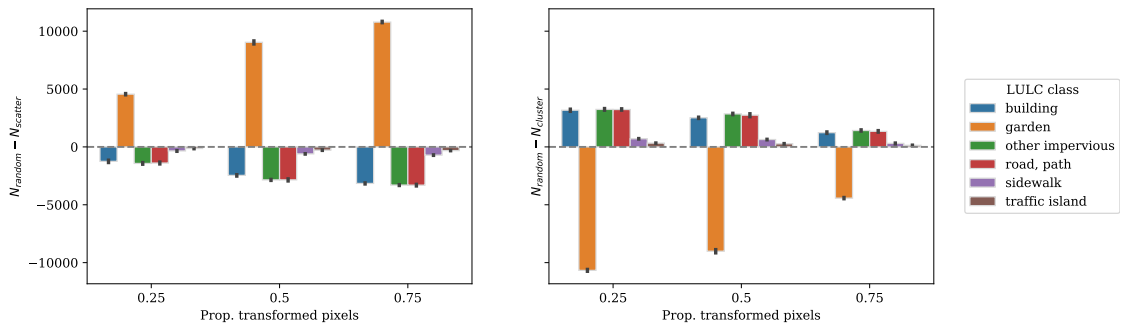


Figure 5.2 – Comparison of between the number of transformed pixels by its original LULC class with the random sampling approach and the clustering ($N_{random} - N_{scatter}$, left subplot) and the clustering ($N_{random} - N_{cluster}$, right subplot) selection approaches, for an overall proportion of transformed pixels of 25, 50 and 75%. The lines at the top of the bars represent the 95% confidence intervals. The bar heights and the confidence intervals are computed out of all the simulation runs. See the Jupyter Notebook at section S2.1 for the detailed numbers of the figure.

5.3.2 Simulated LULC, temperature and heat mitigation maps

The LULC, temperature and heat mitigation maps for the scenarios generated by transforming a 25, 50, 75 and 100% of the candidate pixels are shown in Figure 5.3. When changing 25, 50, 75 and 100% of the candidate pixels, the maximum temperature T for the reference date, i.e., 26.05°C, is progressively reduced to 25.77, 25.30, 24.82 and 24.49°C respectively, while the magnitude of maximum heat mitigation ($T - T_{obs}$) increases from 0.49, 1.17, 1.81 and 2.22°C respectively. The largest heat mitigation magnitudes occur in the most urbanized parts, which

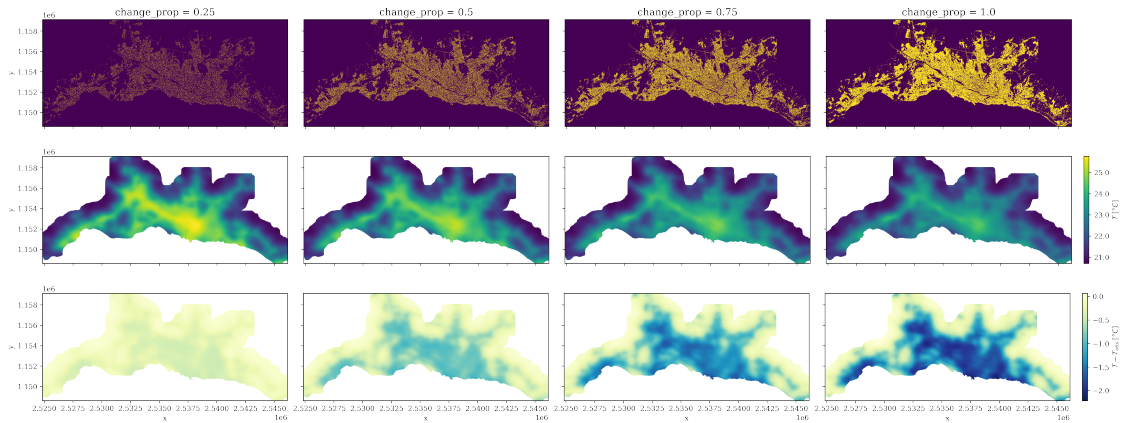


Figure 5.3 – Simulated LULC (top), temperature (middle) and heat mitigation (bottom) maps by transforming a 25, 50, 75 and 100% of the candidate pixels to its corresponding LULC code with high tree canopy cover. The pixel values of each map are aggregated out of all the sampling approaches and simulation runs, i.e., the LULC maps show the mode, whereas the temperature and heat mitigation maps show the average. The axes tick labels display the Swiss CH1903+/LV95 coordinates. See the Jupyter Notebook at section S2.1 for the detailed numbers of the figure.

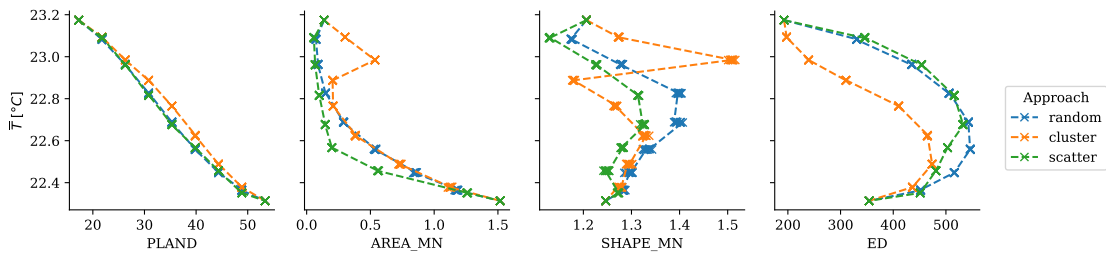


Figure 5.4 – Relationship between landscape metrics and the simulated average temperature \bar{T} for each scenario run, colored to distinguish the sampling approaches. See the Jupyter Notebook at section S2.2 for the detailed numbers of the figure.

are located along the main transportation axes. The relationship between the proportion of candidate pixels transformed and the simulated distribution of air temperature can be approximated as a linear relationship with a negative slope (see Figure A.5 and Figure A.6 for more details about this relationship).

5.3.3 Spatial patterns of tree canopy cover

The relationships between the landscape metrics of each scenario run and the corresponding simulated average temperature \bar{T} (over all the pixels) are displayed in Figure 5.4. The proportion of landscape (PLAND) occupied by pixels with high tree canopy cover range from 17.26 to 53.37%. As a composition metric, PLAND is directly related to the proportion of transformed candidate pixels, and the extreme values of the PLAND range correspond to transforming 0 and 100% of the candidate pixels respectively. The relationship between PLAND and the aver-

age simulated temperature of each scenario \bar{T} shows a sharp monotonic decrease. However, for the same PLAND values, clustering the transformed pixels to other pixels with high tree canopy cover consistently leads to higher \bar{T} than scattering or randomly sampling — the latter approaches show almost indistinguishable PLAND and \bar{T} relationship.

Regarding the configuration metrics, the values of the mean patch area (AREA_MN) show that the clustering and random sampling approaches lead to larger patches of high tree canopy cover than the scattering approach. When transforming a 12.5 and 25% of the candidate pixels, clustering them to other pixels of high tree canopy cover increases AREA_MN from 0.14 to 0.54 hectares respectively (on average over the simulation runs). For 37.5% of transformed candidate pixels in the clustering approach, AREA_MN shows a sudden decline to 0.20 hectares, followed by a monotonic increase that reaches 1.52 hectares when all the candidate pixels are transformed. Such a discernable kink in the computed AREA_MN reveals characteristics of the existing urban fabric, and describes the point after which all the candidate pixels that are adjacent to other pixels of high tree canopy have been transformed and hence new pixels have to be allocated as part of new (and smaller) patches. The same kink is even more notable for the mean shape index (SHAPE_MN), yet the computed values show a very irregular pattern accross the different scenario configurations, and it is the only metric where differences can be noted among scenario runs with the same configuration. The only consistency is that the scattering approach tends to lower SHAPE_MN values than randomly sampling the transformed pixels, which is likely due to the larger abundance of simple single-pixel patches in the former approach. Finally, the clustering approach results in lower edge density (ED) values than in the scattering and random sampling approaches, which show a very similar trend. The observed pattern is consistent with the notion that growing existing patches by clustering the new pixels to them accounts for less total edge length than scattering the same amount of new pixels in a leapfrog manner. In the three approaches, the ED increases monotonically at first until an apex is reached when the proportion of transformed pixels is between 50% and 60%, and then declines monotonically.

The average simulated temperature \bar{T} is overall negatively correlated with AREA_MN, which suggests that for the same amount of high tree canopy pixels, large patches provide lower heat mitigation. On the other hand, configurations with the same proportion of high tree canopy pixels show lower \bar{T} for larger values of ED, which suggests that edge effects between artificial patches and patches of high tree canopy contribute to greater heat mitigation. Nonetheless, as higher proportions of candidate pixels are transformed and the locations of the remaining candidate pixels force the overall ED to decrease, the simulated average temperatures continue to decline. This highlights how the cooling effects of the abundance of tree canopy overshadow those of the spatial configuration, which is consistent with many related research.

5.3.4 Effects on human exposure

The relationship between human exposure to air temperatures higher than 21, 22, 23, 24, 25 and 26°C and the proportion of pixels transformed to their respective high tree canopy cover class is shown in Figure 5.5. The number of dwellers exposed to temperatures higher than 21°C

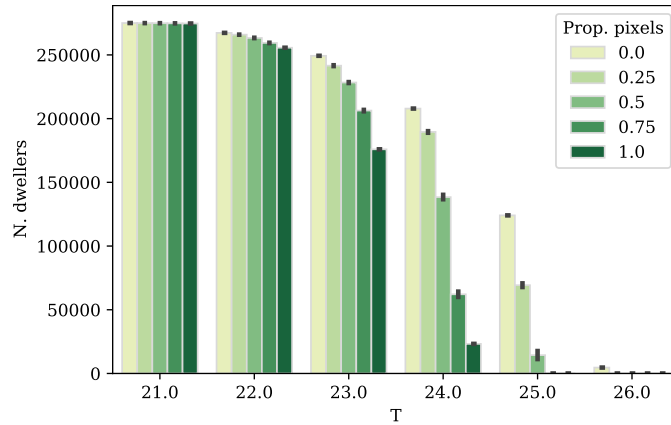


Figure 5.5 – Population exposed to temperatures higher than 21, 22, 23, 24, 25 and 26°C respectively for an overall proportion of transformed pixels of 0, 25, 50, 75 and 100%. The bar heights and the confidence intervals are computed out of all the simulation runs and sampling approaches. See the Jupyter Notebook at section S2.3 for the detailed numbers of the figure.

does not show a significant decrease (even when converting all the candidate pixels), whereas for temperatures higher than 22°C, it diminishes from 269254 to 268601, 267683, 266518 and 264125 when the proportion of transformed pixels is of 25, 50, 75 and 100% respectively, which represents a relative share of 97.25, 97.02, 96.69 96.27 and 95.41% of the population of the study area. Such a decline progressively becomes more notable as temperatures increase, e.g., the share of the population exposed to temperatures over 24°C declines from an initial 78.4% to 72.39, 59.57, 37.53 and 11.52% when transforming a 25, 50, 75 and 100% of the candidate pixels respectively. Finally, the share of dwellers exposed to temperatures over 25°C, which is initially of 47.91%, is diminished to a 24.98 and 5.74% when transforming a 25 and 50% of the pixels respectively, and becomes 0 after that, whereas the 2508 dwellers originally exposed to temperatures over 26°C do no longer meet such temperatures after transforming a 25% of the candidate pixels.

The way in which the transformed pixels are sampled has significant effects on the human exposure to high temperatures (Figure 5.6). Overall, scattering the transformed pixels to avoid forming a continuous tree canopy appears as the most effective approach to reduce the human exposure to the highest temperatures, followed by random sampling. When transforming a 25 and 50% of the candidate pixels with the scattering approach, the number of dwellers exposed to temperatures over 25°C decreases from 124073 to 65108 and 4498 respectively. Such a reduction is larger than its random sampling counterpart by 3125 and 8223 dwellers respectively, and larger than its clustering approach counterpart by 9359 and 21388 dwellers

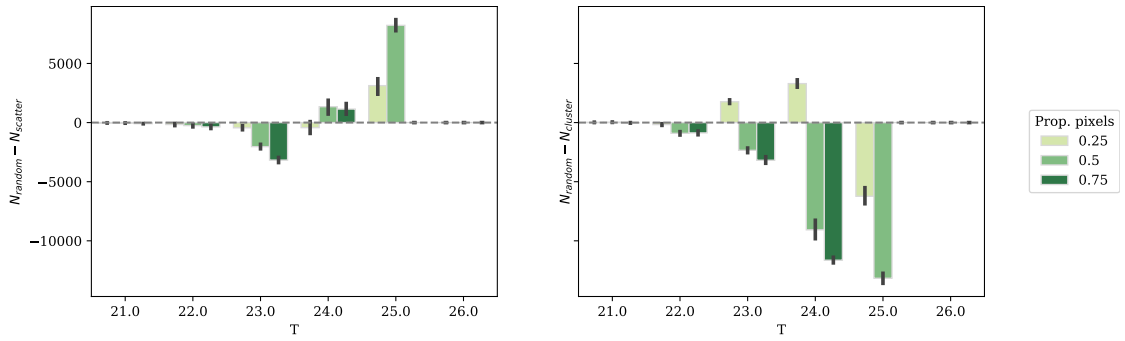


Figure 5.6 – Comparison of between the population exposed to temperatures higher than 21, 22, 23, 24, 25 and 26°C with the random sampling approach and the scattering ($N_{random} - N_{scatter}$, left subplot) and the clustering ($N_{random} - N_{cluster}$, right subplot) selection approaches, for an overall proportion of transformed pixels of 25, 50 and 75%. The lines at the top of the bars represent the 95% confidence intervals. The bar heights and the confidence intervals are computed out of all the simulation runs. See the Jupyter Notebook at section S2.3 for the detailed numbers of the figure.

respectively (Figure 5.6).

5.4 Discussion

5.4.1 Validity and applicability of the proposed approach

The scenarios simulated in this study map locations where the tree canopy cover in the urban agglomeration of Lausanne can be increased, and suggests that such changes can result in urban nighttime temperatures that are up to 2°C lower. The results indicate that given the same proportion of tree canopy cover, a scattered configuration might lead to more effective urban heat mitigation than a clustered one, which is in line with previous studies in humid climates (Zhou et al., 2011; Kong et al., 2014; Estoque et al., 2017; Zhou et al., 2017; Yu et al., 2018; Nastran et al., 2019). Nevertheless, the results suggest that effect of the spatial configuration (measured by the metrics AREA_MN, SHAPE_MN and ED) is secondary when compared to the effect of the composition (measured by the PLAND metric). Overall, the effect of the spatial configuration of trees on its urban heat mitigation depends on how it affects the shading and evapotranspiration processes. Such a relationship is known to be strongly mediated by the tree species, background climatic and environmental conditions as well as the spatial scale (Li et al., 2013b; Estoque et al., 2017; Zhou et al., 2017; Jiao et al., 2017; Yu et al., 2018; Yan et al., 2019; Wang et al., 2020a; Terfa et al., 2020).

The spatial effects observed in the results are due to the InVEST model equations representing air mixing and the effect of parks. In order to ascertain these effects, the InVEST urban cooling model must be further validated with experiments at the neighborhood scale to ensure that it provides an appropriate city-scale depiction of how the urban heat mitigation mechanisms

operate at finer scales. In fact, the InVEST urban cooling model presents limitations regarding the simplified and homogeneous way in which the air is mixed, as well as the cooling effects of large green spaces (Sharp et al., 2020; Bosch et al., *ress*). As a result, the relationship between the proportion of tree canopy cover and the magnitude of the urban heat mitigation reported in this work is practically linear, and the temperature differences between spatially clustering or scattering the new tree canopy cover are limited. Nonetheless, in complex terrains such as the Lausanne agglomeration, models with uniform weighting of space show considerable deviations from the observed spatial patterns of air temperature (Frei, 2014; Labedens et al., 2019). Moreover, the cooling effects of large green spaces have been found to be non-proportional to their area and shape complexity (Chen et al., 2014; Bao et al., 2016; Du et al., 2017). Improving how these non-linear components are represented in the InVEST urban cooling model could enhance not only its validity, but also its value to urban planning by identifying thresholds and regime changes in the cooling efficiency of additional tree planting.

Despite the limitations noted above, a major advantage of the proposed approach is that it can be used to evaluate urban heat mitigation of synthetic scenarios. The simulations presented in this article focus on spatially exploring the effects of an increase of the tree canopy cover, yet there is room for much more experimentation of this kind. On the one hand, the generic sampling approaches explored above can be extended to consider ad-hoc characteristics such as the spatial distribution of the population, and design optimization procedures with specific goals. For instance, the candidate pixels can be selected with the aim of minimizing the exposure of the most vulnerable populations to critical heat thresholds. More broadly, the approach can be used as part of decision support system to explore the trade-offs between ecosystem services provided by trees, perform weighted optimizations and map priority planting locations (Bodnaruk et al., 2017). On the other hand, in line with recent studies (Lemonsu et al., 2015; Yang et al., 2016; Trimmel et al., 2019), the approach could be applied to examine the impact of distinct urbanization scenarios such as densification and urban sprawl on air temperature and human exposure to extreme heat, under current conditions as well as future climate estimates, e.g., by changing the T_{ref} or UHI_{max} parameters. Similarly, InVEST urban cooling model might be coupled with models of LULC change such as cellular automata in order to assess not only which scenarios are most desirable in terms of urban heat mitigation, but also which planning strategies might lead to them (Silva et al., 2008; White et al., 2015; Bosch et al., 2019).

5.4.2 Implications for urban planning in Lausanne

The spatiotemporal patterns of LULC change observed during the last 40 years in the Lausanne agglomeration have been characterized by infilling development and a progressive coalescence of artificial surfaces in its inner ring (Bosch et al., 2020a). Such an infilling trend urges for careful evaluation of the beneficial ecosystem services provided by urban green spaces, which should be balanced against the adverse consequences of urban sprawl (Haaland and van Den Bosch, 2015; Artmann et al., 2019).

The approach proposed in this study maps locations in the current urban fabric where the tree canopy cover can be increased. While part of this urban greening might occur in impervious surfaces (e.g., in sidewalks, next to roads and in other impervious surfaces), most of the candidate locations currently correspond to urban green space (i.e., the “garden” LULC class). Therefore, the potential heat mitigation suggested by the results study is not attainable in a scenario of severe infill development. Additionally, densification strategies should consider that newly created urban green space might result in less provision of ecosystem services than remnant natural patches (Jim, 2013; Sun and Chen, 2017; Wang et al., 2019). Finally, infilling might exacerbate the unevenness of the accessibility to green areas by depriving dwellers of the most dense parts in city core from their few remaining urban green spaces. Spatial heterogeneity of this kind, which are encountered in many socioeconomic and environmental aspects of contemporary cities, are often hard to represent with aggregate indicators and highlight the importance of spatially explicit models to urban planning and decision making.

The explicit representation of space is also crucial when considering the impacts of urban green space on human exposure to extreme heat. Although the simulated scenarios suggest that the impact of the spatial pattern of tree canopy on the air temperature is practically linear, the implications on human exposure to critical temperatures exhibit important thresholds. For example, by increasing the tree canopy cover of a 25% of the candidate pixels, the number of dwellers exposed to nighttime temperatures over 25°C can be reduced from 124073 to 74466, which respectively represents a 45.08 and 27.06% of the total population in the study area. Furthermore, the results suggest by selecting such pixels to prioritize a spatial scattering of the tree canopy cover, such a population can be reduced by an additional 3125 or 6234 dwellers when respectively compared to random sampling such pixels or clustering them to the existing tree canopy cover. In Switzerland, the excess mortality associated to the heat wave of 2003 occurred over-proportionally to urban and sub-urban residents of its largest urban agglomerations (Grize et al., 2005). Furthermore, the association between temperature and mortality in extreme heat events in the largest Swiss urban agglomerations are exponential (Ragetti et al., 2017), which indicates that reducing temperatures by even fractions of a degree can have a dramatic impact on death rates.

5.5 Conclusion

The scenarios simulated in this study represent a new way of spatially exploring the heat mitigation potential provided by modifications of the urban fabric, and allow evaluating the cooling effects of both the abundance and spatial configuration of the tree canopy cover. The results map locations where the existing tree canopy cover of the urban agglomeration of Lausanne can be increased, and show an urban cooling potential for urban nighttime temperatures of more than 2°C. Additionally, the simulations suggest that the spatial configuration in which the tree canopy is increased influences its heat mitigation effects. The configuration effects become more significant when considering the impacts on the urban population, and small increases in the tree canopy can result in important reductions in the number of dwellers

Chapter 5. Urban greening scenarios for urban heat mitigation

exposed to the highest temperatures. Overall, the presented approach provides a novel way to explore how the urban tree canopy can be exploited to reduce heat stress. Future studies can extend the analyses by assessing the provision of other ecosystem services in the various tree canopy strategies presented here.

6 Synthesis and outlook

6.1 Summary of main contributions

This thesis presents important contributions to understand the spatiotemporal patterns of urbanization and its relationship with the UHI effect. Although the staged results are restricted to three Swiss urban agglomerations and only one aspect of environmental performance, namely the UHI effect, the proposed methods are reusable and can thus easily be applied to other regions. Additionally, the overall approach of relating the spatiotemporal patterns of urbanization to the UHI effect can easily be extended to assess other ecosystem services such as flood risk mitigation, air pollution control or recreation opportunities, and more broadly to evaluate further criteria of environmental performance such as the alteration of material and energy flows, the fragmentation of natural habitats or biodiversity indicators.

The first key contribution is the development of PyLandStats (chapter 2), an open-source reusable library to compute landscape metrics in categorical raster maps. Such an accomplishment provides improvements upon the FRAGSTATS software, which hitherto has been the prevalent approach to compute landscape metrics in the literature. In chapter 3, PyLandStats is used to assess the spatiotemporal patterns of urbanization in Bern, Lausanne and Zurich. As noted in the introduction of this thesis, such an endeavor is required in order to quantitatively associate the changes in urban patterns to the observed variations of environmental performance, e.g., the UHI effect. The area-radius scaling of urban patches suggest that the three agglomerations, and especially Bern and Lausanne, are better described by two characteristic spatial extents, i.e., an inner zone where urbanization is essentially complete and an outer zone that is still undergoing intense urbanization. The proposed distinction of two characteristic extents is then exploited to revisit two prominent hypotheses of urbanization patterns, namely the diffusion and coalescence hypothesis and the three growth modes hypothesis. The results suggest that both hypothesis are over-simplistic because urbanization exhibits distinct spatiotemporal patterns in each of the characteristic extents. In the inner zone of the three agglomerations, urban patches are coalescing, and their growth corresponds mostly to infill development. In the outer zone, Lausanne and Bern are seemingly at the transition between

the diffusion and coalescence stages, with urban patches growing mainly by edge expansion yet the influence of infilling increases over time. On the other hand, the outer zone of Zurich also shows the characteristics of coalescence, with an urban growth that is governed by both edge expansion and infilling — yet the latter gains influence over time. Lastly, this article represents an advance over similar studies in terms of the repeatability and reproducibility of the results. The computational workflow to reproduce the results and figures of the manuscript is available at a GitHub repository at <https://github.com/martibosch/swiss-urbanization>, and can be executed interactively in the browser with the Binder web service (Matthias Bussonnier et al., 2018). Additionally, the tool to process the geodata from the SFSO has been packaged into an open-source Python library that has been reviewed and published separately (Bosch, 2019b). The contributions of chapters 2 and 3 serve to achieve the first research objective of this thesis outlined in the introductory chapter, namely quantifying the landscape changes due to urbanization so that they can be linked to variations in the UHI effect.

After the quantitative evaluation of urbanization in Switzerland, chapter 4 is devoted to the spatially-explicit modeling of the UHI effect. To that end, the approach builds upon the InVEST urban cooling model Sharp et al. (2020), which simulates heat mitigation based on three biophysical mechanisms, i.e., shading, evapotranspiration and albedo. An automated calibration procedure based on the simulated annealing algorithm is used to tune the parameters of the model in order to best fit temperature measurements observed in monitoring stations. In the example application in the urban agglomeration of Lausanne, the calibrated model outperforms regression models based on remote sensing features. Besides the performance improvements, the proposed workflow presents two key advantages with respect to the regression models or supervised learning approaches in general. First, the parameters of the InVEST urban cooling model are directly related to the biophysical mechanisms that underpin the UHI effect, which permits their straightforward physical interpretation. Secondly, the calibrated model can be used to simulate urban heat mitigation in synthetic LULC maps such as master plans and urbanization prospects. Supervised learning models based on remote sensing features are not well suited for such an enterprise, since they require inputs such as LST which are hard to obtain other than empirically. Since the ultimate objective is to propose a reusable computational workflow that can be calibrated and applied to any given region, the code materials used to obtain the results and figures are available at a GitHub repository at <https://github.com/martibosch/lausanne-heat-islands>. Furthermore, the automated calibration routine has been released as an open-source Python package, with the source code hosted at a GitHub repository at <https://github.com/martibosch/invest-ucm-calibration>.

In the last part of the thesis, the approach to simulate urban cooling described above is applied to evaluate potential heat mitigation in a variety of greening scenarios in Lausanne (chapter 5). The scenarios are generated by increasing the abundance of the tree canopy cover in distinct spatial configurations. Then, the InVEST urban cooling model is applied to the synthetic LULC map of each scenario in order to simulate the corresponding heat mitigation. The results show an cooling potential for urban nighttime temperatures of more than 2°C, and suggest that scattered configurations of the tree canopy cover mitigate urban heat more efficiently

than clustered ones. When considering the impacts on the urban population, small increases in the tree canopy can result in important reductions in the number of dwellers exposed to the highest temperatures, which can in turn have major impacts on human health and well being. Like in the previous articles, the computational workflow of the study is available at a GitHub repository at <https://github.com/martibosch/lausanne-greening-scenarios>. Overall, chapters 4 5 accomplish the second research objective of the thesis, which is the development of a reusable approach to model the UHI effect in urban areas and to map the heat mitigation potential. The work of these chapters also addresses the third research objective of the thesis, as they provide a reusable method to evaluate the UHI effect in future urbanization scenarios and map the heat mitigation potential of urban green infrastructure. However, the presented results only assess the urban cooling potential in the current urban fabric of Lausanne, and thus do not consider scenarios based in urbanization forecasts or land use plans. Future work should apply the approach to alternative future scenarios in order to explore which urban patterns provide the most desirable heat mitigation outcomes and use that information to support urban planning and decision making.

6.2 Implications of the key findings

The analysis of the spatiotemporal patterns of urbanization from 1980 to 2016 presented in chapter 3 sets the stage for reasonable guesstimation of the future urbanization trends in the main Swiss urban agglomerations. On the one hand, urban growth in Zurich has been characterized by a coalescence of urban patches and an increasing dominance of infilling, which is the dominant growth mode in the inner core as well as in the outer zone during the most recent period of study (i.e., from 2007 to 2016). On the other hand, while the same trend is observed in the inner zones of Bern and Lausanne, their outer zones are seemingly at the transition between diffusion and coalescence of their urban patches. Under these circumstances, urban growth is dominated by edge-expansion of urban patches, yet such a growth mode is losing influence to infilling. From the diffusion and coalescence model of urbanization (Dietzel et al., 2005), the outer zones of Bern and Lausanne can be expected to undergo increasing infilling development, approaching the pattern observed in Zurich. The way in which the outer zones of Bern and Lausanne show a tendency towards the pattern of Zurich can also be noted in the area-radius curves, since the kink that separates the inner and outer zones of Bern and Lausanne is losing prominence as the curve becomes steeper at larger radii (i.e., the outer zones) — hence approaching the straight-line area-radius scaling encountered in Zurich. Therefore, there are plausible grounds that indicate that significant urbanization will occur in the outer zones of Bern and Lausanne in the following years, which is in line with Swiss urbanization scenarios developed in related studies (Price et al., 2015; Gerecke et al., 2019). Nevertheless, the scenarios reviewed above are all based upon the LULC change trends occurred before the major revision of the Swiss Federal Act on Spatial Planning in 2013, which might mediate future urbanization differently, e.g., fostering further intensification of the inner zones (Weilenmann et al., 2017; Rudolf et al., 2018; Gerecke et al.,

2019).

The study of the UHI effect in Lausanne presented in chapters 4 and 5 shows that the highest temperatures occur in the inner core of the urban agglomeration, which concentrates the largest share of urban dwellers. In the greening scenarios evaluated in chapter 5, most of the locations where the tree canopy can be increased correspond to urban green space. These findings reveal that the scenarios that provide the greatest heat mitigation are incompatible with severe urban intensification, hence supporting the central hypothesis of the thesis. This urges for a careful assessment of the potential impacts of further intensification of the main Swiss urban agglomerations, especially regarding the beneficial ecosystem services provided by remnant green space of the urban cores as well as the potential impacts of transforming them to impervious surfaces.

6.3 Methodological aspects and outlook for future research

Improvement of the urban heat island simulation

When compared to the approaches to select tree planting locations with highest urban cooling effectiveness reviewed in the introductory chapter, the application of the InVEST urban cooling model presented in this thesis is the first that implicitly account for the effects of spatial configuration, namely by including the well-documented effect of large green areas. However, the proposed approach is also subject to important limitations that require careful consideration and must be addressed in future work.

Firstly, the study of the UHI effect with the InVEST urban cooling model presented in this thesis only considers the effects at the scale of the urban agglomeration, where the UHI is presumed to be most notable. Nonetheless, the variety of processes that unfold upon urban landscapes operate across multiple spatial and temporal scales, which stresses the importance of multi-scale approaches in the study of urban and ecological systems (Forman, 1995; Pickett et al., 1997; Alberti, 1999; Collins et al., 2000; Zipperer et al., 2000; Pickett et al., 2001; Alberti, 2005; Liu et al., 2007; Wu, 2008; Zhang et al., 2013; Alberti et al., 2018). A variety of micro-scale models of urban climate can be found in the literature, which can be broadly classified into computational fluid dynamics models and energy balance models of the urban canopy (Mirzaei, 2015; Toparlar et al., 2017; Mauree et al., 2019). While computational fluid dynamics can model the urban microclimate at the street and neighborhood scales with great detail, due to their substantial computational requirements, they are not suitable for studying the UHI at the scale of the urban agglomeration. Instead, to reduce the computational costs, energy balance models of the urban canopy do not represent buildings and other features of the urban canyon explicitly, but rather parametrize their effects on a grid where the atmospheric and thermodynamic interactions are represented. In fact, the initial formulations of energy balance models (Masson, 2000; Martilli et al., 2002) have been extended to account for the shadow effects, water and energy exchanges of trees by representing their three-dimensional

6.3. Methodological aspects and outlook for future research

features, which include the height of their trunk and canopy, their cover fraction of the urban canyon as well as their foliage by means of the leaf area index (Krayenhoff et al., 2014; Redon et al., 2017; Krayenhoff et al., 2020; Redon et al., 2020).

When compared to the aforementioned approaches, the InVEST urban cooling model provides a simplified representation of the characteristics of the urban canyon. While such a simplicity is a valuable asset that permits applying the model to a variety of cities and scenarios with results that can be easily interpreted physically, the ability of the model to accurately represent physical processes associated with the heat mitigation should be demonstrated before resolving planning recommendations (Krayenhoff et al., 2021). Therefore, as suggested in the discussion of chapter 5, it is crucial to validate the InVEST urban cooling model against energy balance models with more detailed representations of the urban canyon to ensure that it provides an appropriate city-scale representation of how the urban cooling mechanisms operate at finer scales — or else see how to improve the model by means of more detailed parametrizations.

On the other hand, the distinction between tree species is not addressed explicitly in the InVEST urban cooling model nor in the energy balance models. Some extensions of the latter partly account for these differences when considering the leaf area index, which is characteristic to the tree species and is a key determinant of the shading properties, yet there are large differences in evapotranspirational cooling between species (Peters et al., 2010; Rahman et al., 2015; Gillner et al., 2015; Rahman et al., 2019). Additionally, tree species very different stress tolerance to urban environments (Bassuk, 2003; Swoczyna et al., 2010), and a misappreciation of these factors can lead to adverse outcomes such as reduced heat mitigation, increased tree mortality, as well as excessive maintenance and irrigation costs (Pincetl et al., 2013; Ko et al., 2015; Roman et al., 2020).

However, the research directions outlined above cannot be properly validated with the current spatial sparsity of official monitoring stations. Available means to overcome such a drawback include setting up high-density observation networks (Matte et al., 2013; Chen et al., 2018; Šećerov et al., 2019; Johnson et al., 2020), as well as a variety of crowdsourcing techniques (Muller et al., 2015) such as mobile measurements (Leconte et al., 2015; Tsin et al., 2016; Shi et al., 2018; Ziter et al., 2019; Cao et al., 2020), or citizen weather stations (Wolters and Brandsma, 2012; Schatz and Kucharik, 2015; Meier et al., 2017; Scott et al., 2017; Fenner et al., 2017; Dejmal et al., 2019; Fenner et al., 2019). Furthermore, data from the official monitoring stations can be complemented by measurements from citizen weather stations in order to achieve reliable high-resolution maps of air temperature (Zumwald et al., 2020).

Towards an integrative and long-term approach to urban planning

The importance of incorporating principles from landscape ecology and ecosystem services to the spatial planning of urban agglomerations has long been recognized (McDonnell and Pickett, 1990; Hersperger, 1994; Forman, 1995; Medley et al., 1995; Pickett et al., 1997; Bol-

und and Hunhammar, 1999; Ahern, 1999; Collins et al., 2000; Grimm et al., 2000; Zipperer et al., 2000; Pickett et al., 2001; Leitao and Ahern, 2002). The key goal of such an ecological perspective is to optimize the patch sizes, shapes and connectivity of green areas so that the resulting urban agglomeration provides adequate spaces to accommodate a variety of habitats and species, support ecosystem functioning and enhance the provision of beneficial ecosystem services to urban dwellers (Hersperger, 1994; Forman, 1995; Ahern, 1999; Zipperer et al., 2000; Leitao and Ahern, 2002; Breuste et al., 2008; Ahern, 2013; Jim, 2013). Nevertheless, the practical integration of these principles into urban planning decision making remains a challenge (Ahern, 2013; Haase et al., 2014; Green et al., 2016; Costanza et al., 2017; Hersperger et al., 2018). This thesis proposes an approach to spatially quantify the urban heat mitigation provided by trees that considers the effects of its spatial pattern, and can be easily applied to current urban areas as well as to synthetic LULC maps representing future or alternative scenarios. Altogether, the presented results constitute a cross-sectional evaluation of a single ecosystem service (i.e., urban heat mitigation), which future work should extend in three primary directions.

First, the conceptual framework of this thesis must integrate further models urban ecosystem services so that multiple aspects of environmental performance can be assessed. Ecosystems provide multiple services and can involve trade-offs that increase the provisioning of one service while reducing the provisioning of another, which highlights the importance of considering multiple ecosystem services in planning and decision making (Rodríguez et al., 2006; Raudsepp-Hearne et al., 2010; Seppelt et al., 2011; Haase et al., 2012, 2014; Demuzere et al., 2014; Holt et al., 2015; Kremer et al., 2016; Baró et al., 2017; Turkelboom et al., 2018; Jalogot et al., 2019b,a). Therefore, although chapter 5 might serve to explore spatial patterns of the tree canopy that enhance the urban heat mitigation, the same spatial pattern might have adverse effects in the provision of other ecosystem services. Ensuring an adequate provision of multiple urban ecosystem services is a major challenge for spatial planning that is particularly accentuated in cities undergoing densification, which requires a systematic spatial evaluation of the urban green infrastructure, preventing its degradation during infill development and including guidelines for multifunctionality at the urban agglomeration scale (Jim, 2004; Byrne et al., 2010; Haaland and van Den Bosch, 2015; Hansen et al., 2019)

The second direction for future research concerns extending the cross-sectional assessment of chapter 4 by applying the same approach to other points in time in order to obtain longitudinal trend of the UHI effect. Such an endeavor is complementary to the inclusion of further ecosystem services suggested above, and is also a central requirement to understand the complex temporal synergies and trade-offs of ecosystem services, which are strongly influenced by legacy effects and time lags of historical management (Rodríguez et al., 2006; Haase et al., 2012, 2014; Mouchet et al., 2014; Dallimer et al., 2015; Renard et al., 2015; Tomscha and Gergel, 2016; Tomscha et al., 2016; Hein et al., 2016; Jalogot et al., 2019b,a). Additionally, these proposed extensions would allow a thorough evaluation of the relationships between the spatiotemporal dynamics of ecosystem services and the spatiotemporal patterns of urbanization reported in chapter 3.

6.3. Methodological aspects and outlook for future research

Finally, a third extension consists in integrating the approach of this thesis to assess the environmental performance of synthetic scenarios with LULC change models, which would pave the way not only for the evaluation of potential future scenarios of urbanization, but also to explore which policies and interventions can lead to the most desirable outcomes. A notable example is the integrated fractal planning approach (Tannier et al., 2012; Yamu and Frankhauser, 2015; Frankhauser et al., 2018), which simulates urban development at multiple spatial scales based on a set of rules that allow improving the accessibility to amenities and open space while preventing the fragmentation of green spaces. To that end, fractal structures have the key property that their border is over-proportionally lengthened with respect to their area. Fractal geometry can therefore be exploited in order to satisfy the residential demand for green environments while explicitly considering planning objectives such as protecting natural habitats and improving accessibility to urban and natural amenities. Coupling such an approach with the spatially-explicit evaluation of heat mitigation and other ecosystem services shows great potential to further understand the edge effects between natural and artificial patches and assess how these should be spatially interspersed (Lin and Fuller, 2013; Stott et al., 2015). Another integrated approach consists in coupling cellular automata and agent-based models of urbanization with additional constraining rules that allocate the land conversion in a way that predefined landscape planning goals are met (Silva et al., 2008; Mitsova et al., 2011; Yin et al., 2016). Such goals are determined according to the values of a set of landscape spatial metrics, which can be prescribed to reflect planning strategies aimed at protecting natural habitats and ecosystems. Incorporating the approach of this thesis into such a framework would provide additional grounds to explore how future urbanization might affect the UHI effect (and in turn other ecosystem services), and assess how this might influence the residential behavior, e.g., whether the densification prescribed in Switzerland might prompt dwellers of the urban cores to relocate to suburban areas or nearby municipalities where the UHI effect is of lesser magnitude. Feedback effects of this kind stress how ecosystem services are not simply a benefit of ecosystem functioning but instead are co-produced by humans and ecosystems (Andersson et al., 2015). When dealing with the complex social, ecological, and technological couplings of urban systems, the central advantage of cellular automata and agent-based models with respect to other black-box approaches (e.g., machine learning algorithms) is their ability to explicitly represent socioeconomic principles into their interactions and transition rules, which allows them to not only reproduce the observed patterns but also to explore alternative forms that might emerge when such interactions are mediated by different planning strategies (White et al., 2015; Bosch et al., 2019).

Overall, the high complexity of urban landscapes and their relationships with the socioeconomic and environmental processes that occur upon them highlights the need for a holistic understanding of cities (Wu, 2008, 2014; McHale et al., 2015; McPhearson et al., 2016; Alberti et al., 2018; Artmann et al., 2019). Cities are complex adaptive systems, with coupled human and natural components that co-evolve and adapt to changes in the environment, technology and life modes (Jacobs, 1961; Alexander, 1965; Portugali, 2000; Batty and Torrens, 2001; Batty, 2005; Manson and O'Sullivan, 2006; Irwin et al., 2009; de Roo and Silva, 2010; White et al.,

2015; Bosch et al., 2019). Accordingly, the inability to fully predict or control their evolution is not a shortcoming of the current urban and ecological knowledge but rather an inherent feature of cities. As expressed by Popper (1992) “we cannot predict, scientifically, results which we shall obtain in the course of the growth of our own knowledge” (page 62). From this perspective, the novel insights into the spatiotemporal patterns of urbanization and their impact on the UHI effect provided in this thesis should not be used to predict the evolution of cities and their corresponding UHI effect, but instead be exploited to influence and guide urban development towards more desirable pathways through urban planning and decision-making. Informational networks and technological advances change the urban life modes and thus the physical infrastructure needed to support the functioning of cities. Ecosystems show nonlinear responses to anthropogenic disturbances, such as thresholds, feedback loops, time lags, legacy effects, resilience and multiple modes of stable behavior. Therefore, the only way that urban and environmental knowledge can progress is by continuously monitoring the environmental impacts of cities and updating the urban and ecological knowledge accordingly.

Bibliography

- Ahern, J. (1999). Spatial concepts, planning strategies, and future scenarios: a framework method for integrating landscape ecology and landscape planning. In *Landscape Ecological Analysis*, pages 175–201. Springer.
- Ahern, J. (2013). Urban landscape sustainability and resilience: the promise and challenges of integrating ecology with urban planning and design. *Landscape ecology*, 28(6):1203–1212.
- Akbari, H. and Kolokotsa, D. (2016). Three decades of urban heat islands and mitigation technologies research. *Energy and Buildings*, 133:834–842.
- Akbari, H., Pomerantz, M., and Taha, H. (2001). Cool surfaces and shade trees to reduce energy use and improve air quality in urban areas. *Solar energy*, 70(3):295–310.
- Alberti, M. (1996). Measuring urban sustainability. *Environmental impact assessment review*, 16(4-6):381–424.
- Alberti, M. (1999). Urban patterns and environmental performance: what do we know? *Journal of planning education and research*, 19(2):151–163.
- Alberti, M. (2005). The effects of urban patterns on ecosystem function. *International regional science review*, 28(2):168–192.
- Alberti, M., McPhearson, T., and Gonzalez, A. (2018). Embracing urban complexity. *Urban planet: knowledge towards sustainable cities. First edition. Cambridge University Press, Cambridge, UK. <https://doi.org/10.1017/9781316647554.004>*, pages 45–67.
- Alexander, C. (1965). A city is not a tree. *Architectural forum*, 122(1):58–62.
- Allen, R. G., Pereira, L. S., Raes, D., Smith, M., et al. (1998). Crop evapotranspiration-guidelines for computing crop water requirements - fao irrigation and drainage paper 56. *Fao, Rome*, 300(9):D05109.
- Altshuler, A. A., Womack, J. P., and Pucher, J. P. (1979). *The Urban Transportation System: Politics and Policy Innovation*. MIT Press, Cambridge, Mass.
- Andersson, E., McPhearson, T., Kremer, P., Gomez-Baggethun, E., Haase, D., Tuvendal, M., and Wurster, D. (2015). Scale and context dependence of ecosystem service providing units. *Ecosystem Services*, 12:157–164.

Bibliography

- Angel, S., Blei, A. M., Civco, D. L., and Parent, J. (2012). *Atlas of urban expansion*. Lincoln Institute of Land Policy Cambridge, MA.
- Angel, S., Parent, J., Civco, D. L., Blei, A., and Potere, D. (2011). The dimensions of global urban expansion: Estimates and projections for all countries, 2000–2050. *Progress in Planning*, 75(2):53–107.
- Angel, S., Sheppard, S., Civco, D. L., Buckley, R., Chabaeva, A., Gitlin, L., Kraley, A., Parent, J., and Perlin, M. (2005). *The dynamics of global urban expansion*. Citeseer.
- Anniballe, R., Bonafoni, S., and Pichierri, M. (2014). Spatial and temporal trends of the surface and air heat island over milan using modis data. *Remote Sensing of Environment*, 150:163–171.
- Arnfield, A. J. (2003). Two decades of urban climate research: a review of turbulence, exchanges of energy and water, and the urban heat island. *International Journal of Climatology: a Journal of the Royal Meteorological Society*, 23(1):1–26.
- Artmann, M., Inostroza, L., and Fan, P. (2019). Urban sprawl, compact urban development and green cities. how much do we know, how much do we agree? *Ecological Indicators*, 96:3–9.
- Association pour le Système d'information du Territoire Vaudois (2018). Structure es données cadastrales au format shape (md.01-mo-vd). Available from (in French) <https://www.asitvd.ch/md/508>. Accessed: 3 September 2019.
- Avdan, U. and Jovanovska, G. (2016). Algorithm for automated mapping of land surface temperature using landsat 8 satellite data. *Journal of Sensors*, 2016.
- Bagstad, K. J., Semmens, D. J., Waage, S., and Winthrop, R. (2013). A comparative assessment of decision-support tools for ecosystem services quantification and valuation. *Ecosystem Services*, 5:27–39.
- Balchin, W. G. V. and Pye, N. (1947). A micro-climatological investigation of bath and the surrounding district. *Quarterly Journal of the Royal Meteorological Society*, 73(317-318):297–323.
- Band, L. E., Cadenasso, M. L., Grimmond, C. S., Grove, J. M., and Pickett, S. T. (2005). Heterogeneity in urban ecosystems: patterns and process. In *Ecosystem function in heterogeneous landscapes*, pages 257–278. Springer.
- Bao, T., Li, X., Zhang, J., Zhang, Y., and Tian, S. (2016). Assessing the distribution of urban green spaces and its anisotropic cooling distance on urban heat island pattern in Baotou, China. *ISPRS International Journal of Geo-Information*, 5(2):12.
- Baró, F., Gómez-Baggethun, E., and Haase, D. (2017). Ecosystem service bundles along the urban-rural gradient: Insights for landscape planning and management. *Ecosystem Services*, 24:147–159.

- Bassuk, N. (2003). *Recommended urban trees: Site assessment and tree selection for stress tolerance*. Cornell University, Urban Horticulture Institute.
- Batty, M. (2005). *Cities and Complexity: Understanding Cities with Cellular Automata, Agent-based Models, and Fractals*. MIT Press.
- Batty, M. (2008). The size, scale, and shape of cities. *science*, 319(5864):769–771.
- Batty, M. and Longley, P. (1994). *Fractal Cities: A Geometry of Form and Function*. Academic Press.
- Batty, M. and Torrens, P. M. (2001). Modelling complexity: the limits to prediction. *Cybergeo: European Journal of Geography*.
- Behnel, S., Bradshaw, R., Citro, C., Dalcin, L., Seljebotn, D. S., and Smith, K. (2011). Cython: The best of both worlds. *Computing in Science & Engineering*, 13(2):31.
- Block, A. H., Livesley, S. J., and Williams, N. S. (2012). Responding to the urban heat island: a review of the potential of green infrastructure. Report funded by the Victorian Centre for Climate Change Adaptation Research Melbourne.
- Bodnaruk, E., Kroll, C., Yang, Y., Hirabayashi, S., Nowak, D., and Endreny, T. (2017). Where to plant urban trees? a spatially explicit methodology to explore ecosystem service tradeoffs. *Landscape and Urban Planning*, 157:457–467.
- Bolund, P. and Hunhammar, S. (1999). Ecosystem services in urban areas. *Ecological economics*, 29(2):293–301.
- Bosch, M. (2019a). PyLandStats: An open-source Pythonic library to compute landscape metrics. *PLoS One*, 14(12).
- Bosch, M. (2019b). swisslandstats-geopy: Python tools for preprocessing geodata from the Swiss federal statistical office. *J. Open Source Software*, 4(40):1511.
- Bosch, M. (2020a). Detectree: Tree detection from aerial imagery in Python. *Journal of Open Source Software*.
- Bosch, M. (2020b). Lausanne heat islands, gmd discussions. Zenodo <https://doi.org/10.5281/zenodo.3970608>.
- Bosch, M. (2020c). Urban footprinter: a convolution-based approach to detect urban extents from raster data. Zenodo <https://doi.org/10.5281/zenodo.3699310>.
- Bosch, M. and Chenal, J. (2019). Spatiotemporal patterns of urbanization in three swiss urban agglomerations: insights from landscape metrics, growth modes and fractal analysis. *bioRxiv*, page 645549.
- Bosch, M., Chenal, J., and Joost, S. (2019). Addressing urban sprawl from the complexity sciences. *Urban Science*, 3(2):60.

Bibliography

- Bosch, M., Jaligot, R., and Chenal, J. (2020a). Spatiotemporal patterns of urbanization in three swiss urban agglomerations: insights from landscape metrics, growth modes and fractal analysis. *Landscape Ecology*, pages 1–13.
- Bosch, M., Locatelli, M., Hamel, P., Jaligot, R., Chenal, J., and Joost, S. (2020b). Evaluating urban greening scenarios for urban heat mitigation: a spatially-explicit approach. *Preprint under review in Royal Society Open Science*.
- Bosch, M., Locatelli, M., Hamel, P., Remme, R. P., Chenal, J., and Joost, S. (in press). A spatially-explicit approach to simulate urban heat mitigation with InVEST (v3.8.0). *Geoscientific Model Development*.
- Boumans, R., Roman, J., Altman, I., and Kaufman, L. (2015). The multiscale integrated model of ecosystem services (mimes): Simulating the interactions of coupled human and natural systems. *Ecosystem services*, 12:30–41.
- Bowler, D. E., Buyung-Ali, L., Knight, T. M., and Pullin, A. S. (2010). Urban greening to cool towns and cities: A systematic review of the empirical evidence. *Landscape and urban planning*, 97(3):147–155.
- Breiman, L. (2001). Random forests. *Machine learning*, 45(1):5–32.
- Breuste, J., Niemelä, J., and Snep, R. P. (2008). Applying landscape ecological principles in urban environments. *Landscape ecology*, 23(10):1139–1142.
- Bruegmann, R. (2006). *Sprawl: A compact history*. University of Chicago press.
- Burchell, R. W., Shad, N. A., Listokin, D., Phillips, H., Downs, A., Seskin, S., Davis, J. S., Moore, T., Helton, D., and Gall, M. (1998). *The costs of sprawl-revisited*. Number 39 in Report (Transit Cooperative Research Program). Transportation Research Board.
- Burgstall, A. (2019). Representing the urban heat island effect in future climates. Scientific Report MeteoSwiss No. 105.
- Byrne, J., Sipe, N., and Searle, G. (2010). Green around the gills? the challenge of density for urban greenspace planning in seq. *Australian Planner*, 47(3):162–177.
- Cadenasso, M. L., Pickett, S. T., and Schwarz, K. (2007). Spatial heterogeneity in urban ecosystems: reconceptualizing land cover and a framework for classification. *Frontiers in Ecology and the Environment*, 5(2):80–88.
- Cao, C., Yang, Y., Lu, Y., Schultze, N., Gu, P., Zhou, Q., Xu, J., and Lee, X. (2020). Performance evaluation of a smart mobile air temperature and humidity sensor for characterizing intracity thermal environment. *Journal of Atmospheric and Oceanic Technology*, 37(10):1891–1905.
- Chang, C.-R., Li, M.-H., and Chang, S.-D. (2007). A preliminary study on the local cool-island intensity of taipei city parks. *Landscape and urban planning*, 80(4):386–395.

- Chen, A., Yao, X. A., Sun, R., and Chen, L. (2014). Effect of urban green patterns on surface urban cool islands and its seasonal variations. *Urban forestry & urban greening*, 13(4):646–654.
- Chen, Y.-C., Yao, C.-K., Honjo, T., and Lin, T.-P. (2018). The application of a high-density street-level air temperature observation network (HiSAN): Dynamic variation characteristics of urban heat island in Tainan, Taiwan. *Science of the Total Environment*, 626:555–566.
- Chestnut, L. G., Breffle, W. S., Smith, J. B., and Kalkstein, L. S. (1998). Analysis of differences in hot-weather-related mortality across 44 us metropolitan areas. *Environmental Science & Policy*, 1(1):59–70.
- Clinton, N. and Gong, P. (2013). Modis detected surface urban heat islands and sinks: Global locations and controls. *Remote Sensing of Environment*, 134:294–304.
- Collins, J. P., Kinzig, A., Grimm, N. B., Fagan, W. F., Hope, D., Wu, J., and Borer, E. T. (2000). A new urban ecology modeling human communities as integral parts of ecosystems poses special problems for the development and testing of ecological theory. *American scientist*, 88(5):416–425.
- Conference des Services Cantonaux du Cadastre (2011). Degré de spécification en mensuration officielle - couche d'information de la couverture du sol. Available from (in French) <https://www.cadastre.ch/content/cadastre-internet/fr/manual-av/publication/guidline.download/cadastre-internet/fr/documents/av-richtlinien/Richtlinie-Detaillierungsgrad-BB-fr.pdf>. Accessed: 26 February 2020.
- Connors, J. P., Galletti, C. S., and Chow, W. T. (2013). Landscape configuration and urban heat island effects: assessing the relationship between landscape characteristics and land surface temperature in phoenix, arizona. *Landscape ecology*, 28(2):271–283.
- Costanza, R., De Groot, R., Braat, L., Kubiszewski, I., Fioramonti, L., Sutton, P., Farber, S., and Grasso, M. (2017). Twenty years of ecosystem services: how far have we come and how far do we still need to go? *Ecosystem services*, 28:1–16.
- Dallimer, M., Davies, Z. G., Diaz-Porras, D. F., Irvine, K. N., Maltby, L., Warren, P. H., Armsworth, P. R., and Gaston, K. J. (2015). Historical influences on the current provision of multiple ecosystem services. *Global Environmental Change*, 31:307–317.
- de Roo, G. and Silva, E. A. (2010). *A Planner's Encounter with Complexity*. Ashgate Publishing, Ltd.
- Deilami, K., Kamruzzaman, M., and Liu, Y. (2018). Urban heat island effect: A systematic review of spatio-temporal factors, data, methods, and mitigation measures. *International journal of applied earth observation and geoinformation*, 67:30–42.
- Dejmal, K., Kolar, P., Novotny, J., and Roubalova, A. (2019). The potential of utilizing air temperature datasets from non-professional meteorological stations in Brno and surrounding area. *Sensors*, 19(19):4172.

Bibliography

- Demuzere, M., Orru, K., Heidrich, O., Olazabal, E., Geneletti, D., Orru, H., Bhawe, A., Mittal, N., Feliu, E., and Faehnle, M. (2014). Mitigating and adapting to climate change: Multi-functional and multi-scale assessment of green urban infrastructure. *Journal of environmental management*, 146:107–115.
- Dietzel, C., Herold, M., Hemphill, J. J., and Clarke, K. C. (2005). Spatio-temporal dynamics in california's central valley: Empirical links to urban theory. *International Journal of Geographical Information Science*, 19(2):175–195.
- Du, H., Cai, W., Xu, Y., Wang, Z., Wang, Y., and Cai, Y. (2017). Quantifying the cool island effects of urban green spaces using remote sensing data. *Urban Forestry & Urban Greening*, 27:24–31.
- Estoque, R. C., Murayama, Y., and Myint, S. W. (2017). Effects of landscape composition and pattern on land surface temperature: An urban heat island study in the megacities of Southeast Asia. *Science of the Total Environment*, 577:349–359.
- Ewing, R., Pendall, R., and Chen, D. (2002). Measuring sprawl and its impact. *Smart Growth America*.
- Ewing, R., Richardson, H., Burch, K. B., Nelson, A. C., and Bae, C. (2014). Compactness vs. sprawl revisited: Converging views. *CESifo Working Paper Series*.
- Ewing, R. H. (1995). Characteristics, causes, and effects of sprawl: A literature review. In *Urban Ecology*, pages 519–535. Springer.
- Fabrizi, R., Bonafoni, S., and Biondi, R. (2010). Satellite and ground-based sensors for the urban heat island analysis in the city of rome. *Remote sensing*, 2(5):1400–1415.
- Fan, C., Myint, S. W., and Zheng, B. (2015). Measuring the spatial arrangement of urban vegetation and its impacts on seasonal surface temperatures. *Progress in Physical Geography*, 39(2):199–219.
- Federal Office of Topography (2004). DhM25/200 m the free version of the digital height model of switzerland. Available from https://shop.swisstopo.admin.ch/en/products/height_models/dhm25200. Accessed: 21 March 2020.
- Federal Office of Topography (2019). Swissimage la mosaïque d'orthophotos de la suisse. Available from (in French) https://shop.swisstopo.admin.ch/fr/products/images/ortho_images/SWISSIMAGE. Accessed: 3 March 2020.
- Fenner, D., Holtmann, A., Meier, F., Langer, I., and Scherer, D. (2019). Contrasting changes of urban heat island intensity during hot weather episodes. *Environmental Research Letters*, 14(12):124013.
- Fenner, D., Meier, F., Bechtel, B., Otto, M., and Scherer, D. (2017). Intra and inter 'local climate zone' variability of air temperature as observed by crowdsourced citizen weather stations in Berlin, Germany. *10.14279/depositonce-10378*.

- Forman, R., Foreman, R., and Godron, M. (1986). *Landscape Ecology*. Wiley.
- Forman, R. T. (1995). Some general principles of landscape and regional ecology. *Landscape ecology*, 10(3):133–142.
- Forman, R. T. and Godron, M. (1981). Patches and structural components for a landscape ecology. *BioScience*, 31(10):733–740.
- Fragkias, M., Güneralp, B., Seto, K. C., and Goodness, J. (2013). A synthesis of global urbanization projections. In *Urbanization, biodiversity and ecosystem services: Challenges and opportunities*, pages 409–435. Springer, Dordrecht.
- Frankhauser, P. (1990). Aspects fractals des structures urbaines. *L'Espace géographique*, pages 45–69.
- Frankhauser, P. (1994). *La fractalité des structures urbaines*. Anthropos.
- Frankhauser, P., Tannier, C., Vuidel, G., and Houot, H. (2018). An integrated multifractal modelling to urban and regional planning. *Computers, Environment and Urban Systems*, 67:132–146.
- Frei, C. (2014). Interpolation of temperature in a mountainous region using nonlinear profiles and non-euclidean distances. *International Journal of Climatology*, 34(5):1585–1605.
- Frenkel, A. and Ashkenazi, M. (2008). Measuring urban sprawl: how can we deal with it? *Environment and Planning B: Planning and Design*, 35(1):56–79.
- Gago, E. J., Roldan, J., Pacheco-Torres, R., and Ordóñez, J. (2013). The city and urban heat islands: A review of strategies to mitigate adverse effects. *Renewable and Sustainable Energy Reviews*, 25:749–758.
- Galster, G., Hanson, R., Ratcliffe, M. R., Wolman, H., Coleman, S., and Freihage, J. (2001). Wrestling sprawl to the ground: defining and measuring an elusive concept. *Housing policy debate*, 12(4):681–717.
- Gao, B.-C. (1996). NdwI—a normalized difference water index for remote sensing of vegetation liquid water from space. *Remote sensing of environment*, 58(3):257–266.
- Geneletti, D., Cortinovis, C., Zardo, L., and Esmail, B. A. (2020). *Planning for ecosystem services in cities*. Springer Nature.
- Gennaio, M.-P., Hersperger, A. M., and Bürgi, M. (2009). Containing urban sprawl—Evaluating effectiveness of urban growth boundaries set by the Swiss Land Use Plan. *Land use policy*, 26(2):224–232.
- Georgescu, M., Chow, W. T., Wang, Z., Brazel, A., Trapido-Lurie, B., Roth, M., and Benson-Lira, V. (2015). Prioritizing urban sustainability solutions: coordinated approaches must incorporate scale-dependent built environment induced effects. *Environmental Research Letters*, 10(6):061001.

Bibliography

- Gerecke, M., Hagen, O., Bolliger, J., Hersperger, A. M., Kienast, F., Price, B., and Pellissier, L. (2019). Assessing potential landscape service trade-offs driven by urbanization in Switzerland. *Palgrave Communications*, 5(1):1–13.
- Gill, S. E., Handley, J. F., Ennos, A. R., and Pauleit, S. (2007). Adapting cities for climate change: the role of the green infrastructure. *Built environment*, 33(1):115–133.
- Gillham, O. (2002). *The limitless city: a primer on the urban sprawl debate*. Island Press.
- Gillner, S., Vogt, J., Tharang, A., Dettmann, S., and Roloff, A. (2015). Role of street trees in mitigating effects of heat and drought at highly sealed urban sites. *Landscape and Urban Planning*, 143:33–42.
- Golden, J. S., Brazel, A., Salmond, J., and Laws, D. (2006). Energy and water sustainability: The role of urban climate change from metropolitan infrastructure. *Journal of Green Building*, 1(3):124–138.
- Gómez-Baggethun, E. and Barton, D. N. (2013). Classifying and valuing ecosystem services for urban planning. *Ecological Economics*, 86:235–245.
- Gordon, P. and Wong, H. L. (1985). The costs of urban sprawl: some new evidence. *Environment and planning A*, 17(5):661–666.
- Grădinaru, S. R. and Hersperger, A. M. (2019). Green infrastructure in strategic spatial plans: Evidence from European urban regions. *Urban For. Urban Green*, 40:17–28.
- Green, O. O., Garmestani, A. S., Albro, S., Ban, N. C., Berland, A., Burkman, C. E., Gardiner, M. M., Gunderson, L., Hopton, M. E., Schoon, M. L., et al. (2016). Adaptive governance to promote ecosystem services in urban green spaces. *Urban ecosystems*, 19(1):77–93.
- Grimm, N. B., Faeth, S. H., Golubiewski, N. E., Redman, C. L., Wu, J., Bai, X., and Briggs, J. M. (2008). Global change and the ecology of cities. *science*, 319(5864):756–760.
- Grimm, N. B., Grove, J. G., Pickett, S. T., and Redman, C. L. (2000). Integrated approaches to long-term studies of urban ecological systems: Urban ecological systems present multiple challenges to ecologists—pervasive human impact and extreme heterogeneity of cities, and the need to integrate social and ecological approaches, concepts, and theory. *BioScience*, 50(7):571–584.
- Grimmond, S. and Oke, T. (1999). Evapotranspiration rates in urban areas. In *Proceedings of the Impacts of Urban Growth on Surface Water and Groundwater Quality HS5*, pages 235–243. International Association of Hydrological Sciences Publications.
- Grimmond, S. U. (2007). Urbanization and global environmental change: local effects of urban warming. *Geographical Journal*, 173(1):83–88.
- Grize, L., Huss, A., Thommen, O., Schindler, C., and Braun-Fahrlander, C. (2005). Heat wave 2003 and mortality in Switzerland. *Swiss Medical Weekly*, 135(13-14):200–205.

- Guelton, S., Brunet, P., Amini, M., Merlini, A., Corbillon, X., and Raynaud, A. (2015). Pythran: Enabling static optimization of scientific python programs. *Computational Science & Discovery*, 8(1):014001.
- Haaland, C. and van Den Bosch, C. K. (2015). Challenges and strategies for urban green-space planning in cities undergoing densification: A review. *Urban forestry & urban greening*, 14(4):760–771.
- Haase, D., Larondelle, N., Andersson, E., Artmann, M., Borgström, S., Breuste, J., Gomez-Baggethun, E., Gren, Å., Hamstead, Z., Hansen, R., et al. (2014). A quantitative review of urban ecosystem service assessments: concepts, models, and implementation. *Ambio*, 43(4):413–433.
- Haase, D., Schwarz, N., Strohbach, M., Kroll, F., and Seppelt, R. (2012). Synergies, trade-offs, and losses of ecosystem services in urban regions: an integrated multiscale framework applied to the leipzig-halle region, germany. *Ecology and Society*, 17(3).
- Haines, V. A. (1986). Energy and urban form a human ecological critique. *Urban Affairs Review*, 21(3):337–353.
- Hall, P. (2001). Sustainable cities or town cramming. *Planning for a sustainable future*, pages 101–114.
- Hall, P. and Tewdwr-Jones, M. (2010). *Urban and Regional Planning*. 100 Cases. Taylor & Francis.
- Hamel, P., Tardieu, L., Lemonsu, A., de Munck, C., and Viguié, V. (2020). Co-développement du module rafraîchissement offert par la végétation de l’outil InVEST. Report submitted to the Agence de l’environnement et de la Maîtrise de l’énergie (ADEME).
- Hamstead, Z. A., Kremer, P., Larondelle, N., McPhearson, T., and Haase, D. (2016). Classification of the heterogeneous structure of urban landscapes (sturla) as an indicator of landscape function applied to surface temperature in new york city. *Ecological Indicators*, 70:574–585.
- Hansen, R., Olafsson, A. S., van der Jagt, A. P., Rall, E., and Pauleit, S. (2019). Planning multi-functional green infrastructure for compact cities: what is the state of practice? *Ecological Indicators*, 96:99–110.
- Hargreaves, G. H. and Samani, Z. A. (1985). Reference crop evapotranspiration from temperature. *Applied engineering in agriculture*, 1(2):96–99.
- Harvey, R. O. and Clark, W. A. (1965). The nature and economics of urban sprawl. *Land Economics*, 41(1):1–9.
- Hein, L., van Koppen, C. K., van Ierland, E. C., and Leidekker, J. (2016). Temporal scales, ecosystem dynamics, stakeholders and the valuation of ecosystems services. *Ecosystem Services*, 21:109–119.

Bibliography

- Hersperger, A. M. (1994). Landscape ecology and its potential application to planning. *Journal of Planning Literature*, 9(1):14–29.
- Hersperger, A. M., Oliveira, E., Pagliarin, S., Palka, G., Verburg, P., Bolliger, J., and Grădinaru, S. (2018). Urban land-use change: The role of strategic spatial planning. *Global Environmental Change*, 51:32–42.
- Hesselbarth, M. H., Sciaini, M., With, K. A., Wiegand, K., and Nowosad, J. (2019). landscape-metrics: an open-source r tool to calculate landscape metrics. *Ecography*.
- Heymann, Y., Steenmans, C., Croisille, G., and Bossard, M. (1994). Corine land cover: Technical guide.
- Hirabayashi, S., Nowak, D., Endreny, T., Kroll, C., and Maco, S. (2011). i-tree: Tools to assess and manage structure, function, and value of community forests. In *AGU Fall Meeting Abstracts*, volume 2011, pages B21B–0263.
- Ho, H. C., Knudby, A., Sirovyak, P., Xu, Y., Hodul, M., and Henderson, S. B. (2014). Mapping maximum urban air temperature on hot summer days. *Remote Sensing of Environment*, 154:38–45.
- Holt, A. R., Mears, M., Maltby, L., and Warren, P. (2015). Understanding spatial patterns in the production of multiple urban ecosystem services. *Ecosystem services*, 16:33–46.
- Howard, L. (1818). *The Climate of London: Deduced from Meteorological Observations, Made at Different Places in the Neighbourhood of the Metropolis*. Number vol. 1 in *The Climate of London*. W. Phillips, George Yard, Lombard Street, sold also by J. and A. Arch, Cornhill; Baldwin, Cradock, and Joy, and W. Bent, Paternoster Row; and J. Hatchard, Picadilly.
- Huang, K., Li, X., Liu, X., and Seto, K. C. (2019). Projecting global urban land expansion and heat island intensification through 2050. *Environmental Research Letters*, 14(11):114037.
- Hunter, J. D. (2007). Matplotlib: A 2d graphics environment. *Computing in science & engineering*, 9(3):90.
- Irwin, E. G., Jayaprakash, C., and Munroe, D. K. (2009). Towards a comprehensive framework for modeling urban spatial dynamics. *Landscape ecology*, 24(9):1223–1236.
- Jacobs, J. (1961). *The Death and Life of Great American Cities*. Vintage Books ed. Vintage Books.
- Jaeger, J. A. and Schwick, C. (2014). Improving the measurement of urban sprawl: Weighted Urban Proliferation (WUP) and its application to Switzerland. *Ecological indicators*, 38:294–308.
- Jaganmohan, M., Knapp, S., Buchmann, C. M., and Schwarz, N. (2016). The bigger, the better? the influence of urban green space design on cooling effects for residential areas. *Journal of environmental quality*, 45(1):134–145.

- Jaligot, R., Chenal, J., and Bosch, M. (2019a). Assessing spatial temporal patterns of ecosystem services in Switzerland. *Landscape Ecology*, 34(6):1379–1394.
- Jaligot, R., Chenal, J., Bosch, M., and Hasler, S. (2019b). Historical dynamics of ecosystem services and land management policies in Switzerland. *Ecological Indicators*, 101:81–90.
- Jenerette, G. D. and Potere, D. (2010). Global analysis and simulation of land-use change associated with urbanization. *Landscape ecology*, 25(5):657–670.
- Jiao, M., Zhou, W., Zheng, Z., Wang, J., and Qian, Y. (2017). Patch size of trees affects its cooling effectiveness: A perspective from shading and transpiration processes. *Agricultural and Forest Meteorology*, 247:293–299.
- Jim, C. Y. (2004). Green-space preservation and allocation for sustainable greening of compact cities. *Cities*, 21(4):311–320.
- Jim, C. Y. (2013). Sustainable urban greening strategies for compact cities in developing and developed economies. *Urban Ecosystems*, 16(4):741–761.
- Jin, M. and Dickinson, R. E. (2010). Land surface skin temperature climatology: Benefitting from the strengths of satellite observations. *Environmental Research Letters*, 5(4):044004.
- Johnson, S., Ross, Z., Kheirbek, I., and Ito, K. (2020). Characterization of intra-urban spatial variation in observed summer ambient temperature from the New York City community air survey. *Urban Climate*, 31:100583.
- Jung, M. (2016). Lecos—a python plugin for automated landscape ecology analysis. *Ecological informatics*, 31:18–21.
- Jung, M. C., Dyson, K., and Alberti, M. (2021). Urban landscape heterogeneity influences the relationship between tree canopy and land surface temperature. *Urban Forestry & Urban Greening*, 57:12693p0.
- Kabisch, N., Frantzeskaki, N., Pauleit, S., Naumann, S., Davis, M., Artmann, M., Haase, D., Knapp, S., Korn, H., Stadler, J., et al. (2016). Nature-based solutions to climate change mitigation and adaptation in urban areas: perspectives on indicators, knowledge gaps, barriers, and opportunities for action. *Ecology and Society*, 21(2).
- Kadaverugu, A., Rao, C. N., and Viswanadh, G. (2020). Quantification of flood mitigation services by urban green spaces using InVEST model: a case study of Hyderabad City, India. *Modeling Earth Systems and Environment*, pages 1–14.
- Kadaverugu, R., Gurav, C., Rai, A., Sharma, A., Matli, C., and Biniwale, R. (2021). Quantification of heat mitigation by urban green spaces using InVEST model—a scenario analysis of Nagpur City, India. *Arabian Journal of Geosciences*, 14(2):1–13.
- Kirkpatrick, S., Gelatt, C. D., and Vecchi, M. P. (1983). Optimization by simulated annealing. *science*, 220(4598):671–680.

Bibliography

- Kjellstrom, T., Holmer, I., and Lemke, B. (2009). Workplace heat stress, health and productivity—an increasing challenge for low and middle-income countries during climate change. *Global health action*, 2(1):2047.
- Kluyver, T., Ragan-Kelley, B., Pérez, F., Granger, B. E., Bussonnier, M., Frederic, J., Kelley, K., Hamrick, J. B., Grout, J., Corlay, S., et al. (2016). Jupyter notebooks—a publishing format for reproducible computational workflows. In *Positioning and Power in Academic Publishing: Players, Agents and Agendas*, pages 87–90. IOS Press.
- Ko, Y., Lee, J.-H., McPherson, E. G., and Roman, L. A. (2015). Long-term monitoring of sacramento shade program trees: Tree survival, growth and energy-saving performance. *Landscape and Urban Planning*, 143:183–191.
- Koc, C. B., Osmond, P., and Peters, A. (2018). Evaluating the cooling effects of green infrastructure: A systematic review of methods, indicators and data sources. *Solar Energy*, 166:486–508.
- Kohler, M., Tannier, C., Blond, N., Aguejdad, R., and Clappier, A. (2017). Impacts of several urban-sprawl countermeasures on building (space heating) energy demands and urban heat island intensities. a case study. *Urban Climate*, 19:92–121.
- Kong, F., Yin, H., James, P., Hutyra, L. R., and He, H. S. (2014). Effects of spatial pattern of greenspace on urban cooling in a large metropolitan area of eastern China. *Landscape and Urban Planning*, 128:35–47.
- Koppe, C., Sari Kovats, R., Menne, B., Jendritzky, G., Wetterdienst, D., Organization, W. H., et al. (2004). Heat-waves: risks and responses. Technical report, Copenhagen: WHO Regional Office for Europe.
- Kovats, R. S. and Hajat, S. (2008). Heat stress and public health: a critical review. *Annu. Rev. Public Health*, 29:41–55.
- Krayenhoff, E., Christen, A., Martilli, A., and Oke, T. (2014). A multi-layer radiation model for urban neighbourhoods with trees. *Boundary-layer meteorology*, 151(1):139–178.
- Krayenhoff, E. S., Broadbent, A. M., Zhao, L., Georgescu, M., Middel, A., Voogt, J. A., Martilli, A., Sailor, D. J., and Erell, E. (2021). Cooling hot cities: A systematic and critical review of the numerical modelling literature. *Environmental Research Letters*.
- Krayenhoff, E. S., Jiang, T., Christen, A., Martilli, A., Oke, T. R., Bailey, B. N., Nazarian, N., Voogt, J. A., Giometto, M. G., Stastny, A., et al. (2020). A multi-layer urban canopy meteorological model with trees (bep-tree): Street tree impacts on pedestrian-level climate. *Urban Climate*, 32:100590.
- Kremer, P., Hamstead, Z. A., and McPhearson, T. (2016). The value of urban ecosystem services in new york city: A spatially explicit multicriteria analysis of landscape scale valuation scenarios. *Environmental Science & Policy*, 62:57–68.

- Laaïdi, K., Zeghnoun, A., Dousset, B., Bretin, P., Vandentorren, S., Giraudet, E., and Beaudeau, P. (2012). The impact of heat islands on mortality in Paris during the August 2003 heat wave. *Environmental health perspectives*, 120(2):254–259.
- Labeledens, S., Scartezzini, J.-L., and Mauree, D. (2019). Modeling of mesoscale phenomena using WRF-BEP-BEM-CIM in a complex region. In *Journal of Physics: Conference Series*, volume 1343, page 012012. IOP Publishing.
- Larondelle, N., Hamstead, Z. A., Kremer, P., Haase, D., and McPhearson, T. (2014). Applying a novel urban structure classification to compare the relationships of urban structure and surface temperature in berlin and new york city. *Applied Geography*, 53:427–437.
- Leconte, F., Bouyer, J., Claverie, R., and Pétrissans, M. (2015). Using local climate zone scheme for uhi assessment: Evaluation of the method using mobile measurements. *Building and Environment*, 83:39–49.
- Leitao, A. B. and Ahern, J. (2002). Applying landscape ecological concepts and metrics in sustainable landscape planning. *Landscape and urban planning*, 59(2):65–93.
- Lemonsu, A., Viguie, V., Daniel, M., and Masson, V. (2015). Vulnerability to heat waves: Impact of urban expansion scenarios on urban heat island and heat stress in Paris (France). *Urban Climate*, 14:586–605.
- Li, C., Li, J., and Wu, J. (2013a). Quantifying the speed, growth modes, and landscape pattern changes of urbanization: a hierarchical patch dynamics approach. *Landscape ecology*, 28(10):1875–1888.
- Li, W., Cao, Q., Lang, K., and Wu, J. (2017). Linking potential heat source and sink to urban heat island: Heterogeneous effects of landscape pattern on land surface temperature. *Science of the Total Environment*, 586:457–465.
- Li, X., Zhou, W., and Ouyang, Z. (2013b). Relationship between land surface temperature and spatial pattern of greenspace: What are the effects of spatial resolution? *Landscape and Urban Planning*, 114:1–8.
- Li, X., Zhou, W., Ouyang, Z., Xu, W., and Zheng, H. (2012). Spatial pattern of greenspace affects land surface temperature: evidence from the heavily urbanized beijing metropolitan area, china. *Landscape ecology*, 27(6):887–898.
- Lin, B. B. and Fuller, R. A. (2013). Sharing or sparing? how should we grow the world's cities? *Journal of Applied Ecology*, 50(5):1161–1168.
- Lin, J. (2020). Developing a composite indicator to prioritize tree planting and protection locations. *Science of the Total Environment*, 717:137269.
- Liu, J., Dietz, T., Carpenter, S. R., Alberti, M., Folke, C., Moran, E., Pell, A. N., Deadman, P., Kratz, T., Lubchenco, J., et al. (2007). Complexity of coupled human and natural systems. *science*, 317(5844):1513–1516.

Bibliography

- Liu, X., Li, X., Chen, Y., Tan, Z., Li, S., and Ai, B. (2010). A new landscape index for quantifying urban expansion using multi-temporal remotely sensed data. *Landscape ecology*, 25(5):671–682.
- Liu, Z., He, C., and Wu, J. (2016). General spatiotemporal patterns of urbanization: An examination of 16 world cities. *Sustainability*, 8(1):41.
- Liu, Z., He, C., Zhou, Y., and Wu, J. (2014). How much of the world's land has been urbanized, really? a hierarchical framework for avoiding confusion. *Landscape Ecology*, 29(5):763–771.
- Locke, D. H., Grove, J. M., Lu, J. W., Troy, A., O'Neil-Dunne, J. P., and Beck, B. D. (2010). Prioritizing preferable locations for increasing urban tree canopy in new york city. *Cities and the Environment (CATE)*, 3(1):4.
- Maimaitiyiming, M., Ghulam, A., Tiyp, T., Pla, F., Latorre-Carmona, P., Halik, Ü., Sawut, M., and Caetano, M. (2014). Effects of green space spatial pattern on land surface temperature: Implications for sustainable urban planning and climate change adaptation. *ISPRS Journal of Photogrammetry and Remote Sensing*, 89:59–66.
- Mandelbrot, B. B. (1983). *The fractal geometry of nature*, volume 173. WH freeman New York.
- Mann, S. (2009). Institutional causes of urban and rural sprawl in switzerland. *Land use policy*, 26(4):919–924.
- Manson, S. and O'Sullivan, D. (2006). Complexity theory in the study of space and place. *Environment and Planning A*, 38(4):677–692.
- Martilli, A., Clappier, A., and Rotach, M. W. (2002). An urban surface exchange parameterisation for mesoscale models. *Boundary-layer meteorology*, 104(2):261–304.
- Masson, V. (2000). A physically-based scheme for the urban energy budget in atmospheric models. *Boundary-layer meteorology*, 94(3):357–397.
- Matte, T. D., Ross, Z., Kheirbek, I., Eisl, H., Johnson, S., Gorczynski, J. E., Kass, D., Markowitz, S., Pezeshki, G., and Clougherty, J. E. (2013). Monitoring intraurban spatial patterns of multiple combustion air pollutants in New York City: design and implementation. *Journal of exposure science & environmental epidemiology*, 23(3):223–231.
- Matthias Bussonnier, Jessica Forde, Jeremy Freeman, Brian Granger, Tim Head, Chris Holdgraf, Kyle Kelley, Gladys Nalvarte, Andrew Osherooff, Pacer, M., Yuvi Panda, Fernando Perez, Benjamin Ragan Kelley, and Carol Willing (2018). Binder 2.0 - reproducible, interactive, sharable environments for science at scale. In *Proceedings of the 17th Python in Science Conference*, pages 113–120.
- Mauree, D., Naboni, E., Coccolo, S., Perera, A. T. D., Nik, V. M., and Scartezzini, J.-L. (2019). A review of assessment methods for the urban environment and its energy sustainability to guarantee climate adaptation of future cities. *Renewable and Sustainable Energy Reviews*, 112:733–746.

- McDonnell, M. J. and Pickett, S. T. (1990). Ecosystem structure and function along urban-rural gradients: an unexploited opportunity for ecology. *Ecology*, 71(4):1232–1237.
- McGarigal, K., Cushman, S. A., and Ene, E. (2012). Fragstats v4: spatial pattern analysis program for categorical and continuous maps. Computer software program produced by the authors at the University of Massachusetts, Amherst. Available at: <http://www.umass.edu/landeco/research/fragstats/fragstats.html>.
- McGarigal, K. and Marks, B. J. (1995). Fragstats: spatial pattern analysis program for quantifying landscape structure. *Gen. Tech. Rep. PNW-GTR-351. Portland, OR: US Department of Agriculture, Forest Service, Pacific Northwest Research Station. 122 p*, 351.
- McHale, M. R., Pickett, S. T., Barbosa, O., Bunn, D. N., Cadenasso, M. L., Childers, D. L., Gartin, M., Hess, G. R., Iwaniec, D. M., McPhearson, T., et al. (2015). The new global urban realm: complex, connected, diffuse, and diverse social-ecological systems. *Sustainability*, 7(5):5211–5240.
- McKinney, W. (2010). Data structures for statistical computing in python. In van der Walt, S. and Millman, J., editors, *Proceedings of the 9th Python in Science Conference*, volume 445, pages 51–56. Austin, TX.
- McPhearson, T., Pickett, S. T., Grimm, N. B., Niemelä, J., Alberti, M., Elmqvist, T., Weber, C., Haase, D., Breuste, J., and Qureshi, S. (2016). Advancing urban ecology toward a science of cities. *BioScience*, page biw002.
- Medley, K. E., McDonnell, M. J., and Pickett, S. T. (1995). Forest-landscape structure along an urban-to-rural gradient. *The Professional Geographer*, 47(2):159–168.
- Meehl, G. A. and Tebaldi, C. (2004). More intense, more frequent, and longer lasting heat waves in the 21st century. *Science*, 305(5686):994–997.
- Meentemeyer, V. and Box, E. O. (1987). Scale effects in landscape studies. In *Landscape heterogeneity and disturbance*, pages 15–34. Springer.
- Meier, F., Fenner, D., Grassmann, T., Otto, M., and Scherer, D. (2017). Crowdsourcing air temperature from citizen weather stations for urban climate research. *Urban Climate*, 19:170–191.
- Mirzaei, P. A. (2015). Recent challenges in modeling of urban heat island. *Sustainable cities and society*, 19:200–206.
- Mitsova, D., Shuster, W., and Wang, X. (2011). A cellular automata model of land cover change to integrate urban growth with open space conservation. *Landscape and Urban Planning*, 99(2):141–153.
- Mouchet, M. A., Lamarque, P., Martín-López, B., Crouzat, E., Gos, P., Byczek, C., and Lavorel, S. (2014). An interdisciplinary methodological guide for quantifying associations between ecosystem services. *Global environmental change*, 28:298–308.

Bibliography

- Muller, C., Chapman, L., Johnston, S., Kidd, C., Illingworth, S., Foody, G., Overeem, A., and Leigh, R. (2015). Crowdsourcing for climate and atmospheric sciences: Current status and future potential. *International Journal of Climatology*, 35(11):3185–3203.
- Müller, F. and Burkhard, B. (2012). The indicator side of ecosystem services. *Ecosystem Services*, 1(1):26–30.
- Myint, S. W., Zheng, B., Talen, E., Fan, C., Kaplan, S., Middel, A., Smith, M., Huang, H.-P., and Brazel, A. (2015). Does the spatial arrangement of urban landscape matter? examples of urban warming and cooling in phoenix and las vegas. *Ecosystem Health and Sustainability*, 1(4):1–15.
- Nastran, M., Kobal, M., and Eler, K. (2019). Urban heat islands in relation to green land use in European cities. *Urban Forestry & Urban Greening*, 37:33–41.
- National Center for Climate Services (2018). CH2018 - Climate Scenarios for Switzerland. Available from <https://www.nccs.admin.ch/nccs/en/home/climate-change-and-impacts/swiss-climate-change-scenarios/technical-report.html>. Accessed: 17 Nov 2020.
- Newman, P. W. and Kenworthy, J. R. (1989). Gasoline consumption and cities: a comparison of US cities with a global survey. *Journal of the american planning association*, 55(1):24–37.
- Niemelä, J. (1999). Is there a need for a theory of urban ecology? *Urban Ecosystems*, 3(1):57–65.
- Nistor, M.-M. (2016). Mapping evapotranspiration coefficients in the paris metropolitan area. *GEOREVIEW Scientific Annals of Ștefan cel Mare University of Suceava, Geography Series*, 26(1):138–153.
- Nistor, M.-M., Gualtieri, A. F., Cheval, S., Dezsi, Ș., and Boțan, V. E. (2016). Climate change effects on crop evapotranspiration in the carpathian region from 1961 to 2010. *Meteorological applications*, 23(3):462–469.
- Nistor, M.-M. and Porumb, G. C. G. (2015). How to compute the land cover evapotranspiration at regional scale? a spatial approach of emilia-romagna region. *GEOREVIEW: Scientific Annals of Ștefan cel Mare University of Suceava. Geography Series*, 25(1):38–53.
- Nong, D. H., Lepczyk, C. A., Miura, T., and Fox, J. M. (2018). Quantifying urban growth patterns in Hanoi using landscape expansion modes and time series spatial metrics. *PloS one*, 13(5):e0196940.
- Oke, T. R. (1973). City size and the urban heat island. *Atmospheric Environment (1967)*, 7(8):769–779.
- Oke, T. R. (1982). The energetic basis of the urban heat island. *Quarterly Journal of the Royal Meteorological Society*, 108(455):1–24.

- Oleson, K. W., Bonan, G. B., Feddema, J., and Jackson, T. (2011). An examination of urban heat island characteristics in a global climate model. *International Journal of Climatology*, 31(12):1848–1865.
- Oliveira, E. A., Andrade Jr, J. S., and Makse, H. A. (2014). Large cities are less green. *Scientific reports*, 4.
- O'Neill, R., Krummel, J., Gardner, R., Sugihara, G., Jackson, B., DeAngelis, D., Milne, B., Turner, M. G., Zygmunt, B., Christensen, S., Dale, V., and Graham, R. (1988). Indices of landscape pattern. *Landscape ecology*, 1(3):153–162.
- O'Neill, R. V., Deangelis, D. L., Waide, J. B., Allen, T. F., and Allen, G. E. (1986). *A hierarchical concept of ecosystems*. Number 23 in Monographs in Population Biology. Princeton University Press.
- Pedregosa, F., Varoquaux, G., Gramfort, A., Michel, V., Thirion, B., Grisel, O., Blondel, M., Prettenhofer, P., Weiss, R., Dubourg, V., et al. (2011). Scikit-learn: Machine learning in python. *Journal of machine learning research*, 12(Oct):2825–2830.
- Peters, E. B., McFadden, J. P., and Montgomery, R. A. (2010). Biological and environmental controls on tree transpiration in a suburban landscape. *Journal of Geophysical Research: Biogeosciences*, 115(G4).
- Phelan, P. E., Kaloush, K., Miner, M., Golden, J., Phelan, B., Silva III, H., and Taylor, R. A. (2015). Urban heat island: mechanisms, implications, and possible remedies. *Annual Review of Environment and Resources*, 40:285–307.
- Pickett, S. T., Burch, W. R., Dalton, S. E., Foresman, T. W., Grove, J. M., and Rowntree, R. (1997). A conceptual framework for the study of human ecosystems in urban areas. *Urban ecosystems*, 1(4):185–199.
- Pickett, S. T. and Cadenasso, M. L. (1995). Landscape ecology: spatial heterogeneity in ecological systems. *Science*, 269(5222):331–334.
- Pickett, S. T., Cadenasso, M. L., Grove, J. M., Nilon, C. H., Pouyat, R. V., Zipperer, W. C., and Costanza, R. (2001). Urban ecological systems: linking terrestrial ecological, physical, and socioeconomic components of metropolitan areas. *Annual review of ecology and systematics*, 32(1):127–157.
- Pincetl, S., Gillespie, T., Pataki, D. E., Saatchi, S., and Saphores, J.-D. (2013). Urban tree planting programs, function or fashion? los angeles and urban tree planting campaigns. *GeoJournal*, 78(3):475–493.
- Popper, K. R. (1992). *The Open Universe: An Argument for Indeterminism*. PostScript to the Logic of Scientific Discovery, volume 2. Routledge.
- Portugali, J. (2000). *Self-organization and the city*. Springer Science & Business Media.

Bibliography

- Price, B., Kienast, F., Seidl, I., Ginzler, C., Verburg, P. H., and Bolliger, J. (2015). Future landscapes of Switzerland: Risk areas for urbanisation and land abandonment. *Applied Geography*, 57:32–41.
- Ragettli, M. S., Vicedo-Cabrera, A. M., Schindler, C., and Rösli, M. (2017). Exploring the association between heat and mortality in Switzerland between 1995 and 2013. *Environmental research*, 158:703–709.
- Rahman, M., Armson, D., and Ennos, A. (2015). A comparison of the growth and cooling effectiveness of five commonly planted urban tree species. *Urban Ecosystems*, 18(2):371–389.
- Rahman, M. A., Moser, A., Rötzer, T., and Pauleit, S. (2019). Comparing the transpirational and shading effects of two contrasting urban tree species. *Urban Ecosystems*, 22(4):683–697.
- Raudsepp-Hearne, C., Peterson, G. D., and Bennett, E. M. (2010). Ecosystem service bundles for analyzing tradeoffs in diverse landscapes. *Proceedings of the National Academy of Sciences*, 107(11):5242–5247.
- Real Estate Research Corporation (1974). *The costs of sprawl*. Number v. 1-3 in The Costs of Sprawl: Environmental and Economic Costs of Alternative Residential Development Patterns at the Urban Fringe. U.S. Government. Printing Office.
- Rebetez, M., von Arx, G., Gessler, A., Pannatier, E. G., Innes, J. L., Jakob, P., Jetel, M., Kube, M., Nötzli, M., Schaub, M., et al. (2018). Meteorological data series from swiss long-term forest ecosystem research plots since 1997. *Annals of Forest Science*, 75(2):41.
- Redon, E., Lemonsu, A., and Masson, V. (2020). An urban trees parameterization for modeling microclimatic variables and thermal comfort conditions at street level with the town energy balance model (teb-surfex v8. 0). *Geoscientific Model Development*, 13(2):385–399.
- Redon, E. C., Lemonsu, A., Masson, V., Morille, B., and Musy, M. (2017). Implementation of street trees within the solar radiative exchange parameterization of TEB in SURFEX v8.0. *Geoscientific Model Development*, 10(1):385–411.
- Renard, D., Rhemtulla, J. M., and Bennett, E. M. (2015). Historical dynamics in ecosystem service bundles. *Proceedings of the National Academy of Sciences*, 112(43):13411–13416.
- Rhee, J., Park, S., and Lu, Z. (2014). Relationship between land cover patterns and surface temperature in urban areas. *GIScience & remote sensing*, 51(5):521–536.
- Ridd, M. K. (1995). Exploring a vis (vegetation-impervious surface-soil) model for urban ecosystem analysis through remote sensing: comparative anatomy for cities. *International journal of remote sensing*, 16(12):2165–2185.
- Rüters, K. H., O'Neill, R., Hunsaker, C., Wickham, J. D., Yankee, D., Timmins, S., Jones, K., and Jackson, B. (1995). A factor analysis of landscape pattern and structure metrics. *Landscape ecology*, 10(1):23–39.

- Rodríguez, J. P., Beard Jr, T. D., Bennett, E. M., Cumming, G. S., Cork, S. J., Agard, J., Dobson, A. P., and Peterson, G. D. (2006). Trade-offs across space, time, and ecosystem services. *Ecology and society*, 11(1).
- Roman, L. A., Conway, T. M., Eisenman, T. S., Koeser, A. K., Barona, C. O., Locke, D. H., Jenerette, G. D., Östberg, J., and Vogt, J. (2020). Beyond ‘trees are good’: Disservices, management costs, and tradeoffs in urban forestry. *Ambio*, pages 1–16.
- Ronchi, S., Salata, S., and Arcidiacono, A. (2020). Which urban design parameters provide climate-proof cities? an application of the urban cooling InVEST model in the city of Milan comparing historical planning morphologies. *Sustainable Cities and Society*, 63:102459.
- Rozenfeld, H. D., Rybski, D., Andrade, J. S., Batty, M., Stanley, H. E., and Makse, H. A. (2008). Laws of population growth. *Proceedings of the National Academy of Sciences*, 105(48):18702–18707.
- Rudolf, S. C., Kienast, F., and Hersperger, A. M. (2018). Planning for compact urban forms: local growth-management approaches and their evolution over time. *Journal of environmental planning and management*, 61(3):474–492.
- Santamouris, M. (2016). Innovating to zero the building sector in europe: Minimising the energy consumption, eradication of the energy poverty and mitigating the local climate change. *Solar Energy*, 128:61–94.
- Santamouris, M., Ban-Weiss, G., Osmond, P., Paolini, R., Synnefa, A., Cartalis, C., Muscio, A., Zinzi, M., Morakinyo, T. E., Ng, E., et al. (2018). Progress in urban greenery mitigation science—assessment methodologies advanced technologies and impact on cities. *Journal of Civil Engineering and Management*, 24(8):638–671.
- Santamouris, M., Cartalis, C., Synnefa, A., and Kolokotsa, D. (2015). On the impact of urban heat island and global warming on the power demand and electricity consumption of buildings—a review. *Energy and Buildings*, 98:119–124.
- Saura, S. and Martinez-Millan, J. (2001). Sensitivity of landscape pattern metrics to map spatial extent. *Photogrammetric engineering and remote sensing*, 67(9):1027–1036.
- Schatz, J. and Kucharik, C. J. (2015). Urban climate effects on extreme temperatures in Madison, Wisconsin, USA. *Environmental Research Letters*, 10(9):094024.
- Schneider, A. and Woodcock, C. E. (2008). Compact, dispersed, fragmented, extensive? a comparison of urban growth in twenty-five global cities using remotely sensed data, pattern metrics and census information. *Urban Studies*, 45(3):659–692.
- Schwarz, N., Lautenbach, S., and Seppelt, R. (2011). Exploring indicators for quantifying surface urban heat islands of european cities with modis land surface temperatures. *Remote Sensing of Environment*, 115(12):3175–3186.

Bibliography

- Schwarz, N., Schlink, U., Franck, U., and Großmann, K. (2012). Relationship of land surface and air temperatures and its implications for quantifying urban heat island indicators—an application for the city of leipzig (germany). *Ecological indicators*, 18:693–704.
- Scott, A. A., Zaitchik, B., Waugh, D. W., and O'Meara, K. (2017). Intraurban temperature variability in Baltimore. *Journal of Applied Meteorology and Climatology*, 56(1):159–171.
- Seabold, S. and Perktold, J. (2010). statsmodels: Econometric and statistical modeling with python. In *9th Python in Science Conference*.
- Šećerov, I. B., Savić, S. M., Milošević, D. D., Arsenović, D. M., Dolinaj, D. M., and Popov, S. B. (2019). Progressing urban climate research using a high-density monitoring network system. *Environmental monitoring and assessment*, 191(2):89.
- Seppelt, R., Dormann, C. F., Eppink, F. V., Lautenbach, S., and Schmidt, S. (2011). A quantitative review of ecosystem service studies: approaches, shortcomings and the road ahead. *Journal of applied Ecology*, 48(3):630–636.
- Seto, K. C., Dhakal, S., Bigio, A., Blanco, H., Delgado, G. C., Dewar, D., Huang, L., Inaba, A., Kansal, A., Lwasa, S., et al. (2014). Human settlements, infrastructure and spatial planning. *Climate Change 2014: Mitigation of Climate Change*, pages 923–1000.
- Seto, K. C. and Fragkias, M. (2005). Quantifying spatiotemporal patterns of urban land-use change in four cities of china with time series landscape metrics. *Landscape ecology*, 20(7):871–888.
- Seto, K. C., Fragkias, M., Güneralp, B., and Reilly, M. K. (2011). A meta-analysis of global urban land expansion. *PloS one*, 6(8):e23777.
- Seto, K. C., Güneralp, B., and Hutyrá, L. R. (2012). Global forecasts of urban expansion to 2030 and direct impacts on biodiversity and carbon pools. *Proceedings of the National Academy of Sciences*, 109(40):16083–16088.
- Sharp, R., Tallis, H., Ricketts, T., Guerry, A., Wood, S., Chaplin-Kramer, R., Nelson, E., Ennaanay, D., Wolny, S., Olwero, N., et al. (2020). Invest 3.8.0 user's guide. the Natural Capital Project.
- Sheng, L., Tang, X., You, H., Gu, Q., and Hu, H. (2017). Comparison of the urban heat island intensity quantified by using air temperature and landsat land surface temperature in hangzhou, china. *Ecological Indicators*, 72:738–746.
- Shi, Y., Lau, K. K.-L., Ren, C., and Ng, E. (2018). Evaluating the local climate zone classification in high-density heterogeneous urban environment using mobile measurement. *Urban Climate*, 25:167–186.
- Shiflett, S. A., Liang, L. L., Crum, S. M., Feyisa, G. L., Wang, J., and Jenerette, G. D. (2017). Variation in the urban vegetation, surface temperature, air temperature nexus. *Science of the Total Environment*, 579:495–505.

- Silva, E. A., Ahern, J., and Wileden, J. (2008). Strategies for landscape ecology: An application using cellular automata models. *Progress in Planning*, 70(4):133–177.
- Sobrino, J., Oltra-Carrió, R., Sòria, G., Bianchi, R., and Paganini, M. (2012). Impact of spatial resolution and satellite overpass time on evaluation of the surface urban heat island effects. *Remote Sensing of Environment*, 117:50–56.
- Song, J., Du, S., Feng, X., and Guo, L. (2014). The relationships between landscape compositions and land surface temperature: Quantifying their resolution sensitivity with spatial regression models. *Landscape and Urban Planning*, 123:145–157.
- Steiniger, S. and Hay, G. J. (2009). Free and open source geographic information tools for landscape ecology. *Ecological informatics*, 4(4):183–195.
- Stewart, I. and Oke, T. (2006). Methodological concerns surrounding the classification of urban and rural climate stations to define urban heat island magnitude. *preprints of ICUC6 Göteborg*, 431.
- Stewart, I. D. (2011). A systematic review and scientific critique of methodology in modern urban heat island literature. *International Journal of Climatology*, 31(2):200–217.
- Stewart, I. D. and Oke, T. R. (2012). Local climate zones for urban temperature studies. *Bulletin of the American Meteorological Society*, 93(12):1879–1900.
- Storn, R. and Price, K. (1997). Differential evolution—a simple and efficient heuristic for global optimization over continuous spaces. *Journal of global optimization*, 11(4):341–359.
- Stott, I., Soga, M., Inger, R., and Gaston, K. J. (2015). Land sparing is crucial for urban ecosystem services. *Frontiers in Ecology and the Environment*, 13(7):387–393.
- Sun, R. and Chen, L. (2017). Effects of green space dynamics on urban heat islands: Mitigation and diversification. *Ecosystem Services*, 23:38–46.
- Sun, R., Lü, Y., Yang, X., and Chen, L. (2019). Understanding the variability of urban heat islands from local background climate and urbanization. *Journal of cleaner production*, 208:743–752.
- Swiss Academy of Sciences (2018). Coup de projecteur sur le climat suisse. état des lieux et perspectives. *Swiss Academies Reports*, 11(5).
- Swiss Federal Council (2012). Sustainable development strategy 2012-2015. Available from <https://www.are.admin.ch/are/en/home/media/publications/sustainable-development/strategie-nachhaltige-entwicklung-2012-2015.html>. Accessed: 16 Nov 2020.
- Swiss Federal Office for Spatial Development (2013). Directives techniques sur les zones à bâtir. Available from (in French) https://www.are.admin.ch/are/fr/home/developpement-et-amenagement-du-territoire/droit-de-l_amenagement-du-territoire/revision-de-la-loi-sur-lamenagement-du-territoire--lat-/lat1.html. Accessed: 17 Nov 2020.

Bibliography

- Swiss Federal Office for the Environment (2018). Quand la ville surchauffe.
- Swiss Federal Statistical Office (2013). *Land use in Switzerland: results of the Swiss land use statistics*. Federal Statistical Office: Neuchatel, Switzerland.
- Swiss Federal Statistical Office (2014). L'espace à caractère urbain en Suisse en 2012: Une nouvelle définition des agglomérations et d'autres catégories d'espace urbain. Available from (in French) <https://www.bfs.admin.ch/bfs/fr/home/statistiques/themes-transversaux/analyses-spatiales/niveaux-geographiques.assetdetail.349554.html>. Accessed: 17 April 2019.
- Swiss Federal Statistical Office (2017). Statistique de la superficie selon nomenclature 2004 - standard. Available from (in French) <https://www.bfs.admin.ch/bfs/fr/home/services/geostat/geodonnees-statistique-federale/sol-utilisation-couverture/statistique-suisse-superficie/nomenclature-standard.assetdetail.4103540.html>. Accessed: 18 April 2019.
- Swiss Federal Statistical Office (2018). City statistics (urban audit). Data collection. Available from <https://www.bfs.admin.ch/bfs/en/home/statistics/cross-sectional-topics/city-statistics.html>. Accessed: 16 April 2019.
- Swiss Federal Statistical Office (2020). Statistique de la population et des ménages (statpop), géodonnées 2019. Available from (in French) <https://www.bfs.admin.ch/bfs/fr/home/services/geostat/geodonnees-statistique-federale/batiments-logements-menages-personnes/population-menages-depuis-2010.assetdetail.14027479.html>. Accessed: 23 September 2020.
- Swoczyna, T., Kalaji, H. M., Pietkiewicz, S., Borowski, J., and Zaras-Januszkiewicz, E. (2010). Photosynthetic apparatus efficiency of eight tree taxa as an indicator of their tolerance to urban environments. *Dendrobiology*, 63.
- Taha, H. (1997). Urban climates and heat islands: albedo, evapotranspiration, and anthropogenic heat. *Energy and buildings*, 25(2):99–103.
- Taha, H., Akbari, H., Rosenfeld, A., and Huang, J. (1988). Residential cooling loads and the urban heat island—the effects of albedo. *Building and environment*, 23(4):271–283.
- Tallis, H. and Polasky, S. (2009). Mapping and valuing ecosystem services as an approach for conservation and natural-resource management. *Annals of the New York Academy of Sciences*, 1162(1):265–283.
- Tannier, C., Foltête, J.-C., and Girardet, X. (2012). Assessing the capacity of different urban forms to preserve the connectivity of ecological habitats. *Landscape and urban planning*, 105(1-2):128–139.
- Tannier, C. and Thomas, I. (2013). Defining and characterizing urban boundaries: A fractal analysis of theoretical cities and Belgian cities. *Computers, Environment and Urban Systems*, 41:234–248.

- Terfa, B. K., Chen, N., Zhang, X., and Niyogi, D. (2020). Spatial configuration and extent explains the urban heat mitigation potential due to green spaces: Analysis over Addis Ababa, Ethiopia. *Remote Sensing*, 12(18):2876.
- Tomscha, S. A. and Gergel, S. E. (2016). Ecosystem service trade-offs and synergies misunderstood without landscape history. *Ecology and Society*, 21(1).
- Tomscha, S. A., Sutherland, I. J., Renard, D., Gergel, S. E., Rhemtulla, J. M., Bennett, E. M., Daniels, L. D., Eddy, I. M., and Clark, E. E. (2016). A guide to historical data sets for reconstructing ecosystem service change over time. *BioScience*, 66(9):747–762.
- Toparlar, Y., Blocken, B., Maiheu, B., and Van Heijst, G. (2017). A review on the CFD analysis of urban microclimate. *Renewable and Sustainable Energy Reviews*, 80:1613–1640.
- Torrens, P. M. and Alberti, M. (2000). Measuring sprawl. *CASA Working Paper Series*, 27.
- Tratalos, J., Fuller, R. A., Warren, P. H., Davies, R. G., and Gaston, K. J. (2007). Urban form, biodiversity potential and ecosystem services. *Landscape and urban planning*, 83(4):308–317.
- Trimmel, H., Weihs, P., Faroux, S., Formayer, H., Hamer, P., Hasel, K., Laimighofer, J., Leidinger, D., Masson, V., Nadeem, I., et al. (2019). Thermal conditions during heat waves of a mid-European metropolis under consideration of climate change, urban development scenarios and resilience measures for the mid-21st century. *Meteorologische Zeitschrift*.
- Tsin, P. K., Knudby, A., Krayenhoff, E. S., Ho, H. C., Brauer, M., and Henderson, S. B. (2016). Microscale mobile monitoring of urban air temperature. *Urban Climate*, 18:58–72.
- Turkelboom, F., Leone, M., Jacobs, S., Kelemen, E., García-Llorente, M., Baró, F., Termansen, M., Barton, D. N., Berry, P., Stange, E., et al. (2018). When we cannot have it all: Ecosystem services trade-offs in the context of spatial planning. *Ecosystem services*, 29:566–578.
- Turner, K. G., Anderson, S., Gonzales-Chang, M., Costanza, R., Courville, S., Dalgaard, T., Dominati, E., Kubiszewski, I., Ogilvy, S., Porfirio, L., et al. (2016). A review of methods, data, and models to assess changes in the value of ecosystem services from land degradation and restoration. *Ecological Modelling*, 319:190–207.
- Turner, M. G. (1989). Landscape ecology: the effect of pattern on process. *Annual review of ecology and systematics*, 20(1):171–197.
- Turner, M. G. (1990). Spatial and temporal analysis of landscape patterns. *Landscape ecology*, 4(1):21–30.
- Turner, M. G. and Gardner, R. H. (2015). *Landscape Ecology in Theory and Practice*. Springer New York.
- United Nations (1980). Patterns of urban and rural population growth.

Bibliography

- United Nations (2015). World urbanization prospects: The 2014 revision.
- United Nations (2018). World urbanization prospects: The 2018 revision.
- Van Der Walt, S., Colbert, S. C., and Varoquaux, G. (2011). The numpy array: a structure for efficient numerical computation. *Computing in Science & Engineering*, 13(2):22.
- Villa, F., Bagstad, K. J., Voigt, B., Johnson, G. W., Portela, R., Honzák, M., and Batker, D. (2014). A methodology for adaptable and robust ecosystem services assessment. *PloS one*, 9(3):e91001.
- Voogt, J. A. and Oke, T. R. (2003). Thermal remote sensing of urban climates. *Remote sensing of environment*, 86(3):370–384.
- Wang, J., Zhou, W., Jiao, M., Zheng, Z., Ren, T., and Zhang, Q. (2020a). Significant effects of ecological context on urban trees' cooling efficiency. *ISPRS Journal of Photogrammetry and Remote Sensing*, 159:78–89.
- Wang, J., Zhou, W., Wang, J., and Qian, Y. (2019). From quantity to quality: enhanced understanding of the changes in urban greenspace. *Landscape Ecology*, 34(5):1145–1160.
- Wang, L., Hou, H., and Weng, J. (2020b). Ordinary least squares modelling of urban heat island intensity based on landscape composition and configuration: A comparative study among three megacities along the Yangtze River. *Sustainable Cities and Society*, 62:102381.
- Weilenmann, B., Seidl, I., and Schulz, T. (2017). The socio-economic determinants of urban sprawl between 1980 and 2010 in Switzerland. *Landscape and Urban Planning*, 157:468–482.
- Weng, Q., Lu, D., and Schubring, J. (2004). Estimation of land surface temperature–vegetation abundance relationship for urban heat island studies. *Remote sensing of Environment*, 89(4):467–483.
- Werbin, Z. R., Heidari, L., Buckley, S., Brochu, P., Butler, L. J., Connolly, C., Houttuijn Bloemendaal, L., McCabe, T. D., Miller, T. K., and Hutyra, L. R. (2020). A tree-planting decision support tool for urban heat mitigation. *PloS one*, 15(10):e0224959.
- White, R. and Engelen, G. (1993). Cellular automata and fractal urban form: a cellular modelling approach to the evolution of urban land-use patterns. *Environment and planning A*, 25(8):1175–1199.
- White, R., Engelen, G., and Uljee, I. (2015). *Modeling Cities and Regions as Complex Systems: From Theory to Planning Applications*. MIT Press.
- Wiens, J. A. (1989). Spatial scaling in ecology. *Functional ecology*, 3(4):385–397.
- Windsor, D. (1979). A critique of the costs of sprawl. *Journal of the American Planning Association*, 45(3):279–292.

- Wolters, D. and Brandsma, T. (2012). Estimating the urban heat island in residential areas in the Netherlands using observations by weather amateurs. *Journal of Applied Meteorology and Climatology*, 51(4):711–721.
- Wu, J. (2004). Effects of changing scale on landscape pattern analysis: scaling relations. *Landscape ecology*, 19(2):125–138.
- Wu, J. (2014). Urban ecology and sustainability: The state-of-the-science and future directions. *Landscape and Urban Planning*, 125:209–221.
- Wu, J., Jelinski, D. E., Luck, M., and Tueller, P. T. (2000). Multiscale analysis of landscape heterogeneity: scale variance and pattern metrics. *Geographic information sciences*, 6(1):6–19.
- Wu, J., Jenerette, G. D., Buyantuyev, A., and Redman, C. L. (2011). Quantifying spatiotemporal patterns of urbanization: The case of the two fastest growing metropolitan regions in the united states. *Ecological Complexity*, 8(1):1–8.
- Wu, J. and Loucks, O. L. (1995). From balance of nature to hierarchical patch dynamics: a paradigm shift in ecology. *The Quarterly review of biology*, 70(4):439–466.
- Wu, J., Shen, W., Sun, W., and Tueller, P. T. (2002). Empirical patterns of the effects of changing scale on landscape metrics. *Landscape Ecology*, 17(8):761–782.
- Wu, J. J. (2008). Making the case for landscape ecology an effective approach to urban sustainability. *Landscape journal*, 27(1):41–50.
- Yamu, C. and Frankhauser, P. (2015). Spatial accessibility to amenities, natural areas and urban green spaces: using a multiscale, multifractal simulation model for managing urban sprawl. *Environment and Planning B: Planning and Design*, 42(6):1054–1078.
- Yan, J., Zhou, W., and Jenerette, G. D. (2019). Testing an energy exchange and microclimate cooling hypothesis for the effect of vegetation configuration on urban heat. *Agricultural and Forest Meteorology*, 279:107666.
- Yang, L., Niyogi, D., Tewari, M., Aliaga, D., Chen, F., Tian, F., and Ni, G. (2016). Contrasting impacts of urban forms on the future thermal environment: example of Beijing metropolitan area. *Environmental Research Letters*, 11(3):034018.
- Yang, L., Wu, X., Praun, E., and Ma, X. (2009). Tree detection from aerial imagery. In *Proceedings of the 17th ACM SIGSPATIAL International Conference on Advances in Geographic Information Systems*, pages 131–137. ACM.
- Yin, H., Kong, F., Hu, Y., James, P., Xu, F., and Yu, L. (2016). Assessing growth scenarios for their landscape ecological security impact using the sleuth urban growth model. *Journal of Urban Planning and Development*, 142(2):05015006.

Bibliography

- Young, R. F. (2010). Managing municipal green space for ecosystem services. *Urban forestry & urban greening*, 9(4):313–321.
- Yu, Z., Xu, S., Zhang, Y., Jørgensen, G., and Vejre, H. (2018). Strong contributions of local background climate to the cooling effect of urban green vegetation. *Scientific reports*, 8(1):1–9.
- Yu, Z., Yang, G., Zuo, S., Jørgensen, G., Koga, M., and Vejre, H. (2020). Critical review on the cooling effect of urban blue-green space: A threshold-size perspective. *Urban Forestry & Urban Greening*, 49:126630.
- Zander, K. K., Botzen, W. J., Oppermann, E., Kjellstrom, T., and Garnett, S. T. (2015). Heat stress causes substantial labour productivity loss in australia. *Nature Climate Change*, 5(7):647–651.
- Zanter, K. (2015). Landsat 8 (l8) data user handbook version 1.0. *EROS. South Dakota*.
- Zardo, L., Geneletti, D., Pérez-Soba, M., and Van Eupen, M. (2017). Estimating the cooling capacity of green infrastructures to support urban planning. *Ecosystem services*, 26:225–235.
- Zhang, C., Wu, J., Grimm, N. B., McHale, M., and Buyantuyev, A. (2013). A hierarchical patch mosaic ecosystem model for urban landscapes: model development and evaluation. *Ecological modelling*, 250:81–100.
- Zhou, D., Xiao, J., Bonafoni, S., Berger, C., Deilami, K., Zhou, Y., Frolking, S., Yao, R., Qiao, Z., and Sobrino, J. A. (2019). Satellite remote sensing of surface urban heat islands: progress, challenges, and perspectives. *Remote Sensing*, 11(1):48.
- Zhou, W., Huang, G., and Cadenasso, M. L. (2011). Does spatial configuration matter? understanding the effects of land cover pattern on land surface temperature in urban landscapes. *Landscape and urban planning*, 102(1):54–63.
- Zhou, W., Wang, J., and Cadenasso, M. L. (2017). Effects of the spatial configuration of trees on urban heat mitigation: A comparative study. *Remote Sensing of Environment*, 195:1–12.
- Zipperer, W. C., Wu, J., Pouyat, R. V., and Pickett, S. T. (2000). The application of ecological principles to urban and urbanizing landscapes. *Ecological applications*, pages 685–688.
- Ziter, C. D., Pedersen, E. J., Kucharik, C. J., and Turner, M. G. (2019). Scale-dependent interactions between tree canopy cover and impervious surfaces reduce daytime urban heat during summer. *Proceedings of the National Academy of Sciences*, 116(15):7575–7580.
- Zumwald, M., Knüsel, B., Bresch, D. N., and Knutti, R. (2020). Mapping urban temperature using crowd-sensing data and machine learning. *Urban Climate*, 35:100739.

A Appendix

A.1 Quantifying spatial patterns of landscapes

A.1.1 The PyLandStats library

Availability and installation

The source code of PyLandStats is available in a GitHub repository at <https://github.com/martibosch/pylandstats>, and is licensed under the open source GNU General Public License 3 (GNU GPLv3) to ensure that any derivative work is kept as open source. The easiest way to install PyLandStats is by installing the dedicated conda recipe hosted on the conda-forge channel at <https://anaconda.org/conda-forge/pylandstats>, as in:

```
$ conda install -c conda-forge pylandstats
```

The above command will install all the necessary requirements to run all the features of PyLandStats. Alternatively, a dedicated Python package is hosted on the Python Package Index (PyPI) at <https://pypi.org/project/pylandstats/>, and can be readily installed with pip as in:

```
$ pip install pylandstats
```

Nevertheless, the `BufferAnalysis` and `SpatioTemporalBufferAnalysis` classes have dependencies that cannot be installed with pip, namely the Geospatial Data Abstraction Library (GDAL) and the Geometry Engine Open Source (GEOS). In order to use these two PyLandStats classes, GDAL and GEOS must be present at the time of installing PyLandStats, which in this case will further require specifying the geo extra requirements as in:

```
$ pip install pylandstats[geo]
```

Unit tests are run within the Travis Continuous Integration (Travis CI) platform at <https://travis-ci.org/martibosch/pylandstats> every time that new commits are pushed to the GitHub repository. Additionally, test coverage is reported on Coveralls at <https://coveralls.io/github/martibosch/pylandstats?branch=master>.

The documentation of PyLandStats is hosted in Read the Docs at <https://pylandstats.readthedocs.io/> (see also appendix A.1.2). Additionally, a collection of example notebooks with a thorough overview of PyLandStats's features is provided at a dedicated GitHub repository at <https://github.com/martibosch/pylandstats-notebooks>, which can be executed interactively online by means of the Binder web service (Matthias Bussonnier et al., 2018). Such repository includes unit tests which ensure the correctness of the computations (see appendix A.1.7).

Finally, an example application of PyLandStats in an academic article can be found in the analysis of the spatiotemporal patterns of urbanization of three Swiss urban agglomerations by Bosch and Chenal (2019), and all the code and materials necessary to reproduce the results are available in a dedicated GitHub repository at <https://github.com/martibosch/swiss-urbanization>.

Dependencies and implementation details

The PyLandStats package is fully implemented in Python, and requires the Python packages NumPy, SciPy, pandas, matplotlib, rasterio. The first four are among the most popular packages for scientific and data-centric Python and are used for a wide-variety of scientific needs, whereas rasterio is a popular library to read and write geospatial raster data. In PyLandStats, NumPy arrays are used to represent landscapes and patch-level metrics. In addition, NumPy functions are used in the computations of all the implemented landscape metrics. The SciPy library is used to segment the patches in the landscape arrays, compute the inter-patch nearest-neighbor distances, and to compute the coefficient of variation of the patch-level landscape metrics. The pandas data frames are used to build the data frames of landscape metrics, matplotlib is used to produce the plots and rasterio is used to read raster data, plot the landscapes as well as to rasterize the vector geometries used in `BufferAnalysis` and `SpatioTemporalBufferAnalysis`. As noted above, the foregoing two classes further require the GeoPandas and Shapely Python packages.

The implementation of PyLandStats is organized in Python modules, where the classes described throughout this paper are defined. Such object-oriented design offers many advantages. On the one hand, it allows both for a conceptual separation and reusability of the functionalities, which enhances the maintainability and extensibility of PyLandStats. On the other hand, Python properties serve to cache results that are computationally expensive to obtain, which can later be accessed in constant (almost immediate) time. This mechanism is exploited to cache intermediate results that are later used to compute the metrics (see appendix A.1.8). More precisely, instances of the `Landscape` class cache the list of patches, each with its respective LULC class, area, perimeter and nearest-neighbor distance, as well as

the pixel adjacency matrix, i.e., the number of adjacencies between pixels of each landscape class (including adjacencies between pixels of the same class). Furthermore, such mechanism eases the task of implementing new metrics, since the vast majority of landscape metrics found throughout the academic literature can be straight-forwardly computed out of such cached properties (see the section “List of implemented metrics” of appendix A.1.2 as well as McGarigal et al. (2012)). Finally, as follows from the cache mechanism described above, the memory size of a Landscape instance scales linearly with the number of patches present in the respective raster landscape.

Regarding the performance, the most expensive operations of PyLandStats are the computation of the adjacency matrix, and more importantly, the computation of the inter-patch nearest-neighbor distances. The code for the former is transformed from Python to C++ by means of the Pythran ahead-of-time compiler (Guelton et al., 2015), which achieves speed-ups of an order of magnitude of three. The code for the latter consists of a slow nested Python loop that iterates over each patch of each class and employs SciPy’s implementation of the K-d tree in Cython (Behnel et al., 2011) in order to find the nearest neighbor of each patch. The computation of the inter-patch nearest-neighbor distances is by far the main performance bottleneck of PyLandStats (see appendix A.1.8), and it is therefore recommended that in analysis cases that do not require computing euclidean nearest-neighbor metrics avoid its computation by making use of the `metrics` keyword argument as explained above.

A.1.2 S1 Text

PyLandStats Documentation. <https://pylandstats.readthedocs.io/en/published>

A.1.3 S1 Code

Landscape analysis with PyLandStats for the canton of Vaud (Switzerland), as Jupyter Notebook (IPYNB). <https://github.com/martibosch/pylandstats-notebooks/tree/published/notebooks/01-landscape-analysis.ipynb>

A.1.4 S2 Code

Spatiotemporal analysis with PyLandStats for the canton of Vaud (Switzerland), as Jupyter Notebook (IPYNB). <https://github.com/martibosch/pylandstats-notebooks/tree/published/notebooks/02-spatiotemporal-analysis.ipynb>

A.1.5 S3 Code

Zonal analysis with PyLandStats for the canton of Vaud (Switzerland), as Jupyter Notebook (IPYNB). <https://github.com/martibosch/pylandstats-notebooks/tree/published/notebooks/03-zonal-analysis.ipynb>

A.1.6 S4 Code

Spatiotemporal buffer analysis with PyLandStats for the canton of Vaud (Switzerland), as Jupyter Notebook (IPYNB). <https://github.com/martibosch/pylandstats-notebooks/tree/published/notebooks/04-spatiotemporal-buffer-analysis.ipynb>

A.1.7 S5 Code

Comparison of the metrics computed in FRAGSTATS v4 and PyLandStats for the canton of Vaud (Switzerland), as Jupyter Notebook (IPYNB). <https://github.com/martibosch/pylandstats-notebooks/tree/published/notebooks/A01-fragstats-metrics-comparison.ipynb>

A.1.8 S6 Code

Performance notes and benchmarks comparing FRAGSTATS v4, landscapemetrics and PyLandStats, as Jupyter Notebook (IPYNB). <https://github.com/martibosch/pylandstats-notebooks/tree/published/notebooks/A02-performance-notes.ipynb>

A.2 Spatiotemporal patterns of urbanization in three Swiss urban agglomerations

A.2.1 Code S1

Exploration of the area-radius scaling of each urban agglomerations over the whole period of study, as Jupyter Notebook (IPYNB). https://github.com/martibosch/swiss-urbanization/tree/published/notebooks/area_radius_scaling.ipynb

A.2.2 Code S2

Computation of the time series of landscape metrics and exploration of their correlations over all the urban agglomerations and the whole period of study, as Jupyter Notebook (IPYNB). https://github.com/martibosch/swiss-urbanization/tree/published/notebooks/metrics_time_series.ipynb

A.2.3 Code S3

Computation of the relative dominance of the three growth modes over all the urban agglomerations and the whole period of study, as Jupyter Notebook (IPYNB). https://github.com/martibosch/swiss-urbanization/tree/published/notebooks/growth_modes.ipynb

A.3 Spatially-explicit simulation of urban heat islands

The code materials used in the article of chapter 4 are available at <https://doi.org/10.5281/zenodo.3970608> (Bosch, 2020b) and are maintained in a GitHub repository at <https://github.com/martibosch/lausanne-heat-islands>.

A.3.1 Data

Landsat tiles

The list of product identifiers of the Landsat image tiles are available as comma-separated value (CSV) file at <https://github.com/martibosch/lausanne-heat-islands/blob/master/data/raw/landsat-tiles.csv>

Monitoring stations

Monitoring stations with their operator and their elevation in meters above sea level. The operators are: Agrometeo, Federal roads office (ASTRA), Federal office for the environment (BAFU), General directorate for the environment of the Canton of Vaud (DGE), and the Federal Institute of Forest, Snow and Landscape Research (WSL) (Rebetez et al., 2018). The source CSV file used in the computational workflow is available at <https://github.com/martibosch/lausanne-heat-islands/blob/master/data/raw/tair-stations/station-locations.csv>.

Biophysical table

The crop and water coefficients are based on Allen et al. (1998), while rock, soil and urban coefficients are derived from the results of Grimmond and Oke (1999) in the city of Chicago. Given that the evapotranspiration of the vegetation and crops is subject to seasonal changes in temperate zones such as Switzerland (Allen et al., 1998), the values that correspond to the mid-season estimation (June to August) in Nistor (2016). The albedo values are based on the work of Stewart and Oke (2012). The shade column, which represents the proportion of tree cover of each LULC class, has been computed with a high resolution tree canopy map of Lausanne and is therefore specific to the study area. Rows with a hyphen sign - in the shade column denote that the corresponding LULC class is not present in the study area. The source CSV file used in the computational workflow is available at <https://github.com/martibosch/lausanne-heat-islands/blob/master/data/interim/biophysical-table-shade.csv>.

Reference temperatures and UHI magnitude

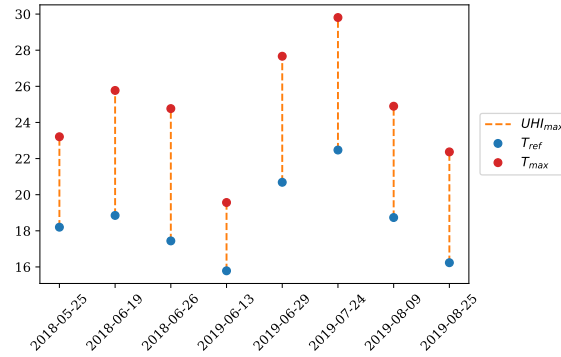


Figure A.1 – Reference temperatures T_{ref} (i.e., minimum T_{air} at 9 p.m. among the monitoring stations) and magnitude of the UHI UHI_{max} (i.e., difference between T_{ref} and the maximum T_{air} at 9 p.m. among the monitoring stations) of the 8 dates considered in this study.

A.3.2 Results

Spatial regression

The code of the spatial regression of air temperature from satellite data is available as a Jupyter Notebook (IPYNB) at <https://github.com/martibosch/lausanne-heat-islands/blob/master/notebooks/spatial-regression.ipynb>.

Feature	Coef.	Std. error	t	P> t	[0.025	0.975]
const	1.1760	3.369	0.349	0.728	-5.534	7.886
lst_0	0.4944	0.584	0.846	0.400	-0.669	1.658
ndwi_0	-6.1852	5.127	-1.206	0.231	-16.396	4.026
lst_200	-0.3267	0.885	-0.369	0.713	-2.089	1.435
ndwi_200	-28.5531	15.581	-1.833	0.071	-59.585	2.479
lst_400	-1.9332	1.765	-1.095	0.277	-5.449	1.583
ndwi_400	124.2456	46.749	2.658	0.010	31.138	217.353
lst_600	1.0526	2.963	0.355	0.723	-4.849	6.955
ndwi_600	-156.7220	55.931	-2.802	0.006	-268.119	-45.325
lst_800	1.7306	1.685	1.027	0.308	-1.626	5.087
ndwi_800	85.4412	22.732	3.759	0.000	40.167	130.715
elev	-0.0026	0.003	-0.810	0.420	-0.009	0.004

Table A.1 – F-test of variable significance of the linear regression.

A.3. Spatially-explicit simulation of urban heat islands

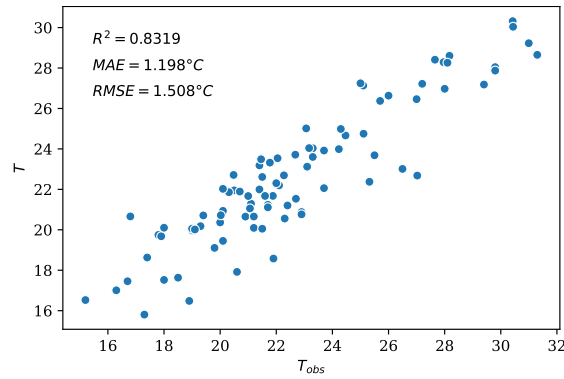


Figure A.2 – Scatter plot of the T_{air} predicted by the linear regression model trained with all the samples (vertical axis) versus the observed measurements (horizontal axis).

Simulation with the InVEST urban cooling model

The code of the spatial simulation of air temperature with the InVEST urban cooling model is available as a Jupyter Notebook (IPYNB) at <https://github.com/martibosch/lausanne-heat-islands/blob/master/notebooks/invest-urban-cooling-model.ipynb>

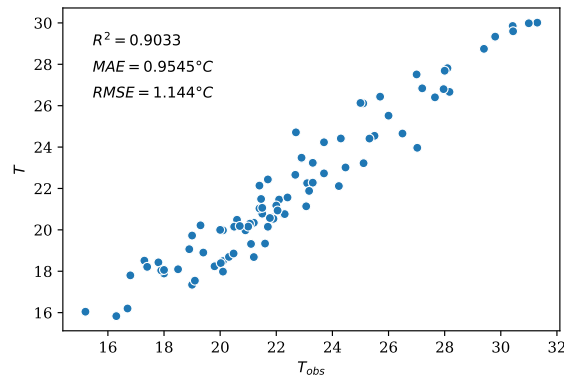


Figure A.3 – Scatter plot of the T_{air} values simulated with the InVEST urban cooling model (vertical axis) versus the observed measurements (horizontal axis).

Comparison

The code used for the comparison of the spatial regression and simulation of air temperature is available as a Jupyter Notebook (IPYNB) at <https://github.com/martibosch/lausanne-heat-islands/blob/master/notebooks/comparison.ipynb>

A.4 Urban greening scenarios for urban heat mitigation

The data materials to required to reproduce the results of the article are available in a dedicated Zenodo repository at <https://zenodo.org/record/4316572>.

A.4.1 Data

Biophysical table

The biophysical table for the LULC codes (before the reclassification) is shown in Table A.2. The crop and water coefficients are based on Allen et al. Allen et al. (1998), while rock, soil and urban coefficients are derived from the results of Grimmond and Oke Grimmond and Oke (1999) in the city of Chicago. Given that the evapotranspiration of the vegetation and crops is subject to seasonal changes in temperate zones such as Switzerland Allen et al. (1998), the values that correspond to the mid-season estimation (June to August) in Nistor (2016). The albedo values are based on the work of Stewart et al. Stewart and Oke (2012). The shade column, which represents the proportion of tree cover of each LULC class, is computed after the reclassification procedure described in section “Refining LULC classes based on tree cover and building density”.

Monitoring stations

The locations of the monitoring stations used to get the T_{ref} and UHI_{max} parameters of the InVEST urban cooling model are shown in Figure A.4. The operators of the stations are: Agrometeo, Federal roads office (ASTRA), Federal office for the environment (BAFU), General directorate for the environment of the Canton of Vaud (DGE), and the Federal Institute of Forest, Snow and Landscape Research (WSL) Rebetez et al. (2018). The source CSV file with the operator, location and elevation in meters above sea level of the monitoring stations used in the computational workflow is available at <https://github.com/martibosch/lausanne-greening-scenarios/blob/master/data/raw/tair-stations/station-locations.csv>. The code to produce Figure A.4 is available as a Jupyter Notebook (IPYNB) at <https://github.com/martibosch/lausanne-greening-scenarios/blob/master/notebooks/stations.ipynb>.

A.4. Urban greening scenarios for urban heat mitigation

Table A.2 – Biophysical table (before the reclassification). The source comma-separated value (CSV) file used in the computational workflow is available at <https://github.com/martibosch/lausanne-heat-islands/blob/master/data/raw/biophysical-table.csv>.

LULC code	Description	Case	K_c	Albedo	Green area
0	building	artificial	0.4	0.1-0.25	0
1	road, path	artificial	0.35	0.15	0
2	sidewalk	artificial	0.35	0.15	0
3	traffic island	artificial	0.35	0.15	0
4	rail	artificial	0.35	0.15	0
5	airfield	artificial	0.4	0.2	0
6	pond	water	0.45	0.15	0
7	other impervious	artificial	0.36	0.15	0
8	field, meadow, pasture	vegetation	0.9	0.2	1
9	vineyards	vegetation	0.7	0.2	1
10	other intensive farming	vegetation	1.05	0.2	1
11	garden	artificial	0.32	0.2	1
12	wetland	water	0.45	0.1	1
13	other green	vegetation	0.45	0.2	1
14	backwater	water	0.65	0.05	1
15	water course	water	0.65	0.05	0
16	reed	water	0.45	0.1	1
17	dense forest	vegetation	1.5	0.15	1
18	densely wooded pasture	vegetation	1.15	0.15	1
19	open wooded pasture	vegetation	1.15	0.2	1
20	other wooded	vegetation	1.15	0.15	1
21	bare rocks	rock and soil	0.2	0.25	0
22	glacier	water	0.52	0.1	0
23	sand	rock and soil	0.3	0.25	0
24	gravel pit	artificial	0.36	0.25	0
25	other non-vegetated	artificial	0.36	0.15	0

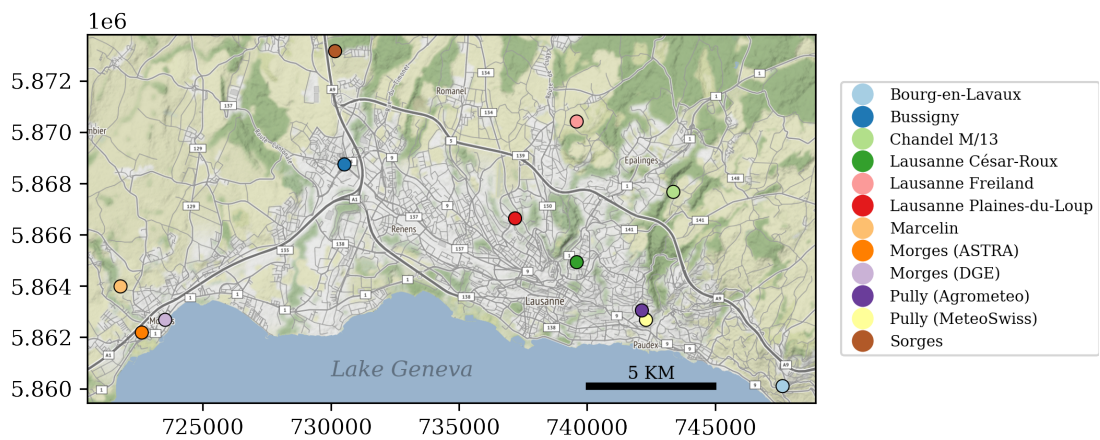


Figure A.4 – Locations of the monitoring stations used to get the T_{ref} and UHI_{max} parameters. The axes tick labels display the Swiss CH1903+/LV95 coordinates. The basemap tile is provided by StamenDesign, under CC BY 3.0, with data from OpenStreetMap, under ODbL.

A.4.2 Results

Scenario LULC, temperature and heat mitigation

The code to produce the figures 5.1, 5.3, A.5 and A.6, as well as tables describing the data of the figures, are available as a Jupyter Notebook (IPYNB) at <https://github.com/martibosch/lausanne-greening-scenarios/blob/master/notebooks/scenarios.ipynb>.

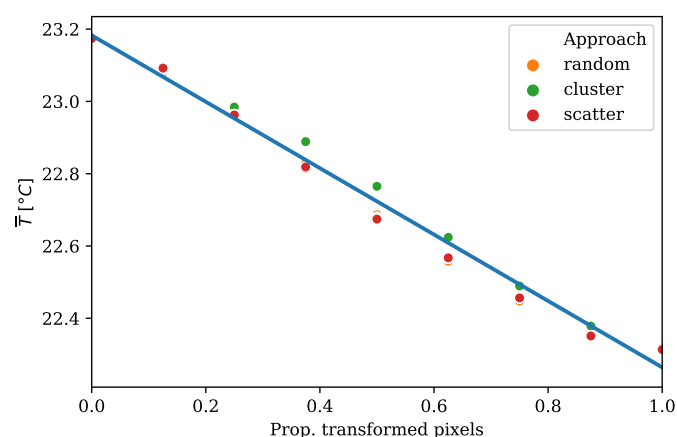


Figure A.5 – Relationship between the proportion of candidate pixels transformed and the average simulated temperature \bar{T} for each scenario sample. The translucent bands around the regression line represent the 95% confidence intervals estimated using a bootstrap.

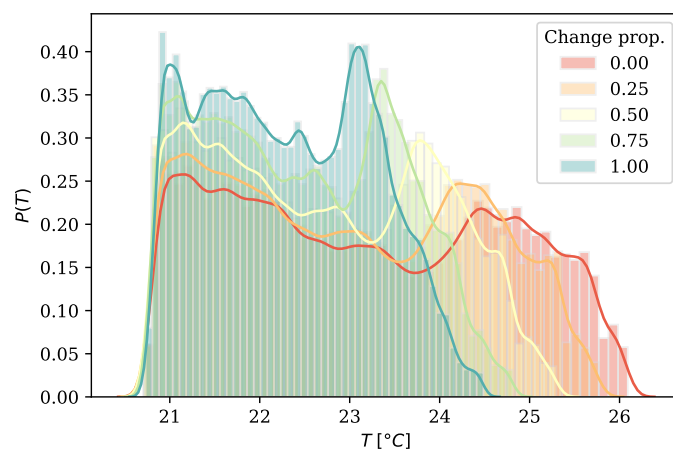


Figure A.6 – Histogram of raster temperature values for a 25, 50, 75 and 100% of the candidate pixels transformed. The temperature rasters for each histogram are computed by averaging the 10 simulations with the same proportion of candidate pixels transformed.

Scenario metrics

The code to produce Figure 5.4 is available as a Jupyter Notebook (IPYNB) at <https://github.com/martibosch/lausanne-greening-scenarios/blob/master/notebooks/scenario-metrics.ipynb>.

Scenario human exposure

The code to produce Figure 5.5 is available as a Jupyter Notebook (IPYNB) at <https://github.com/martibosch/lausanne-greening-scenarios/blob/master/notebooks/human-exposure.ipynb>.

Martí Bosch

Google Scholar: [cutt.ly/Og6JH8C](https://scholar.google.com/citations?user=Og6JH8C) • OrcID: [0000-0001-8735-9144](https://orcid.org/0000-0001-8735-9144)
GitHub: github.com/martibosch • Personal site: martibosch.github.io
EPFL ENAC IA CEAT, BP 3232, Station 16, 1015 Lausanne, Switzerland
marti.bosch@epfl.ch • +41 21 69 34435 • 28 years old

Education

- Sep 2016-Mar 2021 **PhD in Civil and Environmental Engineering; École Polytechnique Fédérale de Lausanne** (Lausanne, Switzerland)
- Sep 2015-Jul 2016 **MSc in Informatics; École Nationale Supérieure d'Informatique et Mathématiques Appliquées de Grenoble** (Grenoble, France)
- Sep 2010-Jul 2014 **BSc in Industrial Technology Engineering; Escola Tècnica Superior d'Enginyeria Industrial de Barcelona** (Barcelona, Spain)

Experience

- Current (since Sep 2016) **Doctoral Assistant; Urban and regional planning community (CEAT)**, EPFL (Lausanne, Switzerland)
Directors: Jérôme Chenal and Stéphane Joost
- Feb 2016-Jul 2016 **Research Intern, STEEP team**, INRIA Rhone-Alpes (Grenoble, France)
Thesis title: A framework for measuring urban sprawl from crowd-sourced data.
Directors: Serge Fenet and Peter Sturm
- Jun 2015-Sep 2015 **Summer Student, IT department**, CERN (Geneva, Switzerland)
Development of the DataTV project, aimed to display a network with the real-time data throughput of CERN's experiments. Director: Xavier Espinal
- Feb 2014-Jul 2014 **Research Intern, Tyrex team**, INRIA Rhone-Alpes (Grenoble, France)
Thesis title: Automated refactoring for size reduction of CSS style sheets. Director: Pierre Genevès

Technical Experience

- PhD Courses** **Scientific programming for Engineers** - Lecturer: Gillaume Anciaux
Topics in Computational Social Science - Lecturer: Robert West
Optimization and simulation - Lecturer: Michel Bierlaire
- Programming Languages** **Python:** expert proficiency in the scientific Python stack and geospatial libraries. Good command of performance-optimization tools like Cython, Numba, Dask and PyBind. Advanced proficiency in Flask and Django web frameworks.

C/C++: good command of object-oriented C++, templates and the standard library

Other: expert proficiency with the Emacs editor, LaTeX and git. Advanced proficiency in bash, Java, Matlab, R, SQL, HTML, CSS, JavaScript.

Languages

- Catalan (mothertongue), Spanish (native)
 - English, French (full professional proficiency, C1)
 - Italian (limited working proficiency, B1)
 - German (elementary proficiency, A1)
-

Publications

Submitted manuscripts

Bosch, M., Locatelli, M., Hamel, P., Jaligot, R., Chenal, J., & Joost, S. (2020): Evaluating urban greening scenarios for urban heat mitigation: a spatially-explicit approach. *Preprint available* at bioRxiv. doi.org/10.1101/2020.11.09.373779

Bosch, M., Locatelli, M., Hamel, P., Remme, R., Chenal, J., & Joost, S. (2020): A spatially-explicit approach to simulate urban heat islands in complex urban landscapes. *Under review* in Geoscientific Model Development. doi.org/10.5194/gmd-2020-174

Peer-reviewed journals

Bosch, M. (2020): DetecTree: Tree detection from aerial imagery in Python. *Journal of Open Source Software*, 5(50), 2172. doi.org/10.21105/joss.02172

Bosch, M., Jaligot, R., & Chenal, J. (2020). Spatiotemporal patterns of urbanization in three Swiss urban agglomerations: insights from landscape metrics, growth modes and fractal analysis. *Landscape Ecology*, 1-13. doi.org/10.1007/s10980-020-00985-y

Bosch, M. (2019). PyLandStats: An open-source Pythonic library to compute landscape metrics. *PLoS One*, 14(12). doi.org/10.1371/journal.pone.0225734

Bosch, M., Chenal, J., & Joost, S. (2019). Addressing urban sprawl from the complexity sciences. *Urban Science*, 3(2), 60. doi.org/10.3390/urbansci3020060

Bosch, M. (2019). swisslandstats-geopy: Python tools for the land statistics datasets from the Swiss Federal Statistical Office. *Journal of Open Source Software*, 4(41), 1511. doi.org/10.21105/joss.01511

Jaligot, R., Chenal, J., & Bosch, M. (2019). Assessing spatial temporal patterns of ecosystem services in Switzerland. *Landscape Ecology*, 34(6), 1379-1394. doi.org/10.1007/s10980-019-00850-7

Jaligot, R., Chenal, J., Bosch, M., & Hasler, S. (2019). Historical dynamics of ecosystem services and land management policies in Switzerland. *Ecological indicators*, 101, 81-90. doi.org/10.1016/j.ecolind.2019.01.007

Kemajou, A., Jaligot, R., Bosch, M., & Chenal, J. (2019). Assessing motorcycle taxi activity in Cameroon using GPS devices. *Journal of transport geography*, 79, 102472. doi.org/10.1016/j.jtrangeo.2019.102472

Conference proceedings

Gervasoni, L., Bosch, M., Fenet, S., & Sturm, P. (2017). Calculating spatial urban sprawl indices using open data. In 15th International Conference on Computers in Urban Planning and Urban Management.

Gervasoni, L., Bosch, M., Fenet, S., & Sturm, P. (2016). A framework for evaluating urban land use mix from crowd-sourcing data. In 2016 IEEE International Conference on Big Data (Big Data) (pp. 2147-2156). IEEE. doi.org/10.1109/BigData.2016.7840844

Bosch, M., Genevès, P., & Layaïda, N. (2015). Reasoning with style. In Twenty-Fourth International Joint Conference on Artificial Intelligence.

Bosch, M., Genevès, P., & Layaïda, N. (2014). Automated refactoring for size reduction of CSS style sheets. In Proceedings of the 2014 ACM symposium on Document engineering (pp. 13-16). doi.org/10.1145/2644866.2644885

Talks

Conferences

Bosch, M. (2020). A reusable computational workflow to assess urban heat islands in Python. GeoPython Conference 2020 (online). Sep 21-22

Bosch, M. (2020). Analysis with PyLandStats of the evolution of the Swiss forests. Workshop in the Young Modellers in Ecology Workshop (online). May 26-28

Bosch, M. (2020). PyLandStats: computing landscape metrics in the Python ecosystem. Talk in the Young Modellers in Ecology Workshop (online). May 26-28

Bosch, M. (2020). DetecTree: a Python library for tree detection from aerial imagery. AI & Cities track, Applied Machine Learning Days. Lausanne. Jan 25-29

Bosch, M. (2019). Spatiotemporal Patterns of Urbanization in Three Swiss Urban Agglomerations: Insights from Landscape Metrics, Growth Modes and Fractal Analysis. Theoretical Geography VVOIP Debates, Debate 3.1 - Fractals and Multifractals. Online colloquium. Nov 15-16

Bosch, M. (2014). Automated refactoring for size reduction of CSS style sheets. ACM symposium on Document engineering. Fort Collins, Colorado. Sep 16-19

Service

Journal peer review

Environmental Research Letters

Geoscientific Model Development

PLOS Computational Biology

Journal of Open Source Software